Limit shapes on the dimer model in multiply-connected domains

Nikolai Kuchumov

SORBONNE UNIVERSITÉ
CRÉATEURS DE FUTURS DEPUIS 1257

LPSM
LABORATOIRE DE PROBABILITÉS STATISTIQUE & MODÉLISATION

THÈSE DE DOCTORAT
Discipline : Mathematique

présentée par

Nikolai Kuchumov

Formes limites pour le modèle de dimères dans des domaines non simplement connexes

sous la direction de Cédric Boutillier

Rapporteurs :

M. **Nicolai Reshetikhin**	UC Berkeley, Tsinghua University
M. **Adrien Kassel**	UMPA - ENS de Lyon

Soutenue le devant le jury composé de :

M. **Cédric Boutillier**	Sorbonne, LPSM	Directeur de thèse
M. **Adrien Kassel**	UMPA ENS de Lyon	Rapporteur
Mme. **Marie Théret**	Université Paris Nanterre	Examinatrice
M. **Thierry Lévy**	Sorbonne, LPSM	Examinateur
Mme. **Beatrice De Tilière**	Université Paris Dauphine	Examinatrice
M. **Sunil Chhita**	University of Durham	Examinateur

Laboratoire de Probabilités, Statistique et Modélisation
Sorbonne Université Campus Pierre et Marie Curie
4 Place Jussieu, Case courrier 158

Remerciements – Acknowledgements

I would like to thank my scientific advisor, Cédric Boutillier, for his extraordinary support over the past two and a half years, for his generosity in hosting me in France, along with related issues. I am also grateful for the careful reading of the manuscript, his numerous suggestions that greatly enhanced its quality, and for our many fruitful discussions. I also wish to thank Nicolai Reshetikhin for his inspiring comments and Adrien Kassel who kindly accepted the invitation to be the reporter and provided valuable reports. I am especially thankful to Adrien Kassel for his remarks on the manuscript. Further, thanks to the Jury Committee members — Cédric Boutillier, Adrien Kassel, Béatrice de Tilière, Thierry Lévy, Marie Théret, and Sunil Chhita — for accepting the invitation to participate in the defense.

Furthermore, I would like to thank Rick Kenyon and István Prause for their ideas, sharing of Mathematica sheets, and help with the tangent plane method, which significantly contributed to Chapter 4. I am also grateful to Vadim Gorin for his stimulating discussions and for sharing his ideas.This thesis would not have been possible without the support and funding from the P.A.U.S.E. program (Programme d'Aide à l'Urgence des Scientifiques et des Artistes en Exil) at Collège de France, which facilitated my move to France. I am also thankful to the hosting laboratory, LPSM (Laboratoire de Probabilités, Statistique et Modélisation) for their warm hospitality. Special thanks to Lorenzo Zambotti, Élise Maspimby, and Valérie Juve with Marouane Abdelaziz for their administrative support over the past two years. I would also like to thank the Mathematical Faculty of the Higher School of Economics for their understanding and hospitality, particularly Andrey Marshakov, Alexey Gorinov, Senya Shlosman, and Pavlo Gavrilenko for our numerous and productive discussions. Additionally, I am grateful to my friends, Kirill Simonov and Alexei Gordeev for their help with computer simulations of random domino tilings of multiply-connected regions. Also, thanks to LPTMC lab and Maxim Dolgushev for providing technical facilities at the end.

My deepest gratitude goes to my family, especially my mother and father, my aunts Anna Schubert and Svetlana Baranova, my uncle Alexander Kolodyazhny, and my cousins Valerie Baranova, Natalie Schubert, Anastasia Kolodyazhnaya, Vladislav Baranov and Stepan Kolodyazhny, and my grandfather Sergei Golodyazhniy with my grandmother Nina Golodyazhnaya for their support throughout this journey. I would also like to thank Masha and Evgenia Smirnova for their various forms of assistance in the lifetime and especially over the past two years. Moreover, this scientific journey would not have been possible without the care provided by the specialists at the St.Petersburg Center of Multiple Sclerosis, particularly my neurologists at the early stages, Maria Shumilina and Gleb Makshakov together with Anna Rogozina and Valentin Piven, who have performed a medical miracle. Finally, I would like to thank my jogging coach, Pavel Menshikov, for helping me maintain and improve my physical condition during the course of writing this thesis, and to Bella Evloeva for an unforgettable jogging experience. Last but not least, I want to thank Daphné Letrosne for her willingness to help organize the PhD defense despite all odds.

Formes limites pour le modèle de dimères dans des domaines non simplement connexes

Résumé

Cette thèse se compose de trois parties, le but de la première partie est d'étudier les pavages aléatoires de dominos d'un domaine non simplement connexe avec une fonction de hauteur définie sur l'espace de revêtement universel du domaine. Nous établissons un principe de grandes déviations pour la fonction de hauteur dans deux régimes asymptotiques. Le premier régime couvre tous les pavages de dominos du domaine. Une loi des grands nombres pour le changement de hauteur dans ce régime est également obtenue. Le second régime couvre les pavages de dominos avec un changement de hauteur asymptotique donné. La deuxième partie de la thèse est une extension de la première partie. Nous prouvons l'existence d'une forme limite pour le modèle de dimères sur des graphes bipartis périodiques planaires avec un domaine fondamental arbitraire et des poids périodiques arbitraires. La troisième partie est consacrée au calcul de la courbe arctique du diamant aztèque avec trous dans deux régimes. Le premier régime, appelé cas non contraint, correspond à la mesure uniforme sur l'ensemble des pavages par dominos. Le second régime, appelé cas contraint, pose une condition sur le changement de hauteur des dominos.

Mots-clés : dimères,pavages,principe variationnel, forme limite, surfaces aléatoires, grandes déviations"

Limit shapes of the dimer model in multiply-connected domains

Abstract

This thesis consists of three parts, the goal of the first part is to study random domino tilings of a multiply-connected domain with a height function defined on the universal covering space of the domain. We establish a large deviation principle for the height function in two asymptotic regimes. The first regime covers all domino tilings of the domain. A law of large numbers for height change in this regime will also be derived. The second regime covers domino tilings with a given asymptotic height change. The second part of thesis is an extension of the first part. We prove the existence of a limit shape for the dimer model on planar periodic bipartite graphs with an arbitrary fundamental domain and arbitrary periodic weights. The third part is devoted to computation of the arctic curve of the multiply-connected Aztec diamond in two regimes. The first regime, called an unconstrained case, corresponds to the uniform measure on a set of domino tilings. The second regime, constrained case, puts a condition on the height change of domino tilings.

Keywords:Dimers, tilings, variational principle, limit shapes

Contents

Chapter 1

Introduction

1.1 Physical motivation

Random objects, like air particles, or crystal surfaces surround us everywhere. Thus, describing their behavior is important. However, what is a reasonable description of a random object? If we look at an air molecule or a crystal atom, we can try to memorize the position and the speed of each particle at every moment in time, in total six numbers for each particle at every moment of time. This would be a complete description, yet extremely difficult to deal with. As we know, the number of atoms in 1 gram has the order of the Avogadro number $N_A \approx 10^{23}$. It means that at any given time, the state of this 1 gram would be described by a vector in a space of dimension dim $\approx 6 \times 10^{23}$, which would be impossible to operate in daily life. Therefore, we would like to come up with a better description. A common way of doing it is to look at the average quantities among all the particles of the system. For example, instead of the speed v of each air particle,we typically use the air temperature, which is proportional to the average kinetic energy of the particles $T \propto m\langle v^2 \rangle/2$, where m is the mass density. The proportionality coefficient is called the *Boltzmann constant* $k \approx 1.38 \times 10^{-23} JK^{-1}$.

Instead of the positions of the particles, we tend to describe their densities. Further, rather than dealing with the Newton equations for each particle, we operate with so-called thermodynamic laws.

In our example of air particles in a room, we may look at molecules of a heavy gas, like carbon dioxide, in two cases: a high temperature $T \gg 100K$, and low temperature $T \approx 100K$. In the first situation, the particles have enough kinetic energy to neglect the force of gravity. Thus, they are distributed uniformly at random in the room. While in the second example, the temperature is low, and the molecules cannot neglect the potential energy, therefore they tend to stay closer to the floor of the room, and one would observe the so-called *barometric formula* from thermodynamics, see § 38 in [LL58]. It describes the normalized density distribution $c(h)$ depending on the height h and the mass density m,

$$c(h) = c_0 e^{-h\frac{gm}{TN_A k}}, \tag{1.1.1}$$

here $g \approx 9.8 m/s^2$ is the acceleration of free fall, and c_0 is the density distribution at $h = 0$.

One could say that this law is a result of the competition between the potential energy, and the temperature (in fact, people refer to it as the competition between energy and

entropy). Indeed, in the high temperature (or low mass m) regime, the concentration almost does not depend on h, while for the high mass m, and low temperature, the particles tend to concentrate around $h = 0$.

The transition from the individual description of each particle simultaneously to the description of the whole system is called the *thermodynamic limit*. Also, one often calls the state of the system in the first parametrization a *microstate*, while in the second parametrization a *macrostate*. Therefore, the latter is thought as the "limit" of a sequence of microstates of a growing sequence of systems. Now, we arrive at two problems: first how to take the thermodynamic limit of a given system, and second, how to parametrize and analyze the system afterwards.

In this thesis, we study analogs of these two problems for a sequence of random systems $\{\Gamma_N\}$:

- How to define the thermodynamic limit of $\{\Gamma_N\}$, such that

$$\lim_{N\to\infty} \Gamma_N = \mathcal{G}, \tag{1.1.2}$$

- How to describe the limit $\mathcal{G}$.

We analyze these two problems for a different model of statistical mechanics called *the dimer model*. This model is describing the arrangement of two-atomic molecules in a two-dimensional plane, and it is sufficiently rich to model physical phenomena such as phase transitions, yet simple enough to study it mathematically rigorously. Let us discuss another example of a model of statistical physics, *the Ising model*, as a warm-up before the main discussion.

1.1.1 Ising crystal

Let us introduce a model of a two-dimensional crystal on the square grid, following the exposition from [Oko15]. Assume that we deal with a finite region $\Gamma \subset \mathbb{Z}^2$ thought to be the union of unit squares of $\mathbb{Z}^2$, or equivalently, Γ is a subset of $\mathbb{Z}^2$ bounded by a finite lattice path. Then, the configuration of the model is a coloring of the faces of Γ by two colors, say blue and white, see Figure 1.1.

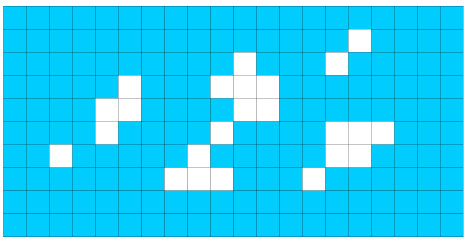

Figure 1.1: Example of a configuration of the Ising model for Γ being a rectangle, taken from [Oko15].

We think of a microstate of the model as an arrangement of white crystals inside the overall blue system, and the energy of the microstate S is proportional to the length of the interface $L(S)$ between the blue and the white squares, $E(S) \propto L(S)$. Then, the probability of observing the system in the state S is given by the Boltzmann distribution $\mathbb{P}_\Gamma$,

$$\mathbb{P}_\Gamma(S) = \frac{1}{Z} e^{-E(S)/kT}. \tag{1.1.3}$$

Where the normalization constant $Z := \sum_S e^{-E(S)/kT}$ is called the partition function, and the sum is taken over all the configurations S on Γ. The Ising model originally describes a

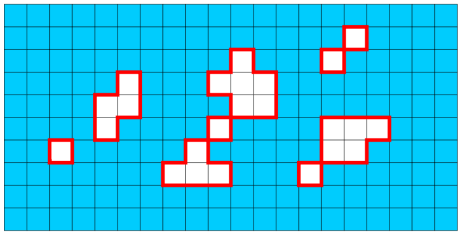

Figure 1.2: The contour representation of the Ising model, contours are in the red color.

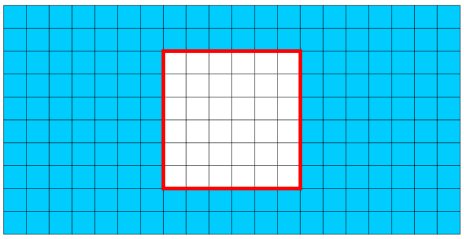

Figure 1.3: The energy minimizing configuration of the Ising model, the figure from [Oko15].

two-dimensional ferromagnetic material. In the first order approximation, the microstates of such materials are given by the magnetic dipole moments of atoms at each lattice site. The dipole moment in this model is oriented either upwards, or downwards. Thus, the microstate of each lattice site takes two possible values, either $+1$ or -1 depending on the orientation. We distinguish them by color, either white or blue. One could also describe the crystal surface in the model by the interface between the two colors. Then, a configuration of the Ising model can be seen as a configuration of lattice contours separating the two phases, blue and white, of the model. Let us concentrate on the situation with the fixed number of the white squares.

Looking at the formula (1.1.3), it is clear that the energy minimizer is the one that minimizes the length of the interface between the white and the blue squares. Clearly, such a state is not the one from Figure 1.1, but rather a square from Figure 1.3,

If the temperature T is low, the only configurations that we may observe are the low energy configurations that have the low interface lengths $L(S)$. Thus, let us look at the corner of the crystal minimizing the energy as on Figure 1.3. While the number of white squares allows formation of the perfect square, the minimizing configuration is the straight angle near its corner. However, if one deletes one or several one white squares (i.e., replacing them by the blue squares), the minimizing energy interface would take the configuration, for example as on Figure 1.4. Call such a modification a *defect*. One can notice that the shape of this interface separating the phases of the Ising model near the corner is given by an arrangement of unit cubes. Moreover, since the interface is supposed to minimize the length of the path separating two colors, the boxes should stick to each other. One can parametrize the defect by the length of each row. A collection of such lengths is naturally ordered from bottom to top and gives an example of a Young diagram corresponding to a partition of the natural number that is the size of the defect. A Young diagram is an ordered partition of integer $N = \sum_k \lambda_k$, $\lambda = \{\lambda_1 \geq \cdots \lambda_i\}$. For instance, on the Figure 1.4, the defect consists of ten white squares replaced by the blue ones, and the partition is $10 = 5 + 3 + 1 + 1$. The integers are the row length starting the bottom row, let us denote the corresponding Young diagram is $\lambda := (5, 3, 1, 1)$. Since configurations are random, so is the interface and the partition. Therefore, we can define a microstate of the Ising model with a defect as random partition of a given natural number for each corner. Moreover, it is reasonable to expect that a macrostate would be a continuous analog of this interface, a so-called *limit shape* for

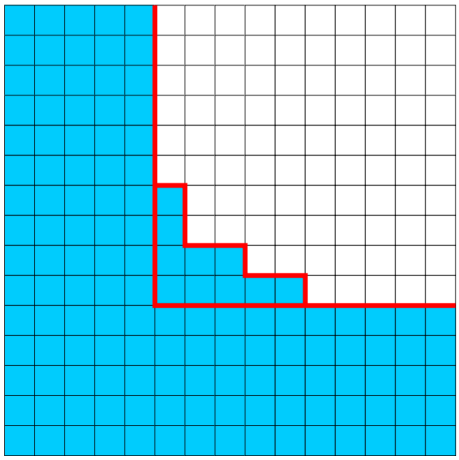

Figure 1.4: Energy minimizer of the Ising model with a defect

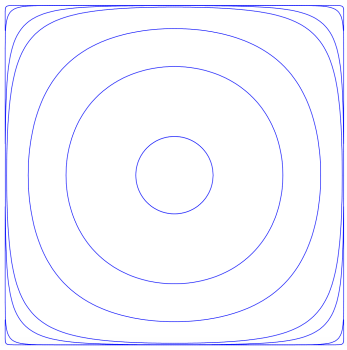

Figure 1.5: The limiting interface of the Ising model for various values of temperature, $T = 0$ corresponds to the square, figure is taken from [Oko15].

the Young diagrams corresponding to the partitions encoding the corners

This means that a typical Young diagram would tend to this shape as its size grows. This phenomenon is well-studied in the literature [Shl07] and §140 in [LL58].

Thus, the question from statistical mechanics turns out to be related to combinatorics, or more precisely to random Young diagrams. We are going to describe the thermodynamic limit in this situation in this language.

1.2 Limit shape of Young diagrams.

Let us describe the random Young diagrams and their limit shape. The *limit shape* is the most probable state of a large system such that nearby states are distributed according to the law, whose maximum is at the limit shape, while probabilities to observe other states are exponentially suppressed. Such law is often the Gaussian law. Let us give the first example of the limit shape, which goes back to the works by A. Vershik and S. Kerov [VK77], and, independently, by B. Logan and L. Shepp [LS77] on asymptotics for the Plancherel measure on Young diagrams. The main ingredient of their proofs is a variational principle. Moreover, the works[Ver96; DVZ00] generalize the works for the uniform measure on Young diagrams of a large fixed size.

Young diagrams are central objects in combinatorics and representation theory. For example, Young diagrams λ with N boxes encode conjugacy classes of the symmetric group S_N, and therefore complex irreducible representations of S_N, the so-called *Specht modules*

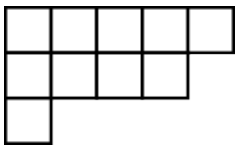

Figure 1.6: Example of Young diagram $(5, 4, 1)$.

$\mathcal{S}_\lambda$. Therefore, information about a large Young diagram would give us information about representation theory of a large symmetric group. One can assign two natural probability distributions on the set of Young diagrams. The first one is the uniform distribution, which is related to the example from the previous section. The second natural choice is the *Plancherel measure*, which is natural from the point of view of the representation theory. The Plancherel measure assigns to a Young diagram λ the probability $\mu(\lambda) = \frac{\dim^2 \lambda}{N!}$, where $\dim \lambda$ is the dimension of the Specht module $\mathcal{S}_\lambda$. This is indeed a well-define probability measure due to Burnside's formula,

$$\sum_{\lambda \vdash N} \frac{\dim \lambda)^2}{N!} = 1 \tag{1.2.1}$$

which follows from the Robinson–Schensted correspondence.

This dimension is usually expressed by the hook length formula discovered by Frame, Robinsonx and Thrall [FRT54]. See also [GNW79] for a probabilistic interpretation of it. Having the cell in position (i, j) of the i-th row and j-th column, the hook $D_\lambda(i, j)$ is the set of cells (a, b) such that $a = i$ and $b \geq j$ or $a \geq i$ and $b = j$. The number of cells of $D_\lambda(i, j)$ is *the hook length* $d_\lambda(i, j)$. Then,

$$\dim \lambda = \frac{N!}{\prod_{(i,j)} d_\lambda(i, j)}. \tag{1.2.2}$$

Here, the product is taken over squares of λ at position (i, j).

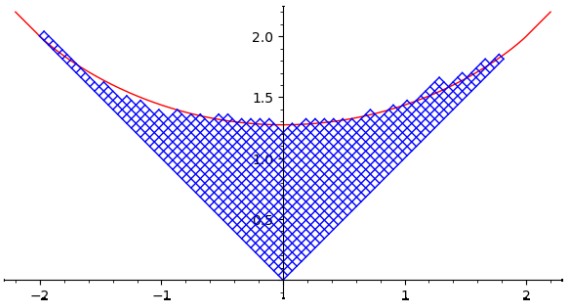

Figure 1.7: The Vershik-Kerov-Logan-Shepp limit shape, figure from [Ros23]. Here we use the standard coordinates rotated by 45° degrees.

1.2.1 Variational principle and Vershik-Kerov-Logan-Shepp curve

The idea of this method is linking the discrete problem of finding of the typical large but finite Young diagram with a continuous problem in the following sense. Fix a probability distribution $\mathbb{P}_N$ on Young diagrams with N boxes, which can be either the uniform measure, or the Plancherel measure μ_N.

First, a Young diagram λ defines a piece-wise constant function h_λ,

$$h_\lambda(x) := \{\text{Number of boxes of } \lambda \text{ above point } x\}. \tag{1.2.3}$$

Call such function the *height function* of λ. Then, consider a coordinate system (X, Y) rotated by 45° degrees as on Figure 1.7, this notation called the Russian notation. In such notation, the height function of a Young diagram is a piecewise linear function of slope ± 1. Therefore, it is reasonable to expect that in the limit of as $N \to \infty$ the normalized height function will approximate a continuous 1-Lipschitz function.

Let us use normalized coordinate $x_N = X/\sqrt{N}$ and $y_N = Y/\sqrt{N}$ and normalized version of the height function $h_\lambda^N := h_\lambda/\sqrt{N}$. We want to find a such a functional $\mathrm{Ent} : \mathfrak{h} \mapsto \mathrm{Ent}(\mathfrak{h})$ that its value $\mathrm{Ent}(\mathfrak{h})$ equals to the asymptotic weight of Young diagrams $\lambda(N)$ with N boxes whose normalized height functions $h^N_{\lambda(N)}$ are close to $\mathfrak{h}$ with respect to the uniform norm.

$$\mathrm{Ent}(f) = \lim_{N\to\infty} N^{-1} \log \mathbb{P}_N \left(\lambda(N) : \left\| h^N_{\lambda(N)} - \mathfrak{h} \right\|_\infty \leq O(N^{-1/2}) \right). \tag{1.2.4}$$

After it, once Ent has a unique minimizerzer $\mathfrak{h}^\star$, then for sufficiently large N the height function of a random Young diagram $h^N_{\lambda(N)}$ will be close to $\mathfrak{h}^\star$ with overwhelming probability. Or in other terms, the probability of observing a Young diagram whose normalized height function is far away from $\mathfrak{h}^\star$ will tend to zero as $N \to \infty$. We call such function $\mathfrak{h}^\star$ the limit shape of Young diagrams with respect to measure $\mathbb{P}_N$.

One can prove such a statement in the following order.

- Find such functional space $\mathcal{H}$ that any $\mathfrak{h} \in \mathcal{H}$ can be realized as $\lim_{N\to\infty} h^N_{\lambda(N)}(x) = \mathfrak{h}(x)$ for a suitable family of Young diagrams $\lambda(N)$ and vice versa, each normalized height function h^N_λ can be approximated by a function from $\mathcal{H}$, that is there exists $\mathfrak{h} \in \mathcal{H}$ such that $\left\| h^N_\lambda - \mathfrak{h} \right\|_\infty \leq N^{-1/2}$.
- Compute the asymptotic growth rate $\mathrm{Ent}(\mathfrak{h})$ of the weight of Young diagrams whose height functions are close to $\mathfrak{h}$, and prove that it has a unique minimizer $\mathfrak{h}^\star \in \mathcal{H}$
- Prove the concentration of measure, that is, the law of large numbers for Young diagrams for every $c > 0$ and sufficiently large N, $\mathbb{P}_N(h^N_{\lambda(N)}(x) - \overline{h^N_\lambda(x)} > c) < e^{-cN}$, where $\overline{h^N_{\lambda(N)}(x)}$ is the expectation value of $h^N_{\lambda(N)}$ at x.

The first two steps allows us to find a unique candidate for the limit shape $\mathfrak{h}^\star$, and the third step helps us to prove that it is, indeed, the limit shape.

Let us describe the case of the Plancherel measure from [VK77; LS77] in more detail following the book [Ker03]. Looking at formula (1.2.1), it is more convenient to use the following expression for the Plancherel measure μ_N of diagrams with N boxes,

$$\mu_N(\lambda) = \frac{N!}{\prod_{i,j} d_{i,j}^2}. \tag{1.2.5}$$

This formula tells us that if we want to maximize the value of the Plancherel measure, we need to minimize the hook length. It turns out that in the limit as $N \to \infty$, one needs to minimize the hook integral that takes the following form[Ker03, Eq.3.1.6] for an $L \in \mathcal{H}$,

$$\Theta(L) := 1 + 2 \iint \log 2(s-t)(1 - L'(s))(1 + L'(t)) ds dt \tag{1.2.6}$$

And it has the unique minimizer

$$\Omega(X) = \frac{2}{\pi}(X \sin X + \sqrt{1 - X^2}) \tag{1.2.7}$$

for $|X| < 1$, and $\Omega(X) = |X|$ for $|X| > 1$. This Ω is the Vershik-Kerov-Logan-Shepp limit shape.

The correspondence between low temperature limit of the Ising model and a typical Young diagram in two dimensions extends to the three-dimensional situation, which we discuss in the next subsection.

1.2.2 Limit shapes of 3d Young diagrams

In our setting, the Ising model in three dimensions is a coloring by two colors of the unit boxes of $\mathbb{Z}^3$ a finite region $\Gamma \subset \mathbb{R}^3$. A generalization of a Young diagram is so-called *plane partition*.

It is a filling of a Young diagram λ by positive integers $\pi_{i,j}$ such that

$$\pi_{i,j} \geq \pi_{i,j+1}$$
$$\pi_{i,j} \geq \pi_{i+1,j}$$

for all boxes of λ in position (i, j), see Figure 1.8. We think of such plane partition as a two-dimensional stepped surface formed by an arrangement of unit boxes inside the three-dimensional space. And the number of boxes, the height, at position (i, j) of λ equals to $\pi_{i,j}$. Therefore, we may think that this surface is a graph of a piece-wise constant function that assigns the height $\pi_{i,j}$ to each square of λ. Such function is called the height function corresponding to the plane partition $\pi_{i,j}$. See example of a plane partition, and the corresponding discrete surface on Figure 1.8.

4	4	3	2	1
4	3	1	1	
3	2	1		
1				

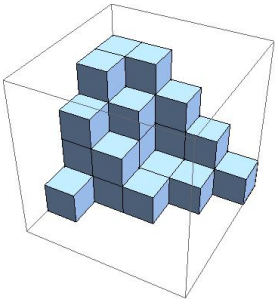

Figure 1.8: Two realizations of a plane partition.

Then, a natural question is what is a typical 3-dimensional Young diagram? First, we need to understand what does "typical" mean in this situation, that is we need to have a probability measure on plane partitions. A common way of doing it is so-called q^{Volume} measure, which for a $|q| < 1$ assigns to a plane partition $\pi_{i,j}$ the weight $q^{\text{number of boxes in } \pi_{i,j}}$. For this measure, limit shape was found in the limit as $q \to 1$ in [CK01], where the authors studied low-temperature asymptotics of the interface of the three-dimensional Ising model and identified it with the limit shape of plane partitions with q^{Volume} measure, the parameter q here is related with the temperature. The limit shape here is given by the Ronkin function $R(X, Y)$, which recall later in the Chapter. The main technique of the paper is the so-called Wulff crystal construction, which describes the limit shape as an envelope of its tangent planes. We describe this approach in Chapter 4 in more detail.

Another interpretation of a plane partition is through the *lozenge tilings*. One may look at a projection of a three-dimensional Young diagram onto the plane $x + y + z = 0$ in $(1, 1, 1)$ direction, as on the Figure 1.8. Each plane partition corresponds to a tiling by three types of *lozenges* of a hexagon. Under this projection, different faces of the boxes are mapped into different lozenges. Since there are three types of faces of a box, parallel to planes $x + y = 0$, $x + z = 0$ and $y + z = 0$, we obtain three types of lozenges. The topic of random tilings, and lozenge tilings in particular, is a popular subject of combinatorics. One of the most famous result about it in the paper [JPS98], where the authors discovered that uniformly-random lozenge tiling of a hexagon with sides $aN \times bN \times cN$ is asymptotically fixed outside the ellipse inscribed into the hexagon. Such an ellipse is called the *arctic curve* meaning that informally, lozenges inside the ellipse are random, while outside the ellipse they are fixed or somehow frozen. One then calls the region outside the ellipse the *frozen region*, while

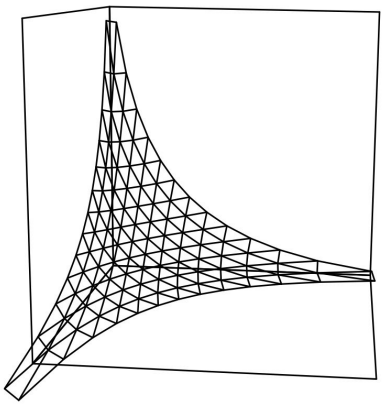

Figure 1.9: The Wulff crystal around which plane partitions concentrate at large scales.

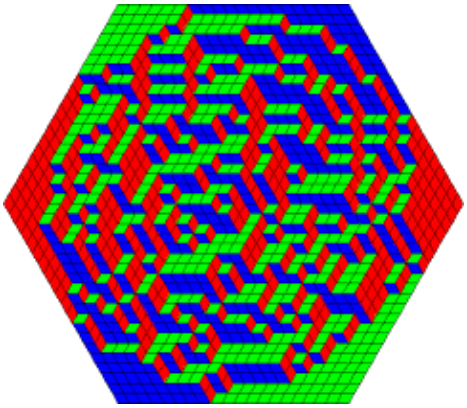

Figure 1.10: A lozenge tiling of a hexagon of side length $N = 20$.

the inner region inside ellipse the *liquid region*. The distinction between the frozen and the liquid regions is also in the behavior of fluctuations, they tend to disappear inside the frozen region, while inside the liquid region they tend to be Gaussian in the limit as $N \to \infty$.

Another famous result concerning the lozenge tilings of the hexagon is the McMahon formula of the number of lozenge tilings of the hexagon

$$Z(A,B,C) = \prod_{i=1}^{A}\prod_{j=1}^{B}\prod_{k=1}^{C}\frac{i+j+k-1}{i+j+k-2}. \tag{1.2.8}$$

The number of lozenge tilings of an arbitrary domain Γ is given by a determinant of a certain matrix, the so-called *Kasteleyn operator*, a suitably signed adjacency matrix of Γ, which we discuss in Section 1.4.

The interpretation of a plane partition by lozenges allows giving a local definition of the height function for other domains as well as for the hexagon $A \times B \times C$,

1.2.3 The height function

Suppose that a planar region Γ on the hexagonal lattice can be tiled by lozenges, i.e., covered by them without gaps or overlaps.

Then, the function H on faces of Γ is the height function of a lozenge tiling D if

- $H(p_0) = 0$ for a fixed $p_0 \in \partial\Gamma$.
- $H(u) = H(v) + 1$ if the edge (u, v) does not cross a lozenge.

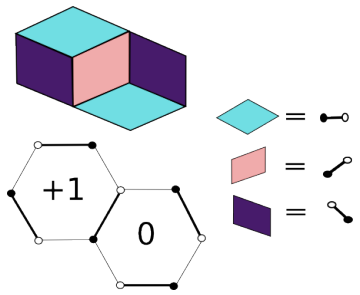

Figure 1.11: Example of lozenge tiling with the corresponding height function and representation by the dimer model.

- $H(u) = H(v) - 2$ if the edge (u, v) crosses a lozenge..

For a simply-connected Γ, the height function is a well-defined map. In fact, the famous Thurston tileability [Thu90] theorem states that a simply-connected domain of the hexagonal lattice Γ is tileable if and only if it admits a well-defined height function.

However, the most famous example of a limit shape goes to [JPS98] and the arctic circle theorem for random domino tiling of the typical random domino tiling of a large Aztec diamond. These examples are quite similar, and we mostly discuss domino tilings. Let us give a glance on this model with necessary details.

1.3 Domino tilings

Counting the number of domino tilings of a region such as the chess board is a classical problem in combinatorics. However, how does a *typical domino tiling of a given region look like*? It turns out that for a large region both the question, and the answer are way deeper than it seems at first glance. Indeed, random domino tilings, or, more generally, dimer configurations provide examples of sharp phase transitions and random surfaces sufficiently rich to be non-trivial, while simple enough to be accessible from the mathematical level of rigor. The mathematical formulation of the problem can be done as follows.

Let Γ be a finite, connected region on the square grid $\Gamma \subset \mathbb{Z}^2$ viewed as a subset of $\mathbb{R}^2$ with the set of vertices $V(\Gamma)$ and a fixed chessboard coloring. We assume that Γ can be seen as a discretization of a planar domain Ω. Suppose also that it can be *tiled by dominoes* (i.e. by 2×1 rectangles), and let $Z(\Gamma)$ be the number of such domino tilings D of Γ. See example on Figure 1.12.

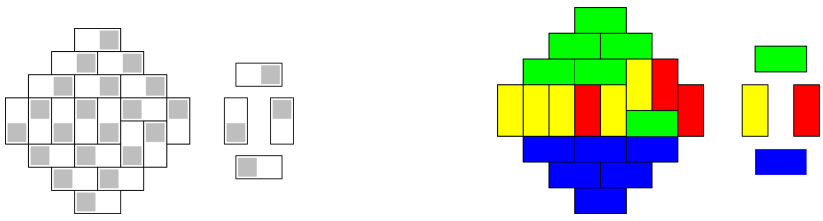

Figure 1.12: The same domino tiling of Aztec diamond AD_4 with two graphical representations. There are four types of dominoes with respect to chess board coloring on the left, and their color representation on the right.

Let $\mathbb{P}_\Gamma$ be the uniform measure on the set of domino tilings of Γ. Then, one might be interested in what is the probability of observing a particular type of domino at a given location of Γ. This type of questions became very popular after the Arctic Circle Theorem

[JPS98], where the authors analyzed a typical domino tiling of a growing sequence of lattice domains, so-called Aztec diamonds AD_N, see Figure 1.12. It was shown that for large N, a uniformly random domino tiling of AD_N forms two kinds of regions separated by the circle inscribed to the normalized domain, the unit square rotated by 45°. Statistics of dominoes in the inner region remains random in the limit as $N \to \infty$, all four types of dominoes w.r.t. their orientation have a positive density. However, regions outside the unit circle, the so-called frozen regions, exhibit a deterministic statistics, each region is covered by a fixed type of domino, see Figure 1.14.

The behavior of domino tilings inside the unit circle is governed by the Gaussian free field, whereas the interface between the frozen and liquid region has a scaling limit described by the Airy point process and is in the KPZ universality class, [BF08; Joh05]. This behavior is known in the literature as the *Arctic boundary* or *Arctic curve*.

Soon after, H.Cohn, R.Kenyon and J.Propp proved that this *limit shape phenomenon* holds for a generic simply-connected domain in [CKP00]. Let us give a glance on their main theorem with the necessary details.

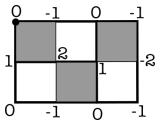

Figure 1.13: Values of the height function of a domino tiling D of a rectangle 2×3.

Let Γ be a simply-connected region and $0 \in \Gamma$, a standard algorithm encodes a domino tiling D of Γ by a height function, $H_D^\Gamma : V(\Gamma) \to \mathbb{Z}$, defined on vertices of Γ by the following combinatorial rule, see example on Figure 1.13.

Definition 1.3.1.

1. Set the value of $H_D^\Gamma(p_0) := 0$ for all D and a fixed point $p_0 \in \partial\Gamma$.
2. If the edge $v := (p_1, p_2)$ has a black square on its left, then $H_D(p_2)$ equals $H_D(p_1) + 1$ if v does not cross a domino in D and $H_D(p_1) - 3$ otherwise.

It is worth mentioning that boundary values for H_D^Γ are fixed by Γ.

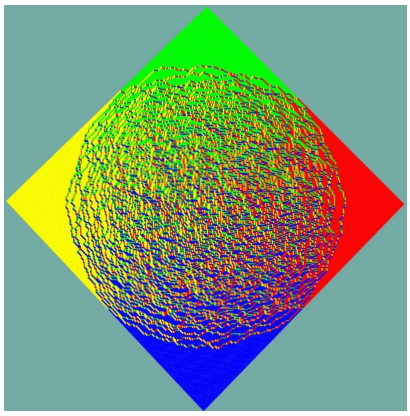

Figure 1.14: Simulation of a uniformly random domino tiling of large Aztec diamond.

The authors of [CKP00] consider a sequence of normalized tilable domains Γ_N with mesh $\frac{1}{N}$ that approximates a continuous simply-connected domain Ω such that discrete boundary conditions for H_D^Γ converge to a continuous one $\mathfrak{b}$. Then, the random normalized height function $\frac{1}{N} H_D^{\Gamma_N}$ converges in probability to a non-random continuous function $\mathfrak{h}^\star$, *the*

limit shape. Moreover, $\mathfrak{h}^\star$ minimizes over the space of Lipschitz functions with prescribed boundary conditions the entropy functional $\mathcal{F} : \mathfrak{h} \mapsto -\int_\Omega \sigma_{\mathbb{Z}^2}(\frac{\partial \mathfrak{h}}{\partial x}, \frac{\partial \mathfrak{h}}{\partial y})dxdy$ for an explicit convex function $\sigma_{\mathbb{Z}^2}$. Further, the normalized logarithm of the number of domino tilings of Γ_N has the following asymptotics,

$$\lim_{N\to\infty} N^{-2} \log Z(\Gamma_N) = -\int_\Omega \sigma_{\mathbb{Z}^2}\left(\frac{\partial \mathfrak{h}^\star}{\partial x}, \frac{\partial \mathfrak{h}^\star}{\partial y}\right) dxdy. \tag{1.3.1}$$

Moreover, $\forall \epsilon > 0$ $\exists c(\epsilon)$ such that for sufficiently large N

$$\mathbb{P}_N\left(|N^{-1}H_D^{\Gamma_N} - \mathfrak{h}^\star|_\infty > \epsilon\right) \le \exp\left(-c(\epsilon)N^2\right) \tag{1.3.2}$$

This statement is known in the literature as a *variational principle* for domino tilings.

The domino tiling and the lozenge tilings are particular cases of a more general model called the dimer model. Let us define it.

1.4 Periodic dimer model

We shall start with a $\mathbb{Z}^2$-periodic bipartite lattice Λ, it means two properties: first: Λ is a bipartite graph, that is the vertices of Λ are either black $\mathcal{B}(\Lambda)$ or white $\mathcal{W}(\Lambda)$ such that only vertices of different colors are connected by edges. Second, translations of $\mathbb{Z}^2$ map black vertices to black, and white vertices to white. Or simply they preserve the color or bipartite structure of Λ. Then, we can define a fundamental cell (fundamental domain) of the lattice by $\Lambda_0 := \Lambda/\mathbb{Z}^2$, see example on Figure 1.16. We mostly interested in dimer covers of a finite connected subset of Λ, usually denoted by Γ and called a *lattice region*.

Then, a dimer configuration (cover) D of Γ is a subset of its edges such that every vertex of Γ is adjacent to an edge from D. One assigns a $\mathbb{Z}^2$-periodic weight to D, call it $\nu(D)$. We focus on the edge weight systems, i.e., abusing notation, define

$$\nu(D) = \prod_{e\in D} \nu(e) \tag{1.4.1}$$

where the product goes over all edges contained in D. More precisely, we fix a positive function ν on edges of Λ_0 and extend it to Λ by periodicity. Then, for a $D \in \mathfrak{Conf}(\Gamma)$ define its probability by the following formula,

$$\mathbb{P}(D) := \frac{\nu(D)}{Z(\Gamma)} \tag{1.4.2}$$

where $Z(\Gamma)$ is a normalization constant called the partition function:

$$Z(\Gamma) = \sum_{D\in\mathfrak{Conf}(\Gamma)} \nu(D). \tag{1.4.3}$$

The height function of a dimer configuration D on Γ is defined by first choosing a *reference dimer cover* D_0, which we keep fixed. Then, a simple combinatorial argument shows that the union of D and D_0 is a collection of double edges and cycles C_i, which can be oriented so that dimers from D are oriented from black vertices to white, whereas dimers from D_0 in the opposite direction. Then, the height function H_{D,D_0} is a level function of these cycles. Then, a probability measure $\mathbb{P}$ on dimer configurations on the whole lattice Λ. Call it a Gibbs measure, for any finite subgraph Γ conditioned on edges that lie outside Γ, the restriction of $\mathbb{P}$ on the dimer configuration inside is given by the weight ν. Further, call it an ergodic Gibbs measure if it is invariant and ergodic under the action of $\mathbb{Z}^2$ by

translations. Define for an ergodic Gibbs measure $\mathbb{P}$ its slope (s,t) to be the expected value of horizontal and vertical height, $s := \mathbb{E}(H(v+(1,0)) - H(v)$, $t := (\mathbb{E}(H(v+(0,1)) - H(v))$.

Then, the question is how to evaluate the partition function $Z(\Gamma)$ for a given example, and the answer for the square grid was found by Kasteleyn in [Kas61].

The partition function of a finite subregion of the square grid can be computed as a determinant of a matrix, the so-called Kasteleyn operator $\mathcal{K}$. This operator is the matrix whose matrix elements labeled by the white and black vertices, i.e., assign a vector space $\mathbb{C}$ to each vertex, then the Kasteleyn operator $\mathcal{K} : \mathbb{C}^{\mathcal{B}(\Gamma)} \to \mathbb{C}^{\mathcal{W}(\Gamma)}$. Its matrix elements $\mathcal{K}(w,b) = \delta(wb)\nu(wb)$, where wb is the edge between w and b, and the sign $\delta(wb) = \pm 1$ is called the Kasteleyn sign. It satisfies the following conditions:

- Each face f with $0 \mod 4$ edges has the odd number of $\delta = -1$ signs.
- Each face f' with $2 \mod 4$ edges has even number of $\delta = -1$ signs.

By the Kasteleyn's theorem [Kas61], such a δ always exists for a planar graph Γ.

Theorem 1.4.1 ([Kas61]). *For any planar graph Γ, there exist Kasteleyn signs.*
Moreover, $Z(\Gamma) = \det \mathcal{K}(\Gamma)$.

This trick can be done in more general context, and these signs have a deep topological meaning in terms of so-called Kasteleyn's orientation or discrete spin structures, see discussion in [CR08].

1.4.1 The Newton polygon

Let us now describe the computation of the Kasteleyn operator $\mathcal{K}$ for the square grid $\mathbb{Z}^2$. Let us pick the following fundamental domain, and attach extra weights to the edges, so-called magnetic altered signs z, w. To an edge e we assign the weight depending on the intersection with the fundamental cycles of the torus, call them A_y, B_x for the horizontal and vertical cycles. That is, We assign the weight $z^{\langle e, A_y\rangle} w^{\langle e, B_x\rangle}$, see Figure 1.16.

The local rule for the height function in this situation becomes as on Figure 1.15.

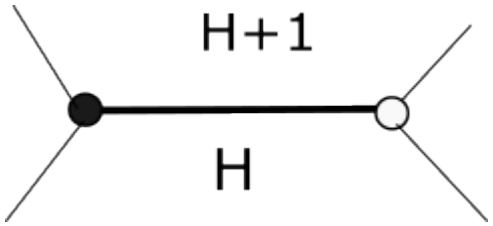

Figure 1.15: The local rule for height function defined on the dual graph. The edge occupied by a dimer is in black.

Now it becomes an operator $\mathbb{C}^{\otimes\mathbb{Z}^2} \to \mathbb{C}^{\otimes\mathbb{Z}^2}$ from the tensor product of vector spaces attached to the white vertices to the tensor product corresponding to the black ones. Thus, a vector $f \in \mathbb{C}^{\otimes\mathbb{Z}}$ can be considered as a function on the white vertices, whose value at a white vertex v equals to the coefficient of f e_v in basis labeled by the white vertices. Now, $\mathbb{Z}^2$ periodicity of the lattice implies that $\mathcal{K}$ takes a block-diagonal form in the basis of $\mathbb{Z}^2$ quasiperiodic functions,i.e., $f(b+(x,y)) = f(b)z^y w^{-x}$. This block is called the Kasteleyn operator $\mathcal{K}(z,w)$.

For example, for the square grid, we can take the fundamental domain represented on Figure 1.16, the corresponding Kasteleyn operator is given by

$$\mathcal{K}(z,w) = 1 + z + w - zw. \tag{1.4.4}$$

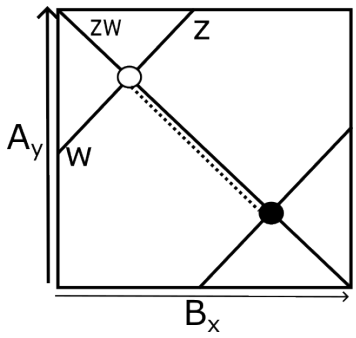

Figure 1.16: Weights of the fundamental domain of the square grid with A_y and B_x cycles. The reference dimer cover is in dashed color.

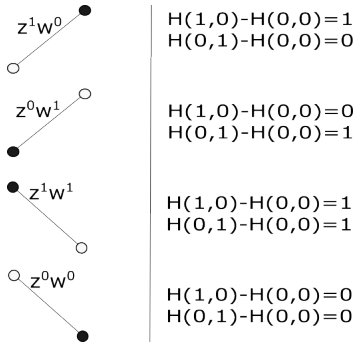

Figure 1.17: Correspondence between heights and monomials in z, w.

The determinant of the Kasteleyn operator is called the *characteristic polynomial* $P(z,w) := \det \mathcal{K}(z,w)$. For the square grid in our conventions, it becomes $P(z,w) = 1 + z + w - zw$, where the minus agrees with the Kasteleyn theorem (we have only one face with four edges around it). Also note that $P(z,w)$ may have negative powers, i.e., it is a Laurent polynomial.

Once we have $P(z,w)$ we define the Newton polygon of it,

$$\mathcal{N} := Conv\{(i,j) : z^i w^j \text{ is monomial in } P(z,w)\}. \tag{1.4.5}$$

The Newton polygon is the set of allowed slopes for the height function by Theorem 3.2 [KOS06], for example for the square grid our conventions give the square with vertices $(0,0), (1,0), (0,1)$ and $(1,1)$. We follow these conventions in Chapter 4. However, in Chapter 2 we use a different normalization of height function. It differs by rotation of the Newton polygon by 45 degrees, thus it has vertices $(\pm 1, 0)$ and $(0, \pm 1)$, and a multiplication by 2. In terms of $P(z,w)$ and the Newton polygon, we can analyze the asymptotic behavior of the model.

1.4.2 Asymptotics on torus, the Ronkin function

Suppose $(s,t) \in \mathbb{R}^2$, and let $\mathfrak{Conf}_{s,t}(\Lambda_N)$ be the set of dimer configurations on torus with the slope $(\lfloor sN \rfloor, \lfloor Nt \rfloor)$. Assuming that it is nonempty, we have a classification of the ergodic Gibbs measures on $\mathfrak{Conf}(\Lambda_N)$,[KOS06, Section 2 and Section 3, Theorem 3.2].

Theorem 1.4.2. *For any $(s,t) \in \mathcal{N}_\Lambda$, there exists a unique Ergodic Gibbs measure $\mu(s,t)$ of slope (s,t), which is a limit of discrete measures $\mu_N(s,t)$ of slopes $(\frac{\lfloor sN \rfloor}{N}, \frac{\lfloor Nt \rfloor}{N})$. Moreover, $\mu_N(s,t)$ exists for sufficiently large N and every ergodic Gibbs measure of slope (s,t) is $\mu(s,t)$*

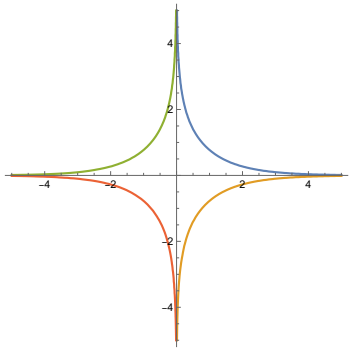

Figure 1.18: Plot of Amoeba for $\mathbb{Z}^2$ and our choice of $P(z,w)$. Quadrants correspond to the frozen regions.

The next question is can we compute the partition function of dimer configurations with a given slope on torus with $N \times N$ fundamental domains? Call this quantity the surface tension σ,

$$\sigma_\Lambda(s,t) = -\lim_{N\to\infty} N^{-2} \log Z_N^\Lambda(\frac{\lfloor sN \rfloor}{N}, \frac{\lfloor tN \rfloor}{N}). \tag{1.4.6}$$

The computation of σ_Λ requires several steps, and the first one is the following partition function.

The partition function of a larger domain, for example the torus made of $N \times N$ fundamental domains, factorizes in $P(z,w)$ and can be computed recursively,

$$\mathcal{K}_N(z,w) = \prod_{z_0^N = z} \prod_{w_0^N = w} P(z_0, w_0) \tag{1.4.7}$$

This formula follows from Fourier transform argument.

This factorization allows us to write the following asymptotics of the partition function by Theorem 3.5 [KOS06],

$$-\frac{1}{N^2} \log Z_N = \frac{1}{(2\pi i)^2} \int_{\mathbb{T}^2} \log|P(z,w)| \frac{dzdw}{zw} + o(1). \tag{1.4.8}$$

We can look at the modified partition function, where we alter the weights z and w in the characteristic polynomial $P(z,w)$ by e^X and e^Y, the resulting asymptotic function is called the *Ronkin function* $\mathcal{R}(X,Y)$,

$$\mathcal{R}(X,Y) := \frac{1}{(2\pi i)^2} \int_{\mathbf{T}^2} \log|P(e^X z, e^Y w)| \frac{dzdw}{zw}. \tag{1.4.9}$$

The curve $\{P(z,w) = 0\}$ in $\mathbb{C}^2$ is called the *spectral curve* $\mathcal{C}(P)$, and a closely related object to it is the image of the spectral curve under the map $(z,w) \mapsto (\log|z|, \log|w|)$, the so-called *amoeba* $\mathcal{A}(P)$. In our example of the square grid, the spectral curve admits a rational parametrization $\lambda \mapsto (\lambda, \frac{\lambda+1}{\lambda-1})$. Therefore, in this case, it has genus 0 thus it is the Riemann sphere. Moreover, it has an obvious involution of complex conjugation, $(z,w) \mapsto (\bar{z}, \bar{w})$, which allows us looking at the upper part isomorphic to the upper-half plane $\mathcal{C}^+ \simeq \mathbb{H}$ and its image under conjugation isomorphic to the lower-half plane $\mathcal{C}^- \simeq \overline{\mathbb{H}}$. The real points of the curve are fixed under the involution. The Ronkin function is strictly convex in the interior of amoeba.

It turns out that $\mathcal{R}$ is a limit shape for a particular boundary condition, see [KO05, Theorem 5]. For example, for the hexagon lattice with $P(z,w) = 1 + w + z$ we have the

limit shape from Figure 1.9. Moreover, the unbounded components of amoeba are frozen regions, thus, they correspond to particular vertices of $\mathcal{N}_\Lambda$ and the corresponding edges.

The Ronkin function $\mathcal{R}$ is related to the surface tension σ, which turns out to be the Legendre transform of $\mathcal{R}$,

$$\sigma(s,t) = \max_{(X,Y)\in\mathcal{A}} \left(sX + tY - \mathcal{R}(X,Y)\right). \tag{1.4.10}$$

The surface tension is defined on the Newton polygon $\mathcal{N}$, and it is strictly convex in the interior of it. However, the exact formulas for σ are relatively complicated, let us give two main examples for the hexagonal lattice and the square grid. First, recall $(s,t) = \nabla\mathfrak{h}$. Introduce the Lobachevsky function $L(z) = -\int_0^z \log|2\sin t|dt$ and quantities $p_a = p_a(s,t), p_b = p_b(s,t), p_c = p_c(s,t), p_d = p_d(s,t)$ that are determined by system expression (1.4.12). Then, the surface tension is the following function,

$$\sigma(s,t) = -\frac{1}{\pi}\left(L(\pi p_a) + L(\pi p_b) + L(\pi p_c) + L(\pi p_d)\right). \tag{1.4.11}$$

Here, p_a, p_b, p_c and p_d are asymptotic probabilities of four types of dominoes on torus that are determined by the following system [CKP00],

$$\begin{aligned} &2(p_a - p_b) = t,\\ &2(p_d - p_c) = s,\\ &p_a + p_b + p_c + p_d = 1\\ &\sin(\pi p_a)\sin(\pi p_b) = \sin(\pi p_c)\sin(\pi p_d). \end{aligned} \tag{1.4.12}$$

Analogously for the hexagonal lattice, we have

$$-\sigma_{Hex}(s,t) = \frac{1}{\pi}\left(L(\pi p_a) + L(\pi p_b) + L(\pi p_c)\right), \tag{1.4.13}$$

where p_a, p_b, p_c are asymptotic probabilities of the three types of lozenges on torus, and satisfy the system

$$\begin{aligned} &p_a + p_b + p_c = 1,\\ &p_a = s,\\ &p_b = t. \end{aligned} \tag{1.4.14}$$

1.5 The presentation of results

1.5.1 A variational principle for multiply-connected domains

In the Chapter 2, we are interested in asymptotic behavior of domino tilings of a multiply-connected domain. The result of [CKP00] does not apply to discretization Γ_N of a multiply-connected domain Ω, see Figure 1.20. The first reason is that $H_D^{\Gamma_N}$ might be a multivalued function. More precisely, when one tries defining it by Definition 2, $H_D^{\Gamma_N}$ may get a non-zero increment (monodromy) after going around a hole in Γ_N, see Figure 1.19. Moreover, the boundary values for the height function are no longer fixed, and, in fact, may depend on D. More precisely, it means that boundary height functions B_{D_1} and B_{D_2} may differ by a multiple of four on a connected boundary component. Thus, boundary conditions a priori do not converge to a continuous function $\mathfrak{b}$. Therefore, the variational problem may be ill-defined.

In the work [Kuc21] we study random domino tilings of a multiply-connected domain. It is known height function H_D is well-defined only as a function on universal cover of a region, see discussion of height functions on torus in [KOS06], and on more general

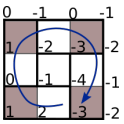

Figure 1.19: Domino tiling D of the ring with multivalued height function (the square in the center is not a part of Γ)

surfaces in [CR08]. We work with the height function H_D^Γ defined this way, as functions $H_D : \tilde{\Gamma} \mapsto \mathbb{Z}$ defined on the universal cover of Γ. Our result shows that as Γ_N with mesh $1/N$ approximates Ω, these functions still converge after appropriate scaling to a deterministic limit $\mathfrak{h}^\star : \tilde{\Omega} \mapsto \mathbb{R}$, which is defined on a universal cover of Ω. The limiting function $\mathfrak{h}^\star$ turns out to be the solution of a variational problem in the spirit of the work by H.Cohn, R.Kenyon and J.Propp, but again, this variational problem gets two extra twists due to the following facts:

- the space $\tilde{\Omega}$ is not compact; the space of optimization of the variational problem is not compact;
- the boundary condition of $\mathfrak{h}^\star$ is the solution of the variational problem for functional $\mathcal{F}$.

Our theorem is the following, recall the surface tension functional $\mathcal{F}_{\mathbb{Z}^2}(h) = \int_\Omega \sigma(\frac{\partial h}{\partial x}, \frac{\partial h}{\partial y})dxdy$,

Theorem 1.5.1 ([Kuc21])**.** *Suppose Γ_N is a sequence of lattice region that approximates a multiply-connected domain Ω. Then,*

$$\lim_{N\to\infty} N^{-2} \log Z(\Gamma_N) = -\mathcal{F}_{\mathbb{Z}^2}(\mathfrak{h}^\star) \tag{1.5.1}$$

and $\frac{1}{N} H^{\Gamma_N} \to \mathfrak{h}^\star$ in probability in ∞-norm topology as $N \to \infty$.

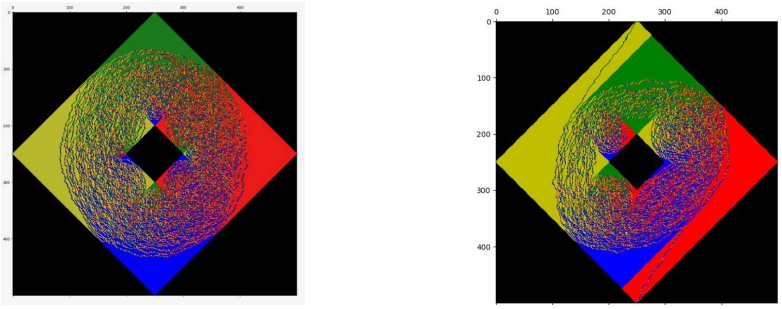

Figure 1.20: Simulation of random domino tilings of multiply-connected versions of the Aztec diamond, Aztec diamond AD_N with removed Aztec diamond $AD_{N/4}$ at the center; monodromy-free version on the left and with monodromy $N/2$ on the right.

One extra corollary of Theorem 1.5.1 is an extension of the arctic circle theorem for multiply-connected domains. In a recent work [ADPZ20] the authors studied a similar variational problem to the one we have, but without connection to dominoes. They were able to prove several geometrical properties of $\mathfrak{h}^\star$ such as the Arctic boundary phenomenon for polygonal domains with sides parallel to sides of $\mathcal{N}_G$, a generalization of arctic circle theorem for other domains. The proof works for multiply-connected regions as well upon the assumption of a variational principle there. Therefore, we have the following corollary

Corollary 1.5.1.1. *The arctic curve is a piecewise algebraic curve with a connected component for each connected boundary component of a polygonal domain Ω.*

1.5.2 A variational principle for the dimer model

In Chapter 3, we generalize Theorem 1.5.1 for other lattices. For example, for the hexagonal lattice as on Figure 1.21.

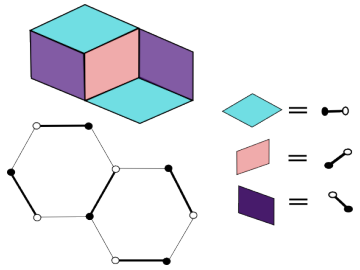

Figure 1.21: Lozenge tilings model and bijection with the dimer model.

Since there is a variational principle for the lozenge tilings of simply-connected domains, also applies to lozenge tilings [CKP00; Ken09]. Therefore, it is reasonable to expect the variational principle for lozenge tilings in multiply-connected domains as well:

Theorem 1.5.2. *Suppose Γ_N is a sequence of lattice regions on the honeycomb lattice that approximates a multiply-connected domain Ω. Then,*

$$\lim_{N\to\infty} N^{-2} \log Z(\Gamma_N) = -\mathcal{F}_{Hex}(\mathfrak{h}^\star) \tag{1.5.2}$$

and $\frac{1}{N} H^{\Gamma_N} \to \mathfrak{h}^\star$ in probability in ∞-norm topology as $N \to \infty$, where

$$\mathcal{F}_{Hex}(h) = \int_\Omega \sigma_{Hex}\left(\frac{\partial h}{\partial x}, \frac{\partial h}{\partial y}\right) dxdy$$

and $\mathfrak{h}^\star$ is the minimizer of $\mathcal{F}_{Hex}$ among the space of Lipschitz functions on Ω with prescribed boundary conditions.

A variational principle for domino (lozenge) tilings can be viewed as a particular case of a variational principle for the generic dimer model.

We use an example of a periodic planar dimer model with an arbitrary fundamental domain and arbitrary periodic weights. Past results for arbitrarily planar domains were done for domino tilings (the fundamental domain correspondent to lattice $\mathbb{Z}^2$ in the dimer model) and weights equal to one [CKP00].

In the work [Kuc17], we prove a generalization of the variational principle from [CKP00] for a generic bipartite periodic lattice Λ instead of $\mathbb{Z}^2$ for a simply-connected region Ω. Here, we prove its generalization for a multiply-connected region Ω.

Theorem 1.5.3. *Suppose $\Gamma_N \in \frac{1}{N}\Lambda$ is a sequence of lattice regions, that approximates a multiply-connected domain with piecewise smooth boundary Ω. Then,*

$$\lim_{N\to\infty} N^{-2} \log Z(\Gamma_N) = -\mathcal{F}_\Lambda(\mathfrak{h}^\star), \tag{1.5.3}$$

where $\mathfrak{h}^\star$ minimizes $\mathcal{F}_\Lambda$ among Lipschitz functions on $\tilde{\Omega}$ with prescribed boundary conditions, and constraint $\nabla\mathfrak{h}(x,y) \in \mathcal{N}_\Lambda$ almost everywhere for the Newton polygon $\mathcal{N}_\Lambda$.

Moreover, $\frac{1}{N} H^{\Gamma_N} \to \mathfrak{h}^\star$ in probability in ∞-norm topology as $N \to \infty$.

This theorem is also applicable to so-called dimer model, particular bipartite lattice with fundamental domain shown on Figure 1.22. Dimer configurations on this lattice are in

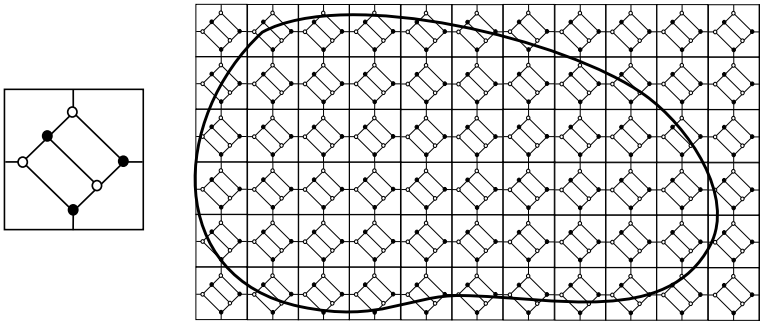

Figure 1.22: Fundamental domain of for dimer city lattice on the left, and approximation Ω_N of region Ω by the dimer city lattice on the right.

bijection with configurations of the six-vertex model at free-fermionic point $\Delta = 0$ [MW73; RS17].

Despite the success and generality of a variational approach, little is known on robust computational methods that determine the arctic curve. One of such methods, developed in [KO05] for a particular case of the honeycomb lattice, involves real algebraic geometry, and reduces the hard analytical problem to a reasonably simple combinatorial task in the so-called tropical limit of the problem. Other methods rely on particular integrable properties, such as a parametrization of domino tilings by family of Young diagrams as in [OR01; Pet12; BK16]. However, extensions of these methods to multiply-connected domains, such as the Aztec diamond with a hole on the right of Figure 1.20, are not known as far as we are aware.

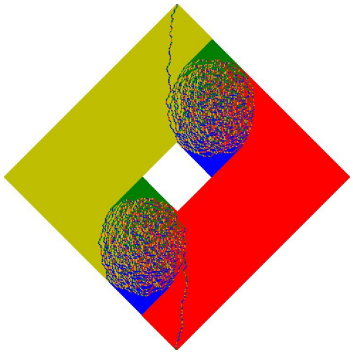

Figure 1.23: Random domino tiling of multiply-connected Aztec diamond with the maximal height change

This domain is defined as the Aztec diamond of size N with a removed Aztec diamond of size $N/4$ in the center supposing that $N/4 \in \mathbb{Z}$. First on all, one can add two defects on the inner and outer connected boundary components so that height function gets monodromy after a turn around the center. Therefore, we deal with a one-parameter family of domains parametrized by monodromy of the height function, or in other words the size of the defects. These modifications create a random path visible on the left of Figure 1.20. Further, random boundary conditions result in emergence of a new parameter of domino tilings, height change, which is equal to the difference between values of the height function between points of the inner boundary, and the outer boundary. While, Theorem 1.5.1 guarantees a law of large numbers for the height change R_N, our computer simulations show that the resulting arctic curve depends on R_N as on a modular parameter, see Figure 1.23 in comparison with the right fig. on Figure 1.20. Furthermore, there are two different regimes, for the

maximal (resp.minimal) height change the arctic curve consists of two independent circles as on Figure 1.23, while for a typical value of R_N the curve forms an inner curve, and an outer one as on Figure 1.20

1.5.3 The tangent plane method

The Chapter 4 is devoted to a new method of computation of arctic curves, the tangent plane method [KP22; KP24].

The method is based on results on generic analytic properties of the limit shape $\mathfrak{h}^\star$ in [ADPZ20]. In the work [KP22], R. Kenyon and I. Prause propose the *tangent plane method*.

Since the surface tension σ is strictly convex in the interior of the Newton polygon $\mathcal{N}$, (which, we recall, is the set of allowed slopes $(s,t) := \nabla\mathfrak{h}$) by [KOS06, Corollary 3.7]. Thus, it defines a non-degenerate metric g on $\mathcal{N}$, let s,t be coordinates on $\mathcal{N}$.

$$g := \sigma_{s,s}ds^2 + 2\sigma_{s,t}dsdt + \sigma_{t,t}dt^2. \tag{1.5.4}$$

After passing to conformal (isothermal) coordinates $u := U(s,t) + iV(s,t)$, the metric writes as $g = e^{\Phi}(dU^2 + dV^2)$ for a function $\Phi = \Phi(s,t)$. Such coordinate is determined by the *Beltrami equation* [Spi79], we give a proof of it in Appendix 4.3.3. Moreover, Beltrami equation for lozenge tilings is equivalent to the complex Burger's equation studied in [KO05] and differential du determines a complex structure on $\mathcal{L}$, also known as the *intrinsic complex structure*.

In [KP22], the authors introduce a function $c(u) := \mathfrak{h}(u) - s(u)x(u) - t(u)y(u)$ called the *intercept* on the liquid region $\mathcal{L}$.

This function allows us to parametrize the planes tangent to the graph of the limit shape in $\mathbb{R}^3$ over a given point $(x_0, y_0) \in \Omega$,

$$\mathcal{P}_{x_0,y_0} = \{(x,y,z) \in \mathbb{R}^3 | \{s(x_0,y_0)x + t(x_0,y_0)y + c(x_0,y_0) = z\}. \tag{1.5.5}$$

Then, if we know three functions s,t and c, we can recover the limit shape as the envelope of its tangent planes. The key observation of the paper is that there is a particular choice of a coordinate u on $\mathcal{L}$ such that s,t and c are harmonic functions of u by Theorem 3.1 [KP22]. Further, they have a piecewise constant boundary conditions, which makes it possible to perform explicit harmonic extension to the bulk. The arctic curve is determined from the following complex equation in u (see (20) in [KP22]),

$$s_u x + t_u y + c_u = 0. \tag{1.5.6}$$

This equation can be viewed as a system of two equations, for the real part, and the imaginary one. In particular, we know the limit shape through its slopes $s(x,y), t(x,y)$. The arctic curve can be found as the boundary of a domain of definition of u. Functions $s(u), t(u)$ does not depend on the boundary conditions, and are determined by σ and $\mathcal{N}$ only. Thus, the limit shape is parametrized by a harmonic function c.

In Chapter 4, we compute the limit shape for the Aztec diamond with a hole from Figure 1.20.

The of the key ingredients of this problem are elliptic functions. Both $s(u), t(u)$ and $c(u)$ viewed as functions on $\tilde{\Omega}$ are periodic with respect to shifts, and expressed in terms of Weierstrass σ functions. Those expressions allow expressing the limit shape $\mathfrak{h}^\star(u)$ in the intrinsic coordinate u as $\mathfrak{h}^\star = x(u)s(u) + y(u)t(u) + c(u)$, where $x(u)$ and $y(u)$ are found from the system (4.2.8). (1.5.5)

However, the program is not totally complete: our harmonic extension have several parameters that need to be fixed by the geometry of the problem. We discuss the condition

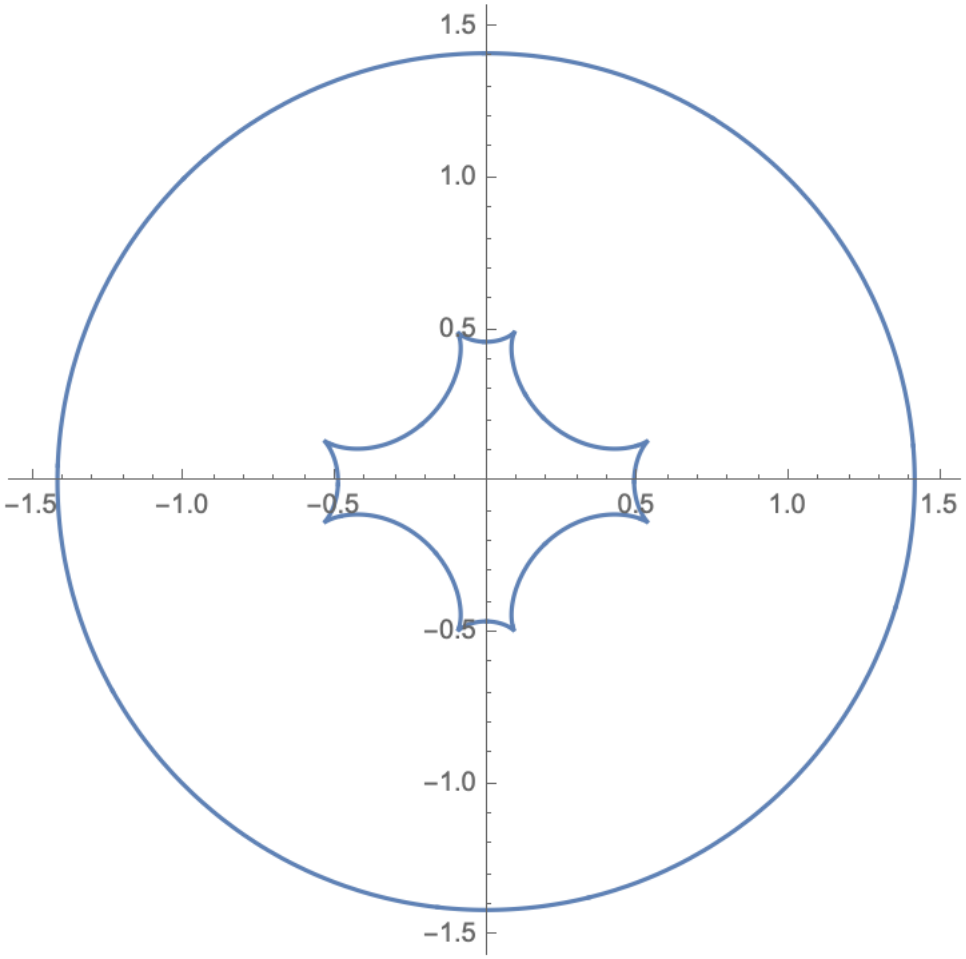

Figure 1.24: Limit shape for unconstrained case.

that one can probably use is to do it in Chapter 4. We also found a one parameter family of the limit shapes for the Aztec diamond with a hole with the parameter r, which is responsible for the relative height between two connected boundary components, i.e., the height of the hole.

We also computed the frozen curve with different size of the torus, i.e., dependence on the elliptic parameter τ in Figure 4.22, which were taken to be $\tau = i$ in the figures above.

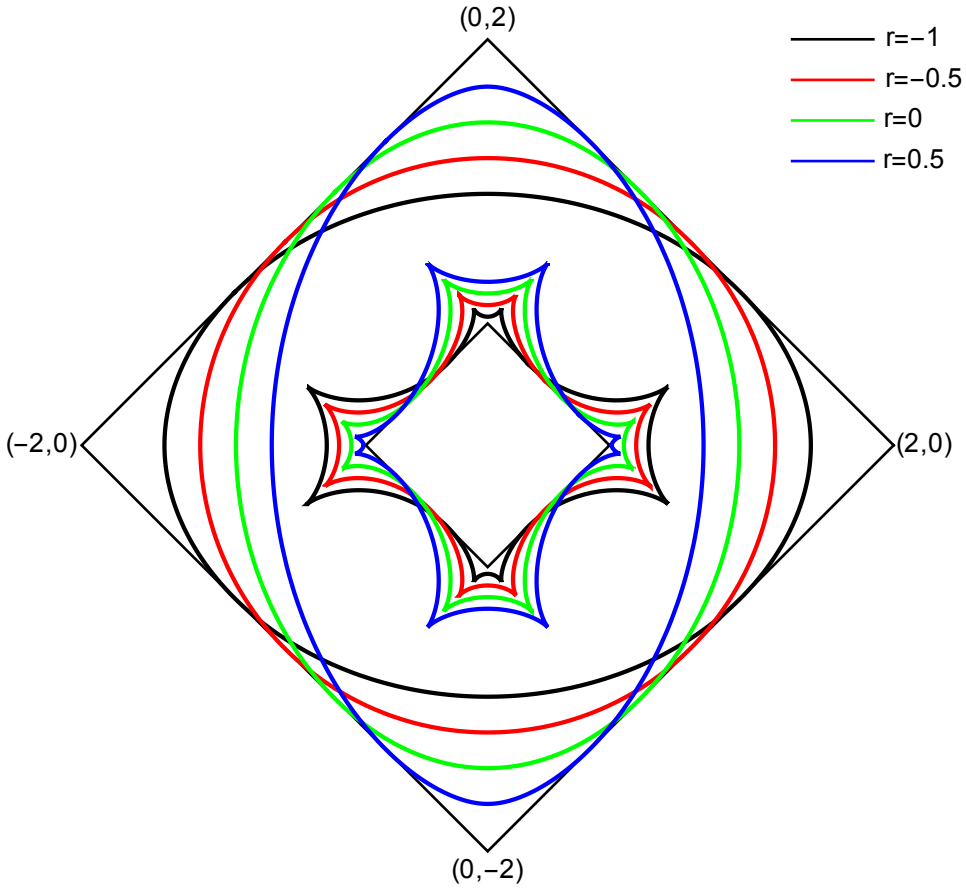

Figure 1.25: One parameter family of limit shapes indexed by r.

Chapter 2

A variational principle for domino tilings of multiply-connected domains

Abstract

We study uniformly random domino tilings of a multiply-connected domain with a multivalued height function according to the usual definition. We consider it as a function on the universal covering space of the domain that makes it a well-defined function. It allows us to prove that as the domain grows, normalized height functions converge in probability to a deterministic continuous function in two regimes. The first regime covers all domino tilings of the domain, for which we also prove a convergence in probability of the height change. In the second regime, we consider domino tilings with a given height change R_N that converges to a fixed asymptotic height change r.

2.1 Introduction

Counting the number of domino tilings of a region such as the chess board is a classical problem in combinatorics. However, how does a *typical domino tiling of a given region look like*? The first attempt answering this question for a simply-connected region is given by the variational principle in [CKP00]. The authors encode a domino tiling D by the *height function* H_D, and show that, after appropriate scaling, the height function of a typical domino tiling is close to a solution of the variational problem. However, for a multiply-connected region this description typically fails, and H_D is a multivalued function. The goal of this paper is to define the height function on a multiply-connected domain, and extend the variational principle for domino tilings of a multiply-connected domain.

Figure 2.1: The same domino tiling of Aztec diamond AD_4 with two graphical representations and four types of dominoes w.r.t. their orientation.

Historically, one of the first such theorems regarding the law of large numbers for geometrical objects coming from combinatorics is the famous Vershik–Kerov–Logan–Shepp limit shape for the Young diagrams [VK77; LS77]. After that, there began a widespread

development in the area starting with the Arctic Circle Theorem in [JPS98]. The authors analyzed typical domino tilings of a growing sequence of lattice domains, so-called Aztec diamonds AD_N(see Figure 2.1). It was shown that for large N, a uniformly random domino tiling of AD_N forms two kinds of regions separated by the circle inscribed to the normalized domain, the unit square rotated by 45°. Statistics of dominoes in the inner region remains non-trivial in the limit as $N \to \infty$, all four types of dominoes w.r.t. their orientation have a positive density. However, regions outside the circle exhibit a deterministic statistics, each of them is tiled by a fixed type of domino.

Soon after, H.Cohn, R.Kenyon and J.Propp proved that this phenomenon holds for a generic simply-connected domain in [CKP00]. Let us give a glance on their main theorem with necessary details.

Let $\Gamma \subset \mathbb{Z}^2$ be a finite, connected region with a fixed chessboard coloring, and viewed as a subset of $\mathbb{R}^2$ consisting of unit squares of $\mathbb{Z}^2$ with set of vertices $V(\Gamma)$. A domino tiling of Γ is a covering of it without gaps or overlaps with dominoes (i.e., 1×2 or 2×1 rectangles) We call a region Γ tileable if it admits a domino tiling. Equip the set of domino tilings of Γ with the uniform measure $\mathbb{P}^\Gamma$. Then, define the boundary of Γ, $\partial\Gamma := \{p \in \Gamma | p \sim \mathbb{Z}^2 \setminus \Gamma\}$, where $\sim$ means graph adjacency on $\mathbb{Z}^2$.

The main technical tool used in [CKP00] is an encoding of a domino tiling D by a height function, $H_D : V(\Gamma) \to \mathbb{Z}$ called *the height function*. Its value is fixed at a reference vertex p_0 by $H_D(p_0) = 0$, and the value $H(p)$ is given by the integral of a natural flow associated to the domino tiling D via The Local rule , for details see Definition 2. Moreover, it turns out that in a simply-connected region, a height function H_D is fixed on the boundary $\partial\Gamma$ and does not depend on a domino tiling.

Then, the authors of [CKP00] consider a sequence of lattice domains $\Gamma_N \subset \frac{1}{N}\mathbb{Z}^2$ that approximates a connected, simply-connected compact set $\Omega \subset \mathbb{R}^2$. Furthermore, it is assumed that the boundary condition $B_N := H_D|_{\partial\Gamma_N}$ after normalization by N^{-1} converges to a deterministic continuous Lipschitz function $\mathfrak{b} : \partial\Omega \to \mathbb{R}$.

Now, let $\mathfrak{h}^\star$ be the unique minimizer over space of Lipschitz functions with boundary condition $\mathfrak{b}$ of *the surface tension functional* $\mathcal{F} : \mathfrak{h} \mapsto \iint_\Omega \sigma_{\mathbb{Z}^2}(\partial_x\mathfrak{h}, \partial_y\mathfrak{h})dxdy$, which we postpone defining until Section 2.5.3. The main theorem of [CKP00] states that the normalized logarithm of the number of domino tilings of Γ_N with a boundary condition B_N, $Z(\Gamma_N, B_N)$, has the following asymptotic behavior as $N \to \infty$.

Theorem 2.1.1 (Cohn Kenyon Propp)**.**

$$N^{-2} \log Z(\Gamma_N, B_N) \xrightarrow{N\to\infty} -\mathcal{F}(\mathfrak{h}^\star). \tag{2.1.1}$$

Furthermore, the normalized height functions $\frac{1}{N}H^{\Gamma_N}$ *converge uniformly in probability to* $\mathfrak{h}^\star$ *as* $N \to \infty$, $\mathbb{P}^{\Gamma_N}\left(|H^{\Gamma_N} - \mathfrak{h}^\star| > \varepsilon\right) \to 0$

However, this theorem does not cover domino tilings of a multiply-connected domain such as the modified Aztec diamond, see Figure 2.2 and Section 2.9.3. The first reason is that a height function H_D defined by The Local rule becomes a multivalued function as one sees by applying it consequently along a non-trivial loop, for instance for annulus from fig 2.3 one gets an extra factor of 4 after each such turn. This gain is the monodromy$M(\delta)$ of a loop $\delta \in \pi_1(\Omega)$, see Figure 2.3. The monodromy $M(\delta)$ is fixed by the domain and δ for all domino tilings.

The second reason is that in a multiply-connected domain, the boundary condition B usually depends on D, see Figure 2.3 and Figure 2.7. More precisely, it means that restrictions of two height functions to $\partial\Gamma$ may differ by a multiple of 4. For instance, it happens for two domino tilings of the region from Figure 2.7. Thus, boundary conditions a

priori do not converge to a continuous function $\mathfrak{h}$. Therefore, the variational problem may be ill-defined.

Despite these difficulties, several results on domino tilings of multiply-connected domains exist. We make a review of these works in Final remarks.

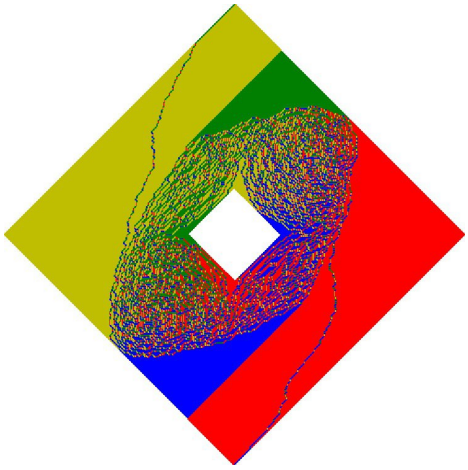

Figure 2.2: Computer simulation of a random domino tiling of $\mathcal{AD}_{500}$ with height change $R = 300$ and monodromy $M = 400$. For further details, see Section 2.9.3.

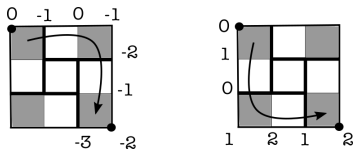

Figure 2.3: Height function $H(p, \gamma)$ and $H(p, \gamma')$ with $M(\gamma'\gamma^{-1}) = 4$, for details see Definition 2.

We formulate a generalization of Theorem 2.1.1 for a multiply-connected domain in Theorem 2.1.2. To the best of our knowledge, it is the first generic result for random domino tilings of a multiply-connected domain that works with a height function with a monodromy.

(2) Instead of defining the height function by The Local Rule, we modify it so that it depends not only on the point $p \in \Gamma$, but also on a path $\gamma_{p_0 \mapsto p}$ from a fixed reference point p_0 to p. This dependence keeps track of the topology and makes the height function a well-defined function. After going around a hole, not only the value of the height function changes, but also the path in the argument. It means the following, suppose that $\delta_{p \mapsto p}$ is the loop around a hole, then we call the transformation $H(p, \gamma_{p_0 \mapsto p}) \mapsto H(p, \delta_{p \mapsto p} \circ \gamma_{p_0 \mapsto p})$ turning around the hole. Or in other words, we apply the local rule consecutively along $\delta_{p \mapsto p}$.

This situation is very similar to the definition of the complex logarithm map, for details see discussion in Remark 2.3.3. We also keep track of relative heights between different points on each connected boundary component. Assuming that the value of the height function at the point p_0 is zero, and fixing the set of paths modulo continuous transformation $\{\gamma_{p_0 \mapsto p_i}\}_{i=1}^{g}$, we end up with a collection of numbers $R_D := \{H_D(p_i, \gamma_{p_0 \mapsto p_i})\}_{i=1}^{g}$ that we call the *height change* of domino tiling D. Here, by a continuous transformation of a path $\gamma_{p_0 \mapsto p} : [0, 1] \mapsto \Omega, \gamma_{p_0 \mapsto p}(0) = p_0, \gamma_{p_0 \mapsto p}(1) = p$ we mean another path $\gamma'_{p_0 \mapsto p}$ which is homotopic to $\gamma_{p_0 \mapsto p}$. That is there exists a such continuous map $F(t, s) : [0, 1] \times [0, 1] \to \Gamma$ that $F[t, 0] = \gamma_{p_0 \mapsto p}(t)$ and $F[t, 1] = \gamma'_{p_0 \mapsto p}(t)$.

Define a similar collection of g of real numbers $r = \{r_i\}_{i=1}^{g}$ for a continuous function

$\mathfrak{h}$. That is, fix a set of points of $\partial\Omega$, $\{x_i \in \partial\Omega_i\}$ on each connected boundary component of Ω denoted as $\partial\Omega_i$. We also fix them together with a set of paths $\gamma_{x_0\mapsto x_i}$ with values $\{r_i\} := \{\mathfrak{h}(x_i, \gamma_{x_0\mapsto x_i})\}$, which we call asymptotic height change.

its values at a fixed point x_0, $\mathfrak{h}(x_0, \gamma_{x_0\mapsto})$

on each connected boundary component with the set of paths $\{\gamma_{x_0\mapsto x_i}\}_{i=1}^{g}$ continuous transformation. Before the main theorem, let $\mathfrak{b}$ be an extendable boundary condition on the universal cover of Ω such that there exists such a function $\mathfrak{h} : \tilde{\Omega} \mapsto \mathbb{R}$ that $\mathfrak{h}\big|_{\partial\tilde{\Omega}} = \mathfrak{b}$.

Then, let $\mathfrak{h}^\star$ be the minimizer of $\mathcal{F}$ over the space of Lipschitz functions on $\tilde{\Omega}$ with boundary condition $\mathfrak{b}$ with an arbitrary height change. Our main result is the following,

Theorem 2.1.2. *The normalized logarithm of the number of domino tilings of Γ_N divided by the area of Ω has the following asymptotic behavior as $N \to \infty$,*

$$N^{-2} \log Z(\Gamma_N, B_N) \xrightarrow{N\to\infty} -\mathcal{F}(\mathfrak{h}^\star). \tag{2.1.2}$$

Moreover, $\frac{1}{N} H_D^{\Gamma_N} \xrightarrow{\mathbb{P}_N} \mathfrak{h}^\star$ uniformly in probability, and the normalized height change of domino tilings converge to the height change of $\mathfrak{h}^\star$, $\frac{1}{N} R_N \xrightarrow{\mathbb{P}_N} r^\star$ as $N \to \infty$.

Note that in $Z(\Gamma_N, B_N)$ we count domino tilings with arbitrary height change. The version of this theorem for a fixed asymptotic height change r also holds, see Corollary 2.6.2. Furthermore, for a simply-connected Ω we recover Theorem 2.1.1 since $\tilde{\Omega}$ becomes Ω itself, and it has only one connected boundary component on which the height function is fixed. What is important is that for a multiply-connected Ω, $\tilde{\Omega}$ is not a compact space unlike the situation for simply-connected domain.

Structure of the paper

- In Section 2.2 we discuss topological notations: universal cover, fundamental domain of it, and quasiperiodic functions together with analogy between the height function and the complex logarithm map.
- Section 2.3 is devoted to the definition of the height function on universal covering space and the bijection between domino tilings and height functions.
- In Section 2.4 we prove several properties of the height functions: we give a formula for the maximal extension with given boundary height function, criterion of extension of height functions in Proposition 2.4.3, and define the space of asymptotic height functions with a given, and an arbitrary) asymptotic height change. Also, in Theorem 2.4.4 we prove compactness of both spaces. We also prove Theorem 2.4.7, which states that discrete height functions approximate asymptotic height functions and vice versa.
- In Section 2.5 we prove the concentration inequality for the uniform measure on domino tilings of multiply-connected domains in Lemma 2.5.1. Then, and we recall the exact formula for function $\sigma_{\mathbb{Z}^2}$ in (2.5.10).
- In Section 2.6 we state and prove the variational principle for arbitrary height change, Theorem 2.6.1, and for a fixed asymptotic height change, Corollary 2.6.2
- In Section 2.7, we prove existence and uniqueness of the minimizer for the variational problem in Proposition 2.7.1.
- Section 2.8 is devoted to Theorem 2.8.1.
- The last Section 2.9 contains final remarks.

2.2 Topological notation

In this section we recall and fix basic topological notations, which we will use later, for details see [Hat02; DC04; Mei08].

2.2.1 Fundamental domain

First, let Ω be a planar domain, that is a compact subset of $\mathbb{R}^2$ with a piecewise smooth boundary $\partial\Omega$, which consists of $g+1$ connected components, $\partial\Omega = \bigsqcup_{i=0}^{g} \partial\Omega_i$, where $\partial\Omega_0$ is the external boundary.

Recall that the universal covering space $\tilde{\Omega}$ is a simply-connected set, and can be realized as a set of pairs (x, γ_x) of points $x \in \Omega$ with paths γ_x that connect x to a fixed base point $x_0 \in \partial\Omega$. Moreover, one can notice a natural action of fundamental group of Ω on $\tilde{\Omega}$. Recall that having two paths modulo continuous transformations, γ_1 connecting p_1 to p_2 and γ_2 connecting p_2 to p_3, one can obtain a third path $\gamma_3 := \gamma_2 \circ \gamma_1$. This path goes first from p_1 to p_2 and then from p_2 to p_3 called a *concatenation* or *composition* of paths γ_1 with γ_2, which is defined also modulo continuous transformations. If we take $p_2 = p_3$ so that γ_2 is a loop, we obtain an action of $\pi_1(\Omega)$ on points of $\tilde{\Omega}$ that maps a point (p, γ) to $(p, \delta \cdot \gamma)$. Denote the action of $\delta \in \pi_1(\Omega)$ on a subset $\mathcal{A} \subset \tilde{\Omega}$ by $\delta \cdot \mathcal{A}$. It is also worth noting that $\Omega = \tilde{\Omega}/\pi_1(\Omega)$.

Definition of fundamental domain

Let us define a fundamental domain $\mathcal{D}(\Omega)$ as follows,

- $\mathcal{D}(\Omega) \subset \tilde{\Omega}$ is a closed set
- $\tilde{\Omega} = \bigcup_{\delta \in \pi_1(\Omega)} \delta \cdot \mathcal{D}(\Omega)$, where $(\delta_1 \cdot \mathcal{D}(\Omega)) \cap (\delta_2 \cdot \mathcal{D}(\Omega))$ has no interior for $\delta_1 \neq \delta_2$.

Below, we give one realization of $\mathcal{D}(\Omega)$ in Construction 2.2.1 that we use later.

Let us explain the definition of $\mathcal{D}(A)$ on a ring A with a radius 1 of the internal circle and radius 2 of the external circle. It can be seen in polar coordinates as

$$A = \{(\ell \cos\phi, \ell \sin\phi) | \ell \in [1,2], \phi \in \mathbb{R}/2\pi\mathbb{Z}\}, \tag{2.2.1}$$

or as $\{(\ell, \phi) | \ell \in [1,2], \phi \in \mathbb{R}/2\pi\mathbb{Z}\}$ in different coordinates. Then, the universal cover can be seen as

$$\tilde{A} = \{(\ell, \phi) | \ell \in [1,2], \phi \in \mathbb{R}\}. \tag{2.2.2}$$

The corresponding fundamental domain is $\mathcal{D}(A) = \{(\ell, \phi) | \phi \in [0, 2\pi], \ell \in [1,2]\}$. Here the fundamental group $\pi_1(A) \simeq \mathbb{Z}$ acts by shifts $(\ell, \phi) \mapsto (\ell, \phi + 2\pi k), k \in \mathbb{Z}$, where the integer k represents the winding number of a loop. Note that here we have $g = 1$.

Construction of fundamental domain.

The example above can be generalized to a construction of $\mathcal{D}(\Omega)$ for a generic multiply-connected domain Ω. First, pick g smooth curves $\{\gamma_i\}_{i=1}^{g}$ on Ω that connect $\partial\Omega_0$ with all other connected boundary components $\{\partial\Omega_i\}_{i=1}^{g}$ and avoid self-intersections such that after the cut along curves $\{\gamma_i\}_{i=1}^{g}$ the resulting domain $\mathcal{D}_0(\Omega)$ is connected and simply-connected. Also note that $\mathcal{D}_0(\Omega)$ can be naturally viewed as a subset of $\tilde{\Omega}$.

Then, we take the closure of $D_0(\Omega)$ in $\tilde{\Omega}$ and obtain $\mathcal{D}(\Omega) = \overline{\mathcal{D}_0(\Omega)}$. It can be proved that at the end we obtain a fundamental domain, for details, see Section 1.1, 1.3 in [Hat02]. Note that the boundary of a fundamental domain consists of an extra $2g$ boundary pieces in addition to $\partial\Omega$, $\partial\mathcal{D}(\Omega) = \partial\Omega \cup \bigcup_{i=1}^{2g} \upsilon_i$, where υ_i and υ_{i+g} are the result of cutting along γ_i. One can also note that $\partial\mathcal{D}(\Omega)$ has one connected boundary component.

2.2.2 Decomposition of paths

Each path γ_x from x_0 to x can be decomposed after a continuous transformation into a product $\gamma_x = \hat{\delta} \cdot \gamma'_x$ of a path γ'_x conditioned to stay inside $\mathcal{D}(\Omega)$, and a loop $\hat{\delta} \in \pi_1(\Omega)$. It is easy to see that such a path γ'_x is unique modulo continuous transformations after choosing $\mathcal{D}(\Omega)$. Also note that the action of $\delta \in \pi_1(\Omega)$ on $\tilde{\Omega}$ maps $\hat{\delta}$ by multiplying by $\delta : \hat{\delta} \mapsto \delta \cdot \hat{\delta}$, while leaving γ'_x unchanged. This allows us to look at a point of $\tilde{\Omega}$ as a pair $(\hat{x}, \delta)$ of a point $x \in \mathcal{D}(\Omega)$ and a loop $\hat{\delta}$, which is changing after going around a loop δ' as $(x, \hat{\delta}) \mapsto (x, \delta' \cdot \hat{\delta})$. Also, it is worth comparing with Definition 2.2.1.

2.2.3 Quasiperiodic functions

Throughout the paper, all functions on $\tilde{\Omega}$ are assumed to be *quasi-periodic*. These functions are similar to the complex logarithm map, which is almost a well-defined map, but it gets the increment $2\pi i$ after one turn around zero in counter-clockwise direction.

Suppose that we have a monodromy map $\mathfrak{m}$, that is a map $\mathfrak{m} : \pi_1(\Omega) \to \mathbb{R}$ that $\mathfrak{m}(\delta' \cdot \delta) = \mathfrak{m}(\delta') + \mathfrak{m}(\delta)$. Then, $f : \tilde{\Omega} \to \mathbb{R}$ is a quasiperiodic function with monodromy $\mathfrak{m}$ if after going along a loop δ on Ω, it changes as

$$f(x, \delta \cdot \hat{\delta}) = f(x, \hat{\delta}) + \mathfrak{m}(\delta), \tag{2.2.3}$$

or in other words upon substitution $\delta = \delta' \cdot \hat{\delta}^{-1}$,

$$f(x, \hat{\delta}) = f(x, \hat{\delta}') - \mathfrak{m}(\delta'_x \cdot \hat{\delta}^{-1}). \tag{2.2.4}$$

The monodromy $\mathfrak{m}$ keeps track of the possible ambiguity of f after going along a loop. Denote the space of quasiperiodic functions for a given monodromy $\mathfrak{m}$ by $\mathcal{H}(\Omega, \mathfrak{m})$.

Two examples of quasiperiodic functions are the complex logarithm map $\log z$ defined on a punctured complex plane (for details see Subsection 2.3.3), and the function $(\phi, \ell) \mapsto \phi + \ell \cos \phi$ defined on the ring A from Example 2.2.1. Since $\pi_1(A) \simeq \mathbb{Z}$, each $\hat{\delta}$ corresponds to an integer, which enumerates "landings of a stairwell" see Figure 2.5.

The action of $\pi_1(\Omega)$ on $\tilde{\Omega}$ naturally extends to an action of $\pi_1(\Omega)$ on quasi-periodic functions on $\mathcal{A} \subset \tilde{\Omega}$. That is, for a quasi-periodic function f and a $\delta \in \pi_1(\Omega)$ define $\delta \cdot f(p, \hat{\delta}) := f(p, \delta \cdot \hat{\delta}) = f(p, \hat{\delta}) + \mathfrak{m}(\delta)$.

Another property of quasi-periodic functions is that the difference between two functions f, f' from $\mathcal{H}(\Omega, \mathfrak{m})$, $f - f'$, is a well-defined function on Ω since $f - f'$ has monodromy 0.

Lemma 2.2.1. *Suppose $f, f' \in \mathcal{H}(\Omega, \mathfrak{m})$. Then, functions defined by $x \mapsto f(x) - f'(x)$ and $x \mapsto \nabla f(x)$ are well-defined as functions on Ω.*

Proof. Indeed, f and f' gain the same increment $\mathfrak{m}(\delta)$ going around the loop δ, therefore $f - f'$ has the trivial monodromy, and thus, it is a well-defined function on Ω. Moreover, if f is differentiable, then its gradient by definition is also a well-defined map on Ω. □

Remark 1. Since the gradient of continuous(discrete) height function is a well-defined map, we could in principle formulate all the statements in the language of continuous/discrete gradients. Discrete gradients parametrize domino tilings without any ambiguity as naively defined height functions. Probably, this is a possible alternative to our approach. However, it would require a more sophisticated technique i.e., topology of the space of continuous gradients as in a recent work[CSW23].

An important fact about quasiperiodic functions is that their behavior is determined by their values on $\mathcal{D}(\Omega)$. It can be formulated as the following proposition.

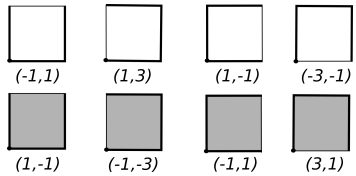

Figure 2.4: Parametrization of domino tilings by the discrete slopes.

Proposition 2.2.2. *Suppose we have two quasi-periodic functions $f, f' \in \mathcal{H}(\Omega, \mathfrak{m})$ that coincide on $\mathcal{D}(\Omega)$. Then, $f = f'$ on $\tilde{\Omega}$.*

Proof. By definition of the fundamental domain, we can express the universal covering space $\tilde{\Omega}$ as the union of fundamental domains,

$$\tilde{\Omega} = \bigcup_{\delta \in \pi_1(\Omega)} \delta \cdot \mathcal{D}(\Omega). \tag{2.2.5}$$

Now, the proof is straightforward, we need to use two facts. The first fact is the assumption that the values of f, f' coincide on $\mathcal{D}(\Omega)$. The second one is that both functions have the same monodromy data $\mathfrak{m}(\delta)$ that gives agreement of their values on $\delta \cdot \mathcal{D}(\Omega)$. □

Proposition 2.2.2 allows recovering a quasi-periodic function f defined on $\tilde{\Omega}$ uniquely from its restriction to $\mathcal{D}(\Omega)$ if we know the monodromy $\mathfrak{m}$.

Call the subspace of functions on $\mathcal{D}(\Omega)$ obtained by restriction of functions from $\mathcal{H}(\Omega, \mathfrak{m})$

$$\mathcal{H}'\left(\mathcal{D}(\Omega), \mathfrak{m}\right) := \{f : f = g\big|_{\mathcal{D}(\Omega)} \text{ for some } g \in \mathcal{H}(\Omega, \mathfrak{m})\}. \tag{2.2.6}$$

Proposition 2.2.3. *Functional spaces $\mathcal{H}'(\mathcal{D}(\Omega), \mathfrak{m})$ and $\mathcal{H}(\Omega, \mathfrak{m})$ are isomorphic with each other. In other words, each function $f' \in \mathcal{H}'(\Omega, \mathfrak{m})$ extends to a function $f \in \mathcal{H}(\Omega, \mathfrak{m})$ uniquely.*

Proof. We have the projection from $\mathcal{H}(\Omega, \mathfrak{m})$ to $\mathcal{H}'(\Omega, \mathfrak{m})$ that is surjective by definition of $\mathcal{H}'(\Omega, \mathfrak{m})$. In order to construct the map in the opposite direction suppose that $\hat{f} := f\big|_{\mathcal{D}(\Omega)}$, so we know the value $\hat{f}(x) = f(x, \mathcal{I})$ for the trivial loop $\mathcal{I}$. Then, $f(x, \delta) = \hat{f}(x, \mathcal{I}) + \mathfrak{m}(\delta \cdot \mathcal{I}) = \hat{f}(x, \mathcal{I}) + \mathfrak{m}(\delta)$. Therefore, once we know that $\hat{f}$ can be extended to a function on $\tilde{\Omega}$ with monodromy $\mathfrak{m}$, we can recover its values on the whole $\tilde{\Omega}$ from the values on $\mathcal{D}(\Omega)$.

□

2.2.4 Boundary condition of quasi-periodic functions.

Let us take a point x_i on a connected boundary component $\partial\tilde{\Omega}_i$ for each $0 \le i \le g$, and let $f \in \mathcal{H}(\Omega, \mathfrak{m})$. Boundary conditions of f is a set of functions $\mathfrak{b}_i : \partial\tilde{\Omega}_i \to \mathbb{R}$ on each connected boundary component, such that $f\big|_{\partial\tilde{\Omega}_i}(x, \delta) - f(x_i, \delta) = \mathfrak{b}_i(x, \delta)$ for $x \in \partial\mathcal{D}(\Omega)_i$. This condition determines f on $\partial\tilde{\Omega}_i$ up to an additive constant that can be fixed by an extra condition $f(x_i, \delta) = r_i$ for an $r_i \in \mathbb{R}$. We also assume that $f(x_0, \mathcal{I}) = 0$

Once we think of f as a surface, the value $r_i := f(x_i, \delta) - f(x_0, \delta)$ represents the relative height of $\partial\tilde{\Omega}_i$ compared to $\partial\tilde{\Omega}_0$. Call $\{r_i\}_{i=1}^g$ the height change. Then, there are two ways to fix the boundary condition of f, the first way is to take $g+1$ functions $\{\mathfrak{b}_i\}_{i=0}^g$ on each connected boundary component $\partial\tilde{\Omega}_i$ and fix $f\big|_{\partial TildeOmega_i}(x, \delta) - f(x_i, \delta) = \mathfrak{b}_i(x, \delta)$. This way we fix f up to an additive shift, denote the space of such quasi-periodic functions on $\tilde{\Omega}$ with monodromy $\mathfrak{m}$ $\mathcal{H}(\Omega, \mathfrak{m}, \{\mathfrak{b}_i\})$. The second option is to further fix value $f(x_i, \mathcal{I}) = r_i$ for $r_i \in \mathbb{R}$, call the space of such functions $\mathcal{H}(\Omega, \mathfrak{m}, \{\mathfrak{b}_i\}, r_i)$.

2.3 Height function on universal covering space of discrete domains

This section is devoted to definitions of height functions and asymptotic height functions.

Our first goal is the definition of the universal cover of a lattice domain. Then, we define the height function and construct a bijection between the set of height functions and the set of domino tilings of a multiply-connected lattice domain Γ.

2.3.1 Universal cover of a lattice domain

Suppose that we have a multiply-connected domain Ω with a lattice domain $\Gamma \subset \Omega$. Let us define the universal cover of Γ denoted by $\tilde{\Gamma}$ as a subset of $\tilde{\Omega}$ as follows. Recall that the expression of the universal cover of Ω, $\tilde{\Omega} = \bigcup_{\delta \in \pi_1(\Omega)} \delta \cdot \mathcal{D}(\Omega)$.

Since Γ is a subset of Ω, define the fundamental lattice domain $\mathcal{D}(\Gamma)$ to be the lattice domain remaining after performing the cuts γ_i from construction 2.2.1, where the cuts are continuously changed so that a path γ_i consists of edges of Γ.

Then, we can define the universal cover of a lattice domain Γ denoted by $\tilde{\Gamma}$ similarly to Definition 2.2.1,

$$\tilde{\Gamma} := \bigcup_{\delta \in \pi_1(\Omega)} \delta \cdot \mathcal{D}(\Gamma). \tag{2.3.1}$$

It is easy to see that $\tilde{\Gamma}$ is a subset of $\tilde{\Omega}$.

2.3.2 Height function

First, recall the usual definition of the height function for a simply-connected domain Γ. Define the boundary of Γ, $\partial\Gamma := \{p \in \Gamma | p \sim \mathbb{Z}^2 \setminus \Gamma\}$, where $\sim$ means graph adjacency on $\mathbb{Z}^2$. Later we will assume that Γ approximate a continuous domain Ω, so that $\partial\Gamma$ will approximate $\partial\Gamma$.

The height function is defined by *the Local Rule* as follows.

Definition 2.3.1. A function $H_D : V(\Gamma) \to \mathbb{Z}$ is called a height function if for a fixed $p_0 \in \partial\Gamma$ the following holds,

1. Set the value of $H_D(p_0) := 0$ for all D and a fixed point $p_0 \in \partial\Gamma$.
2. If the edge $v := (p_1, p_2)$ has a black square on its left, then $H_D(p_2)$ equals $H_D^\Gamma(p_1) + 1$ if v does not cross a domino in D and $H_D(p_1) - 3$ otherwise.

By [Thu90], H_D is a well-defined for a simply-connected Γ. However, in a multiply-connected region, H_D might get a non-zero increment going along a loop around a hole, see Figure 2.3. Therefore, we need to modify this definition so that it will be still a well-defined map.

Let us give an intrinsic definition of the height function H^Γ defined on a connected, multiply-connected lattice domain Γ. Here we follow our conventions from Subsection 2.2.3.

We pick once point $p_i \in \Gamma$ on each connected boundary component $\partial\Gamma_i$, where $\partial\Gamma_0$ is the external connected boundary component of Γ. Fix also a set of paths $\{\gamma_i'\}_{i=1}^g$ from p_0 to each p_i and a path γ from p_0 to a point $p \in \Gamma$.

Also, let $\{R_i\}_{i=0}^g$ be a collection of integers with $R_0 = 0$.

Let us mark a single edge on every lattice square of Γ. We assume that this edge is not a boundary edge. And suppose that M^Γ is a monodromy, that is $M^\Gamma : \pi_1(\Omega) \to 4\mathbb{Z}$ and satisfies $M^\Gamma(\delta \cdot \delta') = M^\Gamma(\delta) + M^\Gamma(\delta')$. Let us proceed to definitions of height function and its boundary condition,

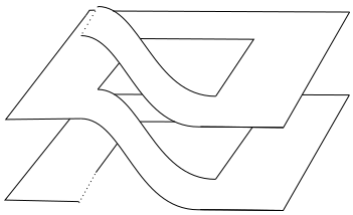

Figure 2.5: "Riemannian Surface" of a ring.

Definition 2.3.2. Call a family of integer functions $B_i^\Gamma : \partial\tilde{\Gamma}_i \to \mathbb{Z}$ the boundary heights if they satisfy the following conditions

- the value of B_i^Γ increases by 1 counterclockwise along the edges of any black square except the marked edge on it.
- the value of B_i^Γ increases by 1 clockwise along all edges of any white square except the marked edge on it.
- going along a loop $\delta_i \in \pi_1(\Omega)$ $B_i^\Gamma(v, \delta_v)$ changes as follows:

$$B_i^\Gamma(v, \delta_i \cdot \delta) = B_i(v, \delta) + M^\Gamma(\delta_i). \tag{2.3.2}$$

Then, we can define the height function with given boundary heights.

Definition 2.3.3. A function $H^\Gamma : \tilde{\Gamma} \to \mathbb{Z}$ is a height function with monodromy M, set of reference points $\{p_i\}_{i=0}^g$, boundary heights B_i and height change $\{R_i\}_{i=0}^g$ if the following holds,

- $H\big|_{\partial\Gamma_i}(p, \delta) - H(p_i, \delta) = B_i(p, \delta)$ for $p \in \partial\tilde{\Gamma}_i$.
- $H(p_i, \gamma_i') = R_i$.
- the value of H increases by 1 counterclockwise along all edges of any black square except the marked edge on it.
- the value of H increases by 1 clockwise along all edges of any white square except the marked edge on it.
- going along a loop $\delta \in \pi_1(\Omega)$ $H(v, \delta_v)$ changes as follows:

$$H(v, \delta \cdot \delta_v) = H(v, \delta_v) + M^\Gamma(\delta). \tag{2.3.3}$$

We think of a marked edge as a dual object to a domino, in other words to a dimer. In fact, the marked edge cuts a domino into two unit squares. Thus, a boundary of a domino is formed by non-marked edges (edges with increment ± 1).

Note that a different choice of points $\{p_i\}_{i=1}^g$ changes $\{R_i\}_{i=1}^g$ by an additive shift. For instance, if we change a point x_i to an adjacent point $p_i' \in \partial\Gamma$, the height change component R_i will change by ± 1 depending on the value $H(p_i')$.

The height function defined this way on the ring is, in fact, a well-defined function only on the corresponding "Riemannian surface" that can be schematically viewed on Figure 2.5.

2.3.3 Analogy with complex analysis

In order to fully grasp the definition of the height function on a multiply-connected domain, it is useful to keep in mind the definition of $\log z$ for complex z through the analytic continuation along a path. Recall that one can define $\log z$ for $z \in \mathbb{C} \setminus \{0\}$ by fixing the value $\log(1) = 0$, and then by the direct analytic continuation along a path γ that connects point 1 with point z via $\log_\gamma(z) = \int_\gamma \frac{d\zeta}{\zeta}$. However, two such logarithms $\log_\gamma z$ and $\log_{\gamma'} z$ defined this way may differ by an integer multiply of $2\pi i$. Therefore, one needs to choose a cut to make $\log_\gamma(z)$ a single-valued function with a branch-cut with a tradeoff of discontinuity at the branch-cut. There is also a way to make $\log z$ a continuous function defined on the corresponding so-called "Riemann surface" [Lan99]. A point of this surface, known as the universal covering space, can be seen as a pair of a point $z \in \mathbb{C} \setminus \{0\}$ with a path connecting z to point 1 modulo continuous transformations in $\mathbb{C} \setminus 0$.

In Definition 2.3.6 we define the height function H_D of domino tiling D of a ring similarly to $\log z$. In order to choose a branch, we make a cut along $\mathbb{R}_{>0}$ and fix a value of H_D at a point p_0. Then, the residue of $\log_\gamma(z)$ is analogous to monodromy of H_D. Globally, the height function H_D is also a well-defined function only on the corresponding "Riemann surface" $\tilde{A}$. Later on, we generalize this setup to a more complicated domain.

In the following discussion, by a path we mean an oriented lattice path on $\mathbb{Z}^2$, that is a sequence of oriented edges. Let also γ, γ' be two paths modulo continuous transformations that connect point p_0 with point p. Note in mind that $\gamma^{-1}\gamma'$ is a loop. Also recall that I is the constant map of the point p_0 to itself. See a summary of this analogy between H and $\log_\gamma$ in Table 2.1.

$\log_\gamma z$	$H_D(p, \gamma)$
Residue of $\frac{1}{z}$ at $z = 0$	Monodromy of H
$\log_I(1) = 0$	$H_D(p_0, I) = 0$
$\log_\gamma(z) = \int_\gamma \frac{d\zeta}{\zeta}$	The Local rule
$\log_\gamma z = \log_{\gamma'} z + \int_{\gamma^{-1}\gamma'} \frac{d\zeta}{\zeta}$	$H_D(p, \gamma) = H_D(p, \gamma') + M(\gamma^{-1}\gamma')$
Branch-cut along $\mathbb{R}_{>0}$	Branch-cut along path connecting different connected boundary components.

Table 2.1: Analogy between height function $H_D(p, \gamma)$ and $\log_\gamma z$

Let us show correctness of the definition of height function H. That is increments of H along any two paths γ, γ' with the same starting point p and ending point p' coincide once the paths can be continuously transformed one into the other.

Lemma 2.3.4. *The increment of H along the path γ equals to its increment along the path γ' if these paths can be continuously transformed one into another.*

$$H(p', \gamma) = H(p', \gamma') \tag{2.3.4}$$

Proof. It is an easy exercise on topology to show that a lattice domain $\Gamma_\gamma^{\gamma'}$ obtained between γ and γ' is simply-connected, for details see Chapter 1 in [Hat02]. Therefore, the height function on $\Gamma_\gamma^{\gamma'}$ is well-defined. Thus, the value of H at p' can be computed along both paths with the same result. □

Monodromy $M^\Gamma(\delta)$ is, in fact, fixed by $\partial\Gamma$ and one can write a formula for it along a single loop δ.

Let e be an edge of Γ and define Δ_e to be $+1$ if e has black square on its left and -1 otherwise. A single loop γ divides $\mathbb{Z}^2$ into two connected components, Γ', the finite component, and Γ'', the infinite component. Denote the number of black squares in Γ' by $\mathcal{B}(\Gamma')$ and the number of white square in Γ' by $\mathcal{W}(\Gamma')$.

Lemma 2.3.5. *The monodromy $M(\delta)$ of a height function H on a lattice domain Γ does not depend on H, and it can be computed by the following formula,*

$$M(\delta) = \sum_{e \in \delta} \Delta_e = \mathcal{B}(\Gamma') - \mathcal{W}(\Gamma'). \tag{2.3.5}$$

Proof. The loop δ can be continuously shrunk to the connected boundary component $\partial\Gamma'$. The increment of H going along $\partial\Gamma'$ can be computed using The Local Rule, and, since there are no marked edges on $\partial\Gamma'$, the value of H changes by $\Delta_e = \pm 1$ only. Therefore, the monodromy can be written as follows,

$$M(\delta) = \sum_{e \in \partial\Gamma'} \Delta_e. \tag{2.3.6}$$

The monodromy $M(\delta)$ divided by 4 equals to the difference between $\mathcal{B}(\Gamma')$ and $\mathcal{W}(\Gamma')$.

$$M(\delta) = \sum_{e \in \partial\Gamma'} \Delta_e = 4\left(\mathcal{B}(\Gamma') - \mathcal{W}(\Gamma')\right) \tag{2.3.7}$$

This formula follows from the Stokes theorem applied to the height function, see section 2 in [Ken09] and [Thu90]. □

The formula from xtends to an arbitrary loop as follows. Suppose we have a loop $\delta \in \pi_1(\Omega)$ and a set of generators of $\pi_1(\Omega)), \{\alpha_i\}_{i=1}$. The loop δ can be decomposed into generators, $\delta = \prod_{i=1} \alpha_i^{a_i}$. From (2.3.7), we have a formula for monodromy around each α_i. Suppose without loss of generality that α_i can be continuously shrunk to $\partial\Gamma_i$. Then, we can express the monodromy $M(\delta)$ as follows,

$$M(\delta) = M\left(\prod_{i=1} \alpha_i^{a_i}\right) = \sum_{i=1} a_i \cdot M(\alpha_i) = \sum_{i=1} a_i \cdot M(\partial\Gamma_i) = 4\sum_{i=1} a_i \cdot (\mathcal{B}(\Gamma_i') - \mathcal{W}(\Gamma_i')). \tag{2.3.8}$$

2.3.4 Height function of a domino tiling

A typical example of a height function can be obtained starting with a domino tiling D. We modify the usual definition of the height function corresponding to a domino tilling from [Thu90; CKP00; Fou96] such that it becomes a well-defined function for a domino tiling of a multiply-connected domain.

Definition 2.3.6. Let D be a domino tiling of a multiply-connected lattice domain Γ. Then, $H_D : \Gamma \to \mathbb{Z}$ is a height function of a domino tiling D if it satisfies the following properties.

- Fix the value of H_D at (p_i, γ_i), $H_D(p_i, \gamma_i) = R_i$.
- if an edge (p, v), does not belong to any domino in D (i.e. intersects) then $H_D(v, \gamma) = H_D(p, \gamma) + 1$ if (p, v) has a black square on the left, and $H_D(v, \gamma) = H_D(p, \gamma) - 3$ otherwise.
- going along a loop $\delta \in \pi_1(\Omega, p_0)$ $H_D(v, \gamma)$ changes as follows:

$$H_D(v, \delta\gamma_v) = H_D(v, \gamma_v) + M(\delta). \tag{2.3.9}$$

Now we are ready to give a proof of the following theorem,

Theorem 2.3.7. *There is a bijection between the set of height functions on* Γ *and domino tilings of it.*

Proof. The height function of a domino tiling defined Defenition 2.3.6 obviously satisfies conditions of Definition 2.3.3, the marked edges are the edges that cross the dominoes.

In the other direction we need to assign a domino tiling to a height function H. Note that H changes by -3 counterclockwise along the marked edge of $\mathcal{S}_b$, which is because there are three non-marked edges of $\mathcal{S}_b$ with increments $+1$. Therefore, there exists a unique edge on every lattice square with increment 3. Moreover, each marked edge is, automatically, the marked edge of two adjacent squares of different colors. Thus, we can declare that the domino covers these two squares. This way we can cover by dominoes all the squares of Γ and obtain a domino tiling.

One can further notice that marked edges are dual to the perfect matching on the dual graph $\Gamma^\star$ in language of the dimer model. □

2.4 Proofs of properties of height functions

We have two kinds of height functions, discrete height functions, which arise from domino tilings, and asymptotic height functions, which are natural limiting objects for sequences of height functions. Both height functions and their continuous counterparts share many properties. Thus, it is worth recalling a basic construction for a usual Lipschitz function f [Val45].

Let M be a metric space with the distance $d(\cdot,\cdot)$. Suppose that $X \subset M$ is a compact subset of M and $f : X \to \mathbb{R}$ is a Lipschitz function. Then, f can be extended to a Lipschitz function on M with the same Lipschitz constant by the following formula:

$$\hat{f}(x) = \min_{y\in X}(f(y) + d(x,y)) \tag{2.4.1}$$

$\hat{f}$ is also the maximal extension of f that is for any extension g of f we have $g \le \hat{f}$.

Let us prove it for the sake of self-completeness,

Proof. We need to show two properties of $\hat{f}$, the Lipschitz property and that $\hat{f}$ agrees with f on X. First, pointwise minimum of Lipschitz functions f_1, f_2 is again a Lipschitz function. Simply, we can express $\hat{(}f) = \min\{f_1, f_2\} = \frac{f_1+f_2-|f_1-f_2|}{2}$ and use that the sum and the difference of Lipschitz functions is again Lipschitz.

Second, let us notice that for any function under the minimum we have $f(x) \le f(y) + d(x,y)$ due to the Lipschitz condition. Therefore, we have $f(x) \le \hat{f}(x)$. The second inequality, $\hat{f}(x) \le f(x)$, holds because for $y = x$, the two functions $f(x)$ and $f(y) + d(x,y)$, coincide with each other. □

For $X = \partial M$ and $X \subset \mathbb{R}^n$ we recover the Kirszbraun theorem for extension of Lipschitz functions in $\mathbb{R}^n$.

Furthermore, one can write a similar formula for the minimal extension,

$$\check{f}(x) := \max_{y\in X}(f(y) + d(x,y)). \tag{2.4.2}$$

For quasiperiodic functions on Ω a similar formula holds, let $f : \partial\tilde{\Omega} \to \mathbb{R}$ be a function with monodromy $\mathfrak{m}$ and $(x,\gamma_x), (y,\gamma_y) \in \mathcal{D}(\Omega)$. Then,

$$\hat{f}(x,\gamma_x) = \inf_{(y,\gamma_y)\in\partial\mathcal{D}(\Omega)}(f(y,\gamma_y) + d((x,\gamma_x),(y,\gamma_y)). \tag{2.4.3}$$

This gives a well-defined map on $\mathcal{D}(\Omega)$ since $\partial\Omega$ is a compact set, and thus the value $\hat{f}(x, \gamma_x)$. Then, we need to check that it also gives a well-defined quasi-periodic function defined on $\tilde{\Omega}$ with the same monodromy data as f. Let us move $\hat{f}(x, \gamma_x)$ around a loop δ. By definition, the expression $f(y, \gamma_x)+d((x, \gamma_x), (y, \gamma_y))$ changes to $f(y, \gamma\cdot\delta)+d((x, \gamma_x), (y, \gamma_y))+\mathfrak{m}(\delta)$ since $d((x, \delta\cdot\gamma_x), (y, \delta\cdot\gamma_y)) = d((x, \gamma_x), (y, \gamma_y))$, and the change is independent of y. Therefore, we have the desired transformation, so $\hat{f}$ is a quasi-periodic function.

2.4.1 Extension of a boundary height function.

In the following discussion, we need functions that satisfy only the second condition of Definition 2.3.6. Let us call them partial height functions. To prove that a partial height function η is an actual height function, we need to check that η has the right boundary conditions. Recall an analog of the Lipschitz condition for height functions from [CEP96]: let Γ be a lattice domain with a height function H defined on it. Let $\beta^\Gamma(p_1, p_2)$ be the length of a minimal path π joining points p_1 and p_2 inside Γ such that every edge of π (oriented from p_1 towards p_2) has a black square on its left. Also, it is not hard to check that $\beta^\Gamma(p_1, p_2)$ satisfy the second condition of Definition 2.3.6 as function of p_1 with a fixed p_2. Thus, $\beta^\Gamma(p_1, p_2)$ is the maximal increment of the height function between p_1 and p_2(β^Γ is only increasing by 1 on the path).

Then, for every two points $p_1, p_2 \in \Gamma$,

$$H(p_1) \le H(p_2) \pm \beta^\Gamma(p_1, p_2) \tag{2.4.4}$$

Let us also set $\beta(p, p) := 0$. Note that this condition implies a constraint for height change of a height function, $-\beta^\Gamma(x_i, x_0) \le R_i \le \beta^\Gamma(x_i, x_0)$.

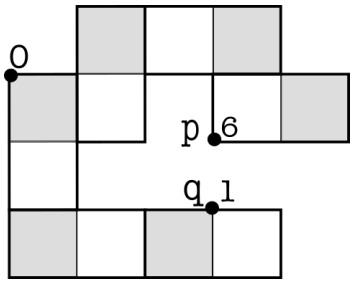

Figure 2.6: Example of a domino tiling of a concave domain, where the height function does not satisfy the Lipschitz condition for points p and q with β defined by (2.4.1).

Call Condition (2.4.9) *the lattice Lipschitz condition*. For points p_1, p_2 at distance d in sup-norm and a convex $\Gamma \subset \mathbb{Z}^2$, $\beta^\Gamma(p_1, p_2) \le 2d(p_1, p_2) + 1$ [CEP96]. Also, one can write an exact expression for $\beta(x, y)$ for such a Γ taken from [Fou96] in the form of lemma 2.1 from [PST16].

Suppose $x = (a, b), y = (a+i, b+j) \in \mathbb{Z}^2$ and set $\kappa(i, j) = i - j \ mod\ 2$. If $a - b = 0 \ mod\ 2$, one sets

$$\beta(x, y) = \begin{cases} 2\|y - x\|_\infty + \kappa(i, j), & \text{if } i \ge j, \\ 2\|y - x\|_\infty - \kappa(i, j), & \text{if } i < j. \end{cases} \tag{2.4.5}$$

If $a - b = 1 \mod 2$, then

$$\beta(x, y) = \begin{cases} 2\|y - x\|_\infty - \kappa(i, j), & \text{if } i \ge j, \\ 2\|y - x\|_\infty + \kappa(i, j), & \text{if } i < j. \end{cases}$$

We need several properties of the height function on a multiply-connected lattice domain that are crucial for the proofs on a simply-connected lattice domain. Let us recall them [PST16], later we extend them to a multiply-connected lattice domain.

These properties are analogous to the basic properties of a usual Lipschitz function. Moreover, we will show that the height function is a discrete analog of the Lipschitz function in a sense that it approximates continuous Lipschitz functions after a suitable normalization on a large lattice domain, see Theorem 2.4.7. In order to show it, we need the following lemma,

Lemma 2.4.1. *Assume that H_D and H' are height functions. Assume also that p is a vertex of Γ. Then, $H(p) = H'(p) \mod 4$*

Proof. By its definition, two height functions coincide at the reference point (p_0, γ_0). Then values at an adjacent point p' may be either H or $H \pm 4$ according to the definition of height function Definition 2.3.6. Or in other words, the discrete gradient of the difference $H - H'$ along any edge always takes its values in $\{-4, 0, 4\}$.

This way we can obtain the proof using induction with respect to the length of a path connecting the point p with the reference point p_0. □

Another important property of the set of height functions is that it has additional operations, which turn this set into a lattice. Namely, we can take pointwise maximum or pointwise minimum of two such functions and obtain another element from this set. For a proof for a simply-connected domain, see discussion in section 1.4 of [CKP00]. Since we use a modified height function, we need to show this property for the functions defined by Definition 2. Suppose that $\{p_i\}_{i=0}^{i=g} \in \partial\Gamma$ points on each connected boundary component of Γ and H and H' are two height functions on Γ with height changes $\{R_i\}_{i=0}^{g}$ and $\{R'_i\}_{i=0}^{g}$. Then,

Lemma 2.4.2. *Pointwise maximum of two height functions H, H' defined on a lattice domain Γ is again a height function $\check{H}$ defined as*

$$\check{H}(p) := \max\{H(p), H'(p)\}. \tag{2.4.6}$$

Further, height change of $\check{H}$ is maximum between height changes of H, H',

$$\check{R}_i = \max\{R_i, R'_i\}. \tag{2.4.7}$$

Proof. We need to show that $\check{H}$ satisfies four conditions from Definition 2. To show the second and the third properties we can use the same arguments as in [CKP00; PST16]. That is supposing that $H(v) \neq H'(v)$ for a point $v \in \Gamma$ (if there is no such a point, it would imply $\check{H} = H = H'$). Then, $H(v)$ must differ from $H'(v)$ by a multiple of 4 by Lemma 2.4.1. Without loss of generality, suppose that $H(v) = H'(v) + 4\ell$ for $\ell \in \mathbb{N}^\star$. Together with the definition of height function, this implies that at all points u adjacent to v, $H(u) \leq H'(u)$. Therefore, $\check{H}$ at points v and u coincides with H. Repeating this argument we obtain the desired.

For the fourth condition note that monodromy of a height function is fixed by the domain by Lemma 2.3.7.

Finally, let us prove the first condition. Note that the height change of $\check{H}$ equals the values of $\check{H}$ at the reference points on the $\partial\Gamma$, $\check{R} = \{\check{R}_i\}_{i=0}^{g} = \check{H}(p_i)_{i=0}^{g}$. These values are maxima between the values of H and H' at reference points. Thus, height change of $\check{H}$ equals to the maximum between height change of H and H', $\check{R}_i = \max\{R_i, R'_i\}$.

Here we assumed that two height functions are defined on $\tilde{Gamma}$ and coincide at the reference point (p_0, γ_0). However, the proof also works with the assumption that they coincide modulo 4 that allows us to use Lemma 2.4.1. Further, monodromies of all height

functions are the same since monodromy is determined by the lattice domain by Lemma 2.3.7.

□

Moreover, the same works for pointwise minimum of the height functions, pointwise minimum of height functions H and H' is, again, the height function, denote it $\tilde{H}$,

$$\tilde{H}(p) = \min\{H(p), H'(p)\}. \tag{2.4.8}$$

Height function on a multiply-connected domain satisfy a refined lattice Lipschitz condition,

$$H(x, \hat{\delta}) - H(y, \delta_y) \leq \beta^{\Gamma}(x, y) + M(\hat{\delta} \cdot \delta_y^{-1}). \tag{2.4.9}$$

This condition can be obtained by applying Condition 2.4.4 to a height function on$\mathcal{C}(\otimes)$. This constraint allows us to formulate a criterion of extension of boundary values to a height function as follows,

Proposition 2.4.3. *Let Γ be a multiply-connected domain with a fixed height function H with monodromy M on a subset $\bar{\Gamma} \subset \Gamma$. And suppose that boundary height function satisfies the following condition for all $x, y \in \partial\Gamma$ and δ, δ',*

$$H(x, \delta) - H(y, \delta') - \pi(x, y) = 0 \mod 4. \tag{2.4.10}$$

Then, H admits an extension to a height function on Γ if there exist a height change $R = \{R_i\}_i = 1^g$ such that two conditions hold all points x, y of $\bar{\Gamma}$,

$$H(x, \hat{\delta}) - H(y, \delta_y) \leq \beta^{\Gamma}(x, y) + M(\hat{\delta} \cdot \delta_y^{-1}) \tag{2.4.11}$$

Proof. Let us take a family of height functions on Γ, $\{\check{H}_y : x \mapsto H(y) + \beta(x, y)\}$ indexed by the points x of $\bar{\Gamma}$. The pointwise minimum of two partial height function from the family is again a partial height function by Lemma 2.4.2 since $\check{H}_y(x)$ satisfies the local rule as a function of x. Then, taking the pointwise minimum over the whole family, we get a height function on Γ

$$H^{\max}(x, \gamma_x) := \min_{y \in \bar{\Gamma}}(H'(y, \gamma_y)) \tag{2.4.12}$$

We need to show that $H^{\max}$ agrees with H on $\bar{\Gamma}$.

Let $x, y, v \in \bar{\Gamma}$, and let us take a function $H'_x : y \mapsto H(y) + \beta^{\Gamma}(x, y)$. It is clear that $H(x) \leq H(y) + \beta^{\Gamma}(x, y)$ holds for every y since it is the lattice Lipschitz condition for H, therefore we have $H(v) \leq H^{\max}(v)$. Inequality $H^{\max}(v) \leq H(v)$ also holds because for $y = x$ we have the equality since $\beta^{\Gamma}(x, x) = 0$.

The height change and monodromy of $H^{\max}$ are given by the boundary condition H.

□

Note that due to (2.4.3) $H^{\max}$ is the maximal extension of H to a height function on Γ. The minimal extension of H can be constructed by almost the same way as the maximal. Let us define the minimal extension H^{min},

$$H^{\min}(x, \gamma) := \max_{y \in \bar{\Gamma}}(H(y, \gamma) - \beta(x, y)). \tag{2.4.13}$$

2.4.2 Asymptotic height function

Here we define an asymptotic height function as a continuous counterpart to the discrete height function. We saw that discrete height functions satisfy the lattice Lipschitz condition. Therefore, it is natural to expect that in a scaling limit they approximate continuous Lipschitz functions. However, as the example on Figure 2.6 suggests we need to consider functions that are 2-Lipschitz in intrinsic sup norm, which can be defined by the following formula

$$\|x-y\|_\infty^\Omega := \inf_\gamma \int_0^1 \|\gamma'(t)\|_\infty \, dt. \tag{2.4.14}$$

Here the curve γ connects x to y by as a path inside Ω, $\gamma(0)=y, \gamma(1)=x$. Moreover, let us use such a path of the minimal length w.r.t. the intrinsic distance on Ω.

Let us note that theorems for the standard sup norm such as Arzela Ascoli theorem and Rademacher's theorem hold for intrinsic norm as well, as one can check using the same arguments as for standard sup norm locally (i.e. by using partition of unity with convex support).

Fix a set of points $\{(x_i,\gamma) \in \mathcal{D}(\Omega) | x_i \in \partial\Omega_i\}$ and a monodromy data, i.e., a map $\mathfrak{m} : \pi_1 \to \mathbb{R}$ such that $\mathfrak{m}(\gamma\cdot\gamma') = \mathfrak{m}(\gamma)+\mathfrak{m}(\gamma')$ and $\mathfrak{m}(\gamma^{-1}) = -\mathfrak{m}(\gamma)$. Also, let $r := \{r_i\}_{i=0}^g$ be a sequence of real numbers and denote point $z=(z_1,z_2)\in\Omega$.

Also define the Newton polygon, which is the set of allowed slopes for the height function arising from domino tilings, $\mathcal{N} := \{(x,y)\in\mathbb{R}^2 | |x|+|y|\le 2\}$ [CKP00; KOS06]

A function $\mathfrak{h}$ is an asymptotic height function with height change $r=\{r_i\}_{i=1}^g$ and monodromy $\mathfrak{m}$ if the following holds,

- $\mathfrak{h}\big|_{\partial\Omega_i}(x) - \mathfrak{h}(x_i) = \mathfrak{b}_i(x)$
- $\mathfrak{h}(x_i,\gamma_i) = r_i$,
- $\mathfrak{h}$ is 2-Lipschitz function with respect to the intrinsic sup norm on Ω, that is $|\mathfrak{h}(x,\delta)-\mathfrak{h}(y,\delta')| \le 2\|x-y\|_\infty^\Omega + \mathfrak{m}(\delta^{-1}\delta')$ and $\nabla\mathfrak{h} : \Omega \to \mathcal{N}$
- after going around a loop δ', values of $\mathfrak{h}$ changes as follows: $\mathfrak{h}(x,\delta'\cdot\delta) = \mathfrak{h}(x,\delta)+\mathfrak{m}(\delta')$.

It is important to mention that numbers r_i for asymptotic height function take their values in intervals due to the Lipschitz constraint, $-2\|x_i-x_0\|_\infty^\Omega \le r_i \le 2\|x_i-x_0\|_\infty^\Omega$.

Let $\mathscr{H}(\Omega,\mathfrak{m},\mathfrak{b}_r)$ be the space of asymptotic height functions with monodromy $\mathfrak{m}$ and boundary condition $\mathfrak{b}_r$. Also define a union of $\mathscr{H}(\Omega,\mathfrak{m},\mathfrak{b}_r)$ over all possible height changes r, $\mathscr{H}(\Omega,\mathfrak{m},\mathfrak{b}) := \bigcup_r \mathscr{H}(\Omega,\mathfrak{m},\mathfrak{b}_r)$.

Theorem 2.4.4. *The spaces $\mathscr{H}(\Omega,\mathfrak{b},\mathfrak{m})$ and $\mathscr{H}(\Omega,\mathfrak{b}_r,\mathfrak{m},r)$ are compact spaces with respect to the intrinsic sup norm.*

Proof. The idea of the proof is to show compactness of the space of functions on the fundamental domain that will lead us to compactness of $\mathscr{H}(\Omega,\mathfrak{b},\mathfrak{m})$. Then, $\mathscr{H}(\Omega,\mathfrak{b}_r,\mathfrak{m},r)$ is compact as a closed subset of $\mathscr{H}(\Omega,\mathfrak{b},\mathfrak{m})$.

Recall that by Proposition 2.2.2, the behavior of these functions is determined by their values on $\mathcal{D}(\Omega)$. Thus, it is sufficient to show compactness of $\mathscr{H}(\mathcal{D}(\Omega),\mathfrak{b})$. In order to show it, one can apply Arzela-Ascoli theorem. The first requirement, the existence of a uniform bound for the functions $f\in\mathscr{H}(\mathcal{D}(\Omega),\mathfrak{b})$, is satisfied because of the boundary condition $\mathfrak{b}$ that is fixed on $\partial\Omega_0$. The equicontinuous follows directly from the Lipschitz condition. Then, these function with a given monodromy data $\mathfrak{m}$ form a closed subspace of $\mathscr{H}(\mathcal{D}(\Omega),\mathfrak{b})$.

Thus, it is a compact space. The same works for the subspace with a given height change r and a fixed monodromy data $\mathfrak{m}$, $\mathscr{H}(\Omega, \mathfrak{b}_r, \mathfrak{m}, r)$. The latter is, again, a compact space as a closed subset of $\mathscr{H}(\Omega, \mathfrak{b}, \mathfrak{m})$. □

Note that the gradient of an asymptotic height function is well-defined on Ω. Further, pointwise difference between two quasi-periodic functions with the same monodromy is, again, a well-defined function on Ω

2.4.3 Approximations of a domain

Assume that $\Omega \subset \mathbb{R}^2$ is a domain and Γ_N tends to Ω as $N \to \infty$ with respect to the Hausdorff distance d_H, $d_H(X, Y) = \inf\{\varepsilon \geq 0 : X \subseteq Y_\varepsilon \text{ and } Y \subseteq X_\varepsilon\}$, where X_ε is ε-neighborhood of X, $d_H(\Omega, \Omega_N) \to 0$, as $N \to \infty$.

Now, let $\Gamma_N \subset \frac{1}{N}\mathbb{Z}^2 \cap \Omega$ be a sequence of lattice domains with normalized boundary conditions $\{B_N\}$. Let us follow ideas from [CKP00; KOS06; Agg20] and call a sequence of regions with boundary conditions (Γ_N, B_N) *an approximation* of $(\Omega, \mathfrak{b})$ if

1. $\Gamma_N \subset \frac{1}{N}\mathbb{Z}^2 \cap \Omega$, where $\frac{1}{N}\mathbb{Z}^2$ is $\mathbb{Z}^2$ with mesh $\frac{1}{N}$.
2. each Γ_N admits at least one domino tiling with normalized boundary condition $B_N^{R_N}$ for each non-trivial $R_N = \{R_N^i\}_{i=1}^g$.
3. for every admissible asymptotic height change r, there exists a sequence of admissible normalized height changes $\{R_N\}$ that converges to r, $R_N^i \to r^i$ as $N \to \infty$.
4. Γ tends to Ω with respect to the Hausdorff distance d_H, $d_H(\Omega, \Gamma) \to 0$, as $N \to \infty$.
5. Further, $|B_N^{R_N}(x_N) - \mathfrak{b}^r(x)| \leq O(N^{-1})$ for the standard Euclid distance for sufficiently large N with $x_N \in \partial\Gamma, x \in \partial\Omega$ such that $|x_N - x| \leq O(N^{-1})$ (the existence of such points is guaranteed by the previous assumption).

Furthermore, note that the convergence of boundary conditions means that the discrete monodromy data $\{\frac{1}{N}M_i\}$ converges to the continuous $\{m_i\}$.

These conditions are modifications of conditions of Theorem 1.1 from [CKP00], which are needed for multiply-connected domains. Convergence of the boundary conditions implies convergence of discrete monodromy $M_N(\delta)$ to its continuous counterpart $\mathfrak{m}(\delta)$.

2.4.4 Convergence of the maximal extensions

In this section we prove convergence of discrete norm $\beta^\Gamma(x, y)$ to continuous intrinsic norm $\|x - y\|_\infty^\Omega$. Firstly, we need to normalize β,

$$\beta_N^{\Gamma_N} := \frac{\beta^\Gamma}{N}. \tag{2.4.15}$$

For $\Gamma = \mathbb{Z}^2$ and convex domains we have an exact formula for β (2.4.1), which tells that $\beta(x, y)$ approximates sup norm up to a factor $\pm 1/N$. For other domains it still holds.

Let Γ_N be an approximation of a domain with a boundary condition Ω. Then,

Proposition 2.4.5. *$\exists C > 0$ such that $\forall p, q \in \Gamma_N$ viewed as points of Ω, the following holds*

$$|\beta_N^{\Gamma_N}(p, q) - \|p - q\|_\infty^\Omega| \leq \frac{C}{N} \tag{2.4.16}$$

Proof. Let us take a path γ connecting x to y that minimizes integral from $\|x-y\|_\infty^\Omega$. Then, cover γ by a family of open balls $\mathcal{B}_i \subset \Omega$ that lie strictly inside Ω, $\gamma \subset \bigcup_{i=1}^C \mathcal{B}_i$, let C be their number. On each ball we have the convergence of $\beta_N(x,y)$ to $\|x-y\|_\infty^\Omega$ by formula (2.4.1), which might give an error $\frac{1}{N}$ on each $\mathcal{B}_i$. Thus, we have the desired estimate on Ω up to an error of $\frac{C}{N}$. □

Let domain Ω be a domain with a fixed boundary condition $\mathfrak{b} : \partial\tilde{\Omega} \to \mathbb{R}$. Further, let (Γ_N, B_N) be an approximation of $(\Omega, \mathfrak{b})$, and let $H_N^{\max}$ be the maximal extension of B_N. Then, $H_N^{\max}$ approximates the maximal extension of $\mathfrak{b}$ as $N \to \infty$,

Proposition 2.4.6. *Then for sufficiently large N and $x \in \Gamma_N$ viewed as point of Ω,*

$$|H_N^{\max}(x) - h^{\max}(x)| \leq O(N^{-1}) \tag{2.4.17}$$

Note that there is a lattice analog of the formula of the maximal extension, where we take the minimum is taken over points of $\partial\Gamma$ instead of $\partial\Omega$. Recall the expression of maximal extension of $\mathfrak{b}$,

$$\mathfrak{h}^{\max}(x) := \min_{y \in \partial\mathcal{D}(\Omega)} (\mathfrak{b}(y) + 2\|(x-y)\|_\infty) \tag{2.4.18}$$

the lattice analog of it is the following,

$$\mathfrak{h}_{\#,N}^{\max}(x) := \min_{y \in \partial\mathcal{D}(\Gamma)} (\mathfrak{b}(y) + 2\|(x-y)\|_\infty). \tag{2.4.19}$$

By the Lipschitz condition, $\mathfrak{h}_{\#,N}^{\max}$ approximates $h^{\max}$ up to an error of order $O(N^{-1})$. Denote approximations obtained this way by subscript $\#, N$. Now, let us prove Proposition 2.4.6.

Proof. The maximal extension of B_N is

$$H_N^{\max}(x) := H^{\max}/N = \min_{y \in \partial\mathcal{D}(\Gamma)} (B_N(y) + \beta_N(x,y)). \tag{2.4.20}$$

It approximates $H_N^{\max}(x)$ up to $O(N^{-1})$ due to the fact that $|\beta_N(x,y) - 2\|(x-y)\|_\infty|^\Omega \leq \frac{C}{N}$ for $C > 0$ independent of x, y. Thus, it approximates $\mathfrak{h}^{\max}$. □

2.4.5 Density lemma

Now we are ready to prove the density Lemma, In the proof we use the following tautological way to express a Lipschitz function in terms of its own values,

$$\mathfrak{h}(x) := \min_{y \in \mathcal{D}(\Omega)} (\mathfrak{h}(y) + 2\|(x-y)\|_\infty^\Omega). \tag{2.4.21}$$

We use the lattice version of the above expression for the lattice $\frac{1}{N}\mathbb{Z}^2$ that gives us an approximation of the function.

$$\mathfrak{h}_{\#,N}(x) := \min_{y \in \mathcal{D}(\Gamma)_N^\#} (\mathfrak{h}(y) + 2\|(x-y)\|_\infty^\Omega) \tag{2.4.22}$$

It is clear that $\mathfrak{h}_{\#,N}$ approximates h to within an error of order of $O(N^{-1})$ due to the Lipschitz condition.

Theorem 2.4.7 (The Density lemma)**.** *Let (Γ_N, B_N) be an approximation of $(\Omega, \mathfrak{b})$. Then, $\exists C > 0$ such that for every $\mathfrak{h} \in \mathscr{H}(\Omega, \mathfrak{b})$ there exists a sequence of normalized height functions H_N, such that $\|\mathfrak{h} - H_N\|_\infty^\Omega \leq \frac{C}{N}$.*

Vice versa, $\exists C' > 0$ such that for every normalized height function H_N on (Γ_N, B_N) there exists an asymptotic height function $\mathfrak{h} \in \mathscr{H}(\Omega, \mathfrak{b})$ such that $\|\mathfrak{h} - H_N\|_\infty^\Omega \leq N^{-1}C'$.

Proof. The strategy is to use (2.4.21) and (2.4.22) for the function $\mathfrak{h}$ and its lattice analog for discrete height functions.

Recall that a function $c'_y : x \mapsto c' + \beta(x, y)$ satisfies the local rule as a function of x. Let us define the partial height function that approximates h. For it let us take an infimum over all height functions that are above $\mathfrak{h}$, one way of doing it is to take such a height function at every lattice point, and then take infimum over these functions.

$$\hat{H}_N(x, \gamma) := \min_{y \in \mathcal{D}(\Gamma)} (\lfloor \mathfrak{h}(y, \gamma_y) \rfloor_{p_0} + \beta_N(x, y)), \tag{2.4.23}$$

where $\lfloor \mathfrak{h}(y, \gamma) \rfloor_{p_0}$ means the following: first, we need to take the integer part of $N \times \mathfrak{h}(y, \gamma)$, second we subtract the fractional part of $N \times (h(p_0, \gamma) - \beta(p_0, x))$ modulo 4, so that the value of height functions under the infimum coincide modulo 4 at point p_0 as they should by Lemma 2.4.1, and second we divide it by N. These modifications change $\hat{H}_N$ by an error of order $\frac{Const}{N}$, and guarantee that all the lattice operations are well-defined, thus we obtain the height function.

Clearly $\hat{H}_N$ approximates $\mathfrak{h}_{\#,N}$ up to $O(N^{-1})$ (see (2.4.22)), and thus approximates $\mathfrak{h}$. Note that so far, $\hat{H}_N$ is just a function on vertices of $\tilde{\Gamma}_N$ with some boundary conditions that satisfy the local rule from Definition 2. However, we need to check all five properties from Definition 2.3.3 to obtain the desired height function, so far we have only two of them, the third and the fourth properties. The rest three can be in fact fixed by the right boundary conditions since all these three properties are basically governed by the boundary conditions.

We can "balance" $\hat{H}_N$ between the maximal and the minimal extensions of B_N that may change the height function only by $O(N^{-1})$ due to the fact that $\hat{H}_N$ is fit to $\mathfrak{h}$ to within $O(N^{-1})$. After it, we have the desired normalized height function H_N

$$H_N := \max(H^N_{\min}, (\min(H^N_{\max}, \hat{H}_N))). \tag{2.4.24}$$

The proof of the second part of the statement easier, let us build such a function $\hat{\mathfrak{h}}$ that is simply a linear interpolation of values of H_N at even points (points with even coordinates). We take even points because of the jumps of the height function by ± 3.

□

2.5 The Concentration Lemma

In this section we prove a concentration inequality for height functions on $\tilde{\Omega}$. (We suppose that Ω is a domain, $\mathfrak{b} : \partial\Omega \to \mathbb{R}$ can be extended to an asymptotic height function on Ω, and (Γ_N, B_N) is an approximation of $(\Omega, \mathfrak{b})$) Also, recall that $\overline{H}_N(\mathrm{p})$ is the expectation value of $H_N(p)$, then the concentration inequality is the following statement:

Lemma 2.5.1 (The Concentration Lemma)**.** *$\exists \ell(\Omega) > 0$ such that $\forall C > 0$ and for sufficiently large N*

$$\mathbb{P}_N \left(\left\| H_N - \overline{H}_N \right\|_\infty > C \right) < \exp\left(-\frac{C^2 N}{\ell(\Omega)} \right). \tag{2.5.1}$$

Proof. The idea of the proof is to deduce Lemma 2.5.1 from the concentration for a simply-connected domain proved in Theorem 21 [CEP96]. Let us recall it.

Suppose that Γ is a tileable connected simply-connected lattice domain with boundary values of height function B, uniform measure $\mathbb{P}^\Gamma$ on the set of domino tilings of Γ. Take a point $p \in \Gamma$ in the interior of Γ such that there is a lattice path from p to $\partial\Gamma$ with m vertices. The concentration inequality from Theorem 21 in [CEP96] is the following statement:

$\forall a > 0$,

$$\mathbb{P}_N^\Gamma \left(|H(p) - \overline{H}(p)| > a \cdot \sqrt{m} \right) < 2 \exp(-a^2/32). \tag{2.5.2}$$

Recall the proof of this result. Let us fix a path $(x_0, \dots, x_m)$ with $m+1$ vertices from $\partial\Gamma$ to the p. Then, the authors considered a filtration of σ algebras $\mathcal{F}_k$ generated by outcomes of $H(x_i)$ for $i \le k$ ($H(x_0)$ is fixed since $x_0 \in \partial\Gamma$). Then, they took the conditional expectation value at point p with respect to $\mathcal{F}_k$, $M_k = \mathbb{E}(H(v)|F_k)$. By the tower property for conditional expectations, $M_k = \mathbb{E}(H(v)|F_k)$ form a martingale with bounded increments, that is $\mathbb{E}(M_{k+1}|F_k) = M_k$, which after applying Azuma's inequality gives the concentration inequality.

Let us renormalize the concentration inequality (2.5.2) for a large N as follows. Denote $\mathbb{P}_N^\Gamma$ the uniform measure on domino tilings of Γ_N. Then divide by N inequality in the left-hand side of (2.5.2) to get that

$$\mathbb{P}_N^\Gamma(|H_N(p) - \overline{H}_N(p)| > N^{-1} a \cdot \sqrt{m}) < 2 \exp(-a^2/32). \tag{2.5.3}$$

Choose a such that $C = N^{-1} a \sqrt{m}$. The length of a path m behaves for large N as $m \approx \ell'(\Omega, p) N$. The quantity $\ell'(\Omega, p)$ is approximately the length of the shortest path inside Ω from point $p \in \Omega$ to $\partial\Omega$. Let us define $\ell'(\Omega) := \max_p \ell(\Omega, p)$, which is finite due to compactness of Ω.

The resulting concentration inequality so far is the following,

$$\mathbb{P}_N^\Gamma(|H_N(p) - \overline{H}_N(p)| > C) < 2 \exp\left(-\frac{NC^2}{32\ell'(\Omega)} \right), \tag{2.5.4}$$

To obtain the probability $\mathbb{P}_N^\Gamma(\left\| H_N - \overline{H}_N \right\|_\infty^\Omega \ge C)$, we need to sum over all point $p \in \Gamma$ probabilities that $|H_N(p) - \overline{H}_N(p)| \ge C$,

$$\mathbb{P}_N^\Gamma \left\| H_N - \overline{H}_N \right\|_\infty^\Omega > C) = \sum_{p \in \Gamma} \mathbb{P}(|H_N(p) - \overline{H}_N(p)| \ge C) \tag{2.5.5}$$

The number of terms in the letter expression is bounded from above by $N^2|\Omega|$, where $|\Omega|$ is the area of Ω, which is due to the fact that the number of vertices of Γ_N is approximately $|\Omega| \times N^2$,

$$\mathbb{P}_N^\Gamma \left(\left\| H_N - \overline{H}_N \right\|_\infty^\Omega > C \right) < 2|\Omega| N^2 \exp\left(-\frac{C^2 N}{32\ell'(\Omega)} \right). \tag{2.5.6}$$

One can further choose an $\ell(\Omega) < 32\ell'(\Omega))$ to absorb the prefactor $12|\Omega|N^2$ for sufficiently large N, and factor 32 in front of ℓ'

$$\mathbb{P}_N^\Gamma \left(\left\| H_N - \overline{H}_N \right\|_\infty^\Omega > C \right) < \exp\left(-\frac{C^2 N}{\ell(\Omega)} \right). \tag{2.5.7}$$

Once we have a multiply-connected domain Γ, the situation slightly changes, however, the original bound still holds. In fact, there are two ways to get the desired inequality.

The first way is a straightforward repetition of the same arguments as in Theorem 21 in [CEP96]. One can always find a lattice path from a vertex of $\tilde{\Gamma}_0$ to its boundary, where boundary values of the height function are fixed, and then apply the same arguments with the Azuma inequality.

Another way is to notice that it is sufficient to show the concentration inequality on $\mathcal{D}(\Omega)$ by Proposition 2.2.3. Since $\Gamma \cap \mathcal{D}(\Omega)$ is a finite simply-connected domain, therefore we can use theorem 21 from [CEP96] in the form of Lemma 2.5.1. □

2.5.1 Piecewise linear approximations of asymptotic height functions

In this subsection we recall piecewise linear approximations of Lipschitz functions that we use in the proofs.

Let us take $\ell > 0$ and take a triangular mesh with equilateral triangles of side ℓ. We map an asymptotic height function $h \in \mathscr{H}(\Omega)$ to a piecewise linear approximation, that is linear on every triangle, moreover it is a unique linear function that agrees with h at vertices of the triangle. Let us denote this approximation of h by $\hat{h}$. In Lemma 2.2 [CKP00] the authors show that in a simply-connected domain, h approximates $\hat{h}$ on the majority of triangles. In a multiply-connected domain, we can build a piecewise linear approximation of h on $\mathcal{D}(\Omega)$. Moreover, one can use such a triangulation of Ω that $\partial\mathcal{D}(\Omega)$ consists of sides of the triangles. The resulting approximation $\hat{h}$ has the same increments between connected boundary components ν_i and ν_{i+g} as h. The latter fact allows us to extend $\hat{h}$ to $\tilde{\Omega}$ with the same monodromy data as h and with the desired approximation property. Thus, we have the following.

Claim 1. *Let $h \in \mathscr{H}(\Omega)$ be asymptotic height function and let $\varepsilon > 0$. Then for sufficiently small $\ell > 0$, on at least $1 - \varepsilon$ fraction of the triangles in the ℓ-mesh that intersect Ω, we have the following two properties: first, piecewise linear approximation h_ℓ is fit to within $\varepsilon\ell$ to h. Second, on at least $1 - \varepsilon$ fraction(in measure) of points x, $\nabla h(x)$ exists and is within ε to ∇h_ℓ.*

2.5.2 The cutting rule

Suppose that we have a domain with a boundary condition $(\Gamma, \mathfrak{b})$ and a subset ρ on the dual lattice from the boundary of Γ to itself (thus, Γ/ρ consists of several components, let us denote them Γ^i). We want to calculate the partition function of Γ and one way to do it is to calculate partition functions $Z(H(\rho))$ with the given height function $H(\rho)$ along ρ. Then to sum up $Z(H(\rho))$ over all $H(\rho)$. The result is the original partition function because we just permute terms in a finite sum.

Then, we can interpret each $Z(H(\rho))$ as the product of the partition functions saying that ρ cuts Γ.

$$Z(\Gamma, \kappa) = \sum_{B_\rho} \prod_i Z(\Gamma^i, B^i_\rho) \tag{2.5.8}$$

where B^i_ρ is the boundary height function on Γ^i that coincide with the original boundary height function B and B_ρ where it is possible.

2.5.3 Surface tension

Recall from [CKP00] that the asymptotic growth rate $\sigma_{\mathbb{Z}^2}(s,t)$ of the number of domino tilings of a rectangle $N \times N$ with periodic boundary conditions with the slope (s,t) is defined by the following formula as $N \to \infty$,

$$Z(R_N(s,t)) \approx \exp\left(-N^2\sigma_{\mathbb{Z}^2}(s,t) + O(N)\right). \tag{2.5.9}$$

The precise expression of $\sigma_{\mathbb{Z}^2}(s,t)$ is the following. Recall the Lobachevsky function $L(z) = -\int_0^z \log|2\sin t|dt$ and quantities $p_a = p_a(s.t), p_b = p_b(s.t), p_c = p_c(s.t), p_d = p_d(s.t)$ that are determined by expression (2.5.11). Then, the surface tension is the following function,

$$\sigma_{\mathbb{Z}^2}(s,t) = -1/\pi\left(L(\pi p_a) + L(\pi p_b) + L(\pi p_c) + L(\pi p_d)\right). \tag{2.5.10}$$

The probabilities of four types of dominoes p_a, p_b, p_c and p_d that are determined by the following system in the limit as $N \to \infty$ [CKP00],

$$\begin{aligned} 2(p_a - p_b) &= t, \\ 2(p_d - p_c) &= s, \\ p_a + p_b + p_c + p_d &= 1 \\ \sin(\pi p_a)\sin(\pi p_b) &= \sin(\pi p_c)\sin(\pi p_d). \end{aligned} \tag{2.5.11}$$

2.6 The variational principle

In this section we formulate and prove Theorem 2.1.2 and its corollary,Theorem 2.6.2.

2.6.1 Statement of theorems

Suppose Ω is a domain with an boundary condition $\mathfrak{b}$ and let (Γ_N, B_N) be an approximation of $(\Omega, \mathfrak{b})$, further r is a continuous height change.

We also need to assume that the boundary condition $\mathfrak{b}$ is non-degenerate, that is it admits an extension to an asymptotic height function $\mathfrak{h}$ whose gradient is in the interior of the newton polygon $\mathcal{N}$ on the set of positive measure. We need to assume this to guarantee the uniqueness of the limit shape $\mathfrak{h}^\star$, which is not the case for pathological boundary conditions, which could have only linear extensions of slope $\partial\mathcal{N}$, i.e., extensions with only frozen regions, where we can not use convexity of $\sigma_{\mathbb{Z}^2}$.

Also recall that $H_N := \frac{1}{N}H$ is a normalized height function together with the normalized height change $\frac{1}{N}R_N$. Finally, let $\mathfrak{h}^\star$ be the unique minimizer of $\mathcal{F}$ over $\mathscr{H}(\Omega, \mathfrak{b})$. And let $r^\star$ be the continuous height change of $\mathfrak{h}^\star$. Then,

Theorem 2.6.1. *In the limit as $N \to \infty$*

$$\lim_{N\to\infty} |\Omega|^{-1} N^{-2} \log Z(\Gamma_N, B_N) = -\mathcal{F}(\mathfrak{h}^\star) = -\iint_\Omega \sigma_{\mathbb{Z}^2}(\nabla \mathfrak{h}^\star) dxdy. \tag{2.6.1}$$

Moreover, there exists $\ell > 0$ such that for all $\delta > 0$ as $N \to \infty$ we have

$$\mathbb{P}_N\left(\max_{x_N \in \Gamma} |H_N(x_N) - \mathfrak{h}^\star(x_N)| > \delta\right) \le \exp\left(-\frac{N\delta^2}{\ell}\right). \tag{2.6.2}$$

and R_N converge to $r^\star$ with respect to $\mathbb{P}_N$ as $N \to \infty$.

This theorem can be formulated for a fixed height change $r \in \mathbb{R}^g$, assume also that $\frac{1}{N}R_N \to r$ and $N \to \infty$. Then we have the following Corollary,

Theorem 2.6.2. *There exists $\mathfrak{h}_r^\star \in \mathscr{H}(\Omega, \mathfrak{b}, r)$ such that in the limit $N \to \infty$ and then $\delta \to 0$*

$$\lim_{N\to\infty} |\Omega|^{-1} N^{-2} \log Z(\Gamma_N, B_N, R_N) = -\iint_\Omega \sigma_{\mathbb{Z}^2}(\nabla \mathfrak{h}_r^\star) dxdy. \tag{2.6.3}$$

Furthermore, there exists $\ell > 0$ such that for all $\delta > 0$ and $N \to \infty$ the following holds,

$$\mathbb{P}_N^R\left(\max_{x_N \in \Gamma} |H_N(x_N) - \mathfrak{h}_r^\star(x_N)| > \delta\right) \le \exp\left(-\frac{N\delta^2}{\ell}\right). \tag{2.6.4}$$

In the remaining section we prove Theorem 2.6.1 in three steps, and deduce from it Theorem 2.6.2. The steps are

2.6.2 Convergence of height functions to the limit shape

Here, we give a proof of a law of large numbers for height function. More precisely, we show that a normalized height function converges in both regimes to its expected value that is approximately the unique solution to the variational problem. We write it for an arbitrary height change, and later discuss the modifications for a fixed height change.

Consider a sequence $\{\overline{H}_N\}$ of expectation values of normalized height functions on (Γ_N, B_N). We know that by Theorem 2.4.7 there exists a sequence of asymptotic height functions $\{\mathfrak{h}_N\}$, such that $\left\|\mathfrak{h}_N - \overline{H}_N\right\|_\infty^\Omega \leq \frac{C}{N}$. By Proposition 2.4.4 $\{\mathfrak{h}_N\}$ has a convergent subsequence, denote its limit by $\mathfrak{h}$. Without loss of generality, we suppose that the convergent subsequence is $\{\mathfrak{h}_N\}$ itself. We will see later that $\mathfrak{h} = \mathfrak{h}^\star$

Lemma 2.6.3. *One can find such an ℓ' that for $\forall \delta > 0$ and for sufficiently large N*

$$\mathbb{P}(\|H_N - \mathfrak{h}\|_\infty^\Omega > \delta) \leq \exp(-N\delta^2/\ell'). \tag{2.6.5}$$

Proof. We deduce it from a combination of Lemma 2.5.1 applied to H_N and convergence of h_N to $\mathfrak{h}$. The goal is to show that the inequality $\|H_N - \mathfrak{h}\|_\infty^\Omega \leq \delta$ holds for sufficiently large N with probability exponentially close to 1.

By the triangle inequality we have

$$\|H_N - \mathfrak{h}\|_\infty^\Omega \leq \left\|\bar{H}_N - \mathfrak{h}_N\right\|_\infty^\Omega + \|\mathfrak{h}_N - \mathfrak{h}\|_\infty^\Omega + \left\|H_N - \bar{H}_N\right\|_\infty^\Omega. \tag{2.6.6}$$

The first term in the right-hand side of (2.6.6) is smaller than $\delta/3$ for sufficiently large N by definition of $\mathfrak{h}_N$, that is by Lemma 2.4.7 we have $C > 0$ such that $\left\|\mathfrak{h}_N - \bar{H}_N\right\|_\infty^\Omega < \frac{C}{N}$, which is smaller than $\delta/3$ for sufficiently large N. The second terms of (2.6.6) is smaller than $\delta/3$ for sufficiently large N due to convergence of $\mathfrak{h}_N$ to $\mathfrak{h}$, which holds by definition of $\mathfrak{h}$.

The third term (2.6.6) is smaller than $\delta/3$ with the probability $1 - \exp(-\frac{\delta^2 N}{\ell})$, where we defined $\ell = 3\ell'$ for ℓ' from Lemma 2.5.1. Therefore, we have $\|H_N - \mathfrak{h}\|_\infty^\Omega > \delta$ with probability bounded by $\exp(-N\delta^2/\ell')$.

□

So far, we know that up to extracting a subsequence, normalized height functions converge with respect to the uniform norm in probability to $\mathfrak{h}$ and the contribution of height functions that are far away from $\mathfrak{h}$ are exponentially suppressed. Thus, $\mathfrak{h}$ is the limit shape. Since height change R_N is a continuous function of H_N, it converges to the height change of the limit shape, which is r. Later, we prove that $\mathfrak{h} = \mathfrak{h}^\star$.

2.6.3 Convergence of partition function

Let us show that one can find an asymptotic expression of the partition function, which is a straightforward corollary of the convergence of height functions to the limit shape. The following proof holds for a fixed height change r after replacing $\mathfrak{h}$ by $\mathfrak{h}_r$ and $Z(\Gamma_N, B_N)$ by $Z(\Gamma_N, B_N, R_N)$.

Define $U_\delta^N(\mathfrak{h}^\star)$ to be the set of height functions on Γ_N that are fit to within δ to $\mathfrak{h}^\star$, $\|H_N - \mathfrak{h}^\star\|_\infty^\Omega \leq \delta$.

Then, the following holds due to the concentration inequality above,

$$\mathbb{P}_N \|H_N - \mathfrak{h}^\star\|_\infty^\Omega \leq \delta) = 1 - \mathbb{P}_N(\|H_N - \mathfrak{h}^\star\|_\infty^\Omega > \delta). \tag{2.6.7}$$

Or more precisely,

$$\frac{Z(\Gamma_N, B_N|\mathfrak{h}^\star, \delta)}{Z(\Gamma, B_N)} = 1 + O(\exp(-\delta^2 N/\ell)). \tag{2.6.8}$$

Now, let us take the logarithm of both sides and normalize them by N^{-2}. Also introduce the notation $S(N, \delta) := 1 + O(\exp(-\delta^2 N/\ell))$ for the simplicity.

$$N^{-2} \log Z(\Gamma_N, B_N) = N^{-2} \log(Z(\Gamma_N, B_N|\mathfrak{h}^\star, \delta)) + N^{-2} \log(S(N, \delta)). \tag{2.6.9}$$

Now we can take limit as $N \to \infty$ to make $\log S(N, \delta)$ converge to zero. Finally, we obtain the desired expression by Theorem 2.8.1,

$$N^{-2} \log Z(\Gamma_N, B_N) \xrightarrow[N\to\infty]{} -\mathcal{F}(\mathfrak{h}^\star). \tag{2.6.10}$$

2.6.4 The Surface tension functional and the limit shape

We still need to show that h minimizes $\mathcal{F}$, that is $h = \mathfrak{h}^\star$. Again, it follows easily from the concentration of height functions around $\mathfrak{h}$.

Assume that $\mathfrak{h} \neq \mathfrak{h}^\star$. We need to show that $\mathcal{F}(\mathfrak{h}) \geq \mathcal{F}(\mathfrak{h}^\star)$. Suppose the opposite, that is $\mathcal{F}(\mathfrak{h}) < \mathcal{F}(\mathfrak{h}^\star)$. By Theorem 2.8.1, $\mathcal{F}(\mathfrak{h}^\star)$ (resp.$\mathcal{F}(\mathfrak{h})$) is the limit of the normalized number of domino tilings whose normalized height functions are fit within δ to $\mathfrak{h}^\star$ (resp.$\mathfrak{h}$) for $\delta \to 0$. Then, we can use that normalized height functions H_N concentrate around $\mathfrak{h}$, which can be separated from $\mathfrak{h}^\star$ by the choice of a smaller $\delta > 0$. The contradiction follows from the fact that the overwhelming majority of domino tilings are δ-close to $\mathfrak{h}$, but not to $\mathfrak{h}^\star$ and thus, we are done.

The proof for the fixed asymptotic height change r works the same way after replacing of $\mathfrak{h}$ by $\mathfrak{h}_r$.

2.7 Existence of the minimizer

Here we show the existence of solution of the variational problems, for an arbitrary height change, and for a given asymptotic height change.

Before formulating the theorems, we need an extra assumption on the boundary conditions. Recall that $\sigma_{\mathbb{Z}^2} : \mathcal{N} \to \mathbb{R}$ is convex only in the interior of $\mathcal{N}$, thus in order to guarantee the uniqueness, we must have $\nabla\mathfrak{h} \in \mathcal{N}^\circ$ on a set of positive Lebesgue measure. Therefore, call a boundary condition non-degenerate if it admits an extension to such an asymptotic height function $\mathfrak{h}$ that there exists a proper subset $\Omega' \subseteq \Omega$ that $\forall p \Omega'\ \nabla\mathfrak{h}(p) \in \mathcal{N}^\circ$. This way we have a subregion of Ω where we can use the strict convexity of $\sigma_{\mathbb{Z}^2}$ following proposition 2.4 from [CKP00]. It is easy to construct counterexamples in the situation where this condition does not hold, and the boundary condition admits two different totally frozen extensions, see discussion of figure 39 from [CSW23].

Proposition 2.7.1. *There exists a unique minimizer $\mathfrak{h}^\star$ of $\mathcal{F}$ over the space $\mathscr{H}(\Omega, \mathfrak{m}, \mathfrak{b})$.*

There exists a unique minimizer $\mathfrak{h}_r^\star$ of $\mathcal{F}$ over the space $\mathscr{H}(\Omega, \mathfrak{m}, \mathfrak{b}_r, r)$.

Proof. Consider a fundamental domain $\mathcal{D}(\Omega)$ for action of $\pi_1(\Omega)$ on the universal covering space of Ω. Recall that by Proposition 2.2.3, it is sufficient to find a minimizer of $\mathcal{F}$ on $\mathcal{D}(\Omega)$.

The boundary $\partial\mathcal{D}(\Omega)$ consists of two parts, $\partial\mathcal{D}(\Omega) = \partial\Omega \bigsqcup \partial\mathcal{D}^1(\Omega)$, the first one is supplemented with boundary condition $\mathfrak{b}$ and the other one is the union of $2g$ curves $\{\upsilon_i\}_{i=1}^{2g}$ matched in pairs υ_i, υ' with free boundary conditions subject to periodicity across the pairs so that the values on υ_i coincide with the values on υ_i'(recall that υ_i and υ_i' were obtained by the cut along the curve γ_i)

The space $\mathscr{H}(\Omega, \mathfrak{m}, \mathfrak{b})$(resp. $\mathscr{H}(\Omega, \mathfrak{m}, \mathfrak{b}_r, r)$) is compact by Theorem 2.4.4. Then, $\mathcal{F}$ is upper semi-continuous on spaces $\mathscr{H}(\Omega, \mathfrak{m}, \mathfrak{b}_r, r)$ and $\mathscr{H}(\Omega, \mathfrak{m}, \mathfrak{b})$. This follows from Lemma 2.1 from [CKP00], which uses only the convexity of $\sigma_{\mathbb{Z}^2}$ and the Lipschitz condition, and thus, trivially extends to partially free periodic boundary conditions.

Therefore, there exists the minimizer $\mathfrak{h}^\star$ of $\mathcal{F}$ on $\mathscr{H}(\Omega, \mathfrak{m}, \mathfrak{b})$ (resp. there exists the minimizer $\mathfrak{h}_r^\star$ on $\mathscr{H}(\Omega, \mathfrak{m}, \mathfrak{b}_r, r)$). By the same convexity argument as in Lemma 2.4 from [CKP00], this minimizer is unique.

A priori $\mathfrak{h}^\star$ and $\mathfrak{h}_r^\star$ depend on a particular choice of the fundamental domain $\mathcal{D}(\Omega)$. However, since gradients of functions from $\mathscr{H}(\tilde{\Omega}, \mathfrak{b})$ are well-defined objects on Ω by Lemma 2.2.1 and $\sigma_{\mathbb{Z}^2}$ is strictly convex everywhere in the interior of the domain of definition [CKP00; KOS06], we can use Proposition 4.5 from [DS08] to show uniqueness. See also the discussion in Section 5.6 in [ADPZ20]. □

2.8 The Surface Tension Theorem.

In this section we formulate Theorem 2.8.1 and give a proof of it.

Theorem 2.8.1. *Let Ω be a domain in $\mathbb{R}^2$ and $\mathfrak{h} \in \mathscr{H}(\Omega, \mathfrak{b})$. Suppose that (Γ_N, B_N) is an approximation of $(\Omega, \mathfrak{b})$.*

Then, for $\forall \delta > 0$ sufficiently small,

$$\lim_{N\to\infty} \sup \left| \frac{1}{|\Omega|} N^{-2} \log Z(\Gamma_N, B_N \mid \mathfrak{h}, \delta) + \int_\Omega \sigma_{\mathbb{Z}^2}(\partial_x \mathfrak{h}, \partial_y \mathfrak{h}) dxdy) \right| = o_\delta(1), \tag{2.8.1}$$

Mind that we have a plus sign since we subtract a negative quantity, that is $-\int_\Omega \sigma_{\mathbb{Z}^2}(\partial_x \mathfrak{h}, \partial_y \mathfrak{h}) dxdy)$.

Proof. Fix a fundamental domain $\mathcal{D}(\Omega)$ with branch-cuts made along curves $\{\gamma_i\}_{i=1}^g$.

For the proof we need a triangular mesh a side length ℓ and piecewise linear approximations of Lipschitz functions from Claim 1. Consider a triangular mesh of length size ℓ that triangulates $\mathcal{D}(\Omega)$ into triangles T^j of the standard area $\mathcal{A}(T^j)$. Let also $\mathfrak{h}_\ell$ be the piecewise linear approximation of $\mathfrak{h}$ that is linear on each triangle and coincides with the values of h at the vertices of the triangles.

Then, we choose small ε and take ℓ such that $\ell\varepsilon < \delta$, and on at least at $1 - \epsilon$ fraction of points of a triangle in measure we have two properties: first, $|\mathfrak{h}_\ell - \mathfrak{h}| \le \ell\varepsilon$, and second, the gradient of $\mathfrak{h}$ exists and fit within ε to the gradient of $\mathfrak{h}_\ell$ in ℓ_2 norm, which is possible by Lemma 2.2 [CKP00]. We need these properties in order to write $\mathcal{F}(\mathfrak{h}_\ell) = \mathcal{F}(\mathfrak{h}) + o_\delta(1)$ as $\varepsilon \to 0$.

Let us use the (2.5.8) for a subset ρ obtained from the intersection of the triangular mesh with the domain. Note that the subset ρ cuts Γ_N into triangles with boundary conditions along ρ. Denote the triangles by $\{T^j\}$ and their boundary height functions by $\{B_\rho^j\}$.

$$Z(\Gamma_N, B_N|\mathfrak{h}, \delta) = \sum_{\mathfrak{b}_\rho} Z(\Gamma_N, B_\rho|\mathfrak{h}, \delta) = \sum_{\mathfrak{b}_\rho} \prod_j Z(T^j, B_\rho^j|\mathfrak{h}, \delta), \tag{2.8.2}$$

There are two types of triangles $\{T^j\}$. The included triangles (the first type) that do not intersect the boundary of the fundamental domain and where $\mathfrak{h}_\ell$ is fit to within $\ell\varepsilon$ to $\mathfrak{h}$. The excluded triangles (the second type) intersect the boundary of the fundamental domain or where $\mathfrak{h}_\ell$ does not approximate $\mathfrak{h}$.

We make an upper and a lower bound for the normalized partition function $N^{-2}\log Z(\Gamma_N, B_N|\mathfrak{h}, \delta)$. In both cases, we can estimate the two types of triangles separately.

For the included triangles we use Corollary 4.2 from [CKP00], and for the excluded we make a rough estimate. Then, after taking limit as $N \to \infty$, the normalized estimates differ from each other by $o_\delta(1)$.

2.8.1 The lower bound.

In the lower bound, it is sufficient to include some height functions that are δ-close to $\mathfrak{h}$. To do this, we can take only one term from (2.8.2) corresponding to one boundary height function B_ρ (for instance, we can take B_ρ obtained from the restriction of H'_N) (Theorem 2.4.7 gives us a sequence of normalized height functions $\{H'_N\}$ that converges to $\mathfrak{h}$ as $N \to \infty$).

Let us estimate the triangles of the first type by the product that includes only triangles of this type.

$$Z(\Gamma_N, B_N|\mathfrak{h}, \delta) \geq \prod_{T_j \text{of 1st type}} Z(T^j, B^j_\rho|\mathfrak{h}_\ell, \delta) \tag{2.8.3}$$

The bound for the included triangles obtained by using Corollary 4.2 [CKP00] to count δ-close height functions to make sure that we include only height functions δ-close to h. Thus, for triangles of the first type, we have the following,

$$N^{-2} \log \prod_{T_j \text{of 1st type}} Z(T^j, B^j_\rho|\mathfrak{h}_\ell, \delta) = \sum_{T_j \text{of 1st type}} -\sigma_{\mathbb{Z}^2}(s^j, t^j) \times \mathcal{A}(T^j) + o(N^{-1}) + O(\varepsilon^{1/2} \log \varepsilon), \tag{2.8.4}$$

where (s^j, t^j) is a slope of $\mathfrak{h}_\ell$ on the triangle T^j and $\mathcal{A}(T^j)$ is the area of the triangle T^j. Finally, for sufficiently large, N the lower bound is the following,

$$N^{-2} \log Z(\Gamma_N, B_N|\mathfrak{h}, \delta) \geq \sum_j (-\sigma_{\mathbb{Z}^2}(s^j, t^j))\mathcal{A}(T^j) + o(N^{-1}) + O(\varepsilon^{1/2} \log \varepsilon), \tag{2.8.5}$$

where we fixed a height function on the excluded triangles to be H'_N.

2.8.2 The upper bound.

We can use almost the same strategy to make an upper bound. First, we have to include all height function δ-close to $\mathfrak{h}$. Let us estimate the included triangles the same way as for the lower bound to count height functions δ-close to $\mathfrak{h}$. For the excluded triangles we make a rough estimate since the area of those triangles is proportional to ε, the number of configurations is bounded from above by $\exp(\varepsilon)$ times the number of terms in the cutting rule, which is $2^{O(N)}$ since it is the number of configurations of a line of size N.

$$Z(\Gamma, B_N|\mathfrak{h}, \delta) \leq \prod_{T_j \text{of 1st type}} Z(T^j, B^j_\rho|\mathfrak{h}_\ell, \delta))2^{O(N)} + N^2\varepsilon \tag{2.8.6}$$

And after taking limit as $N \to \infty$, the normalized upper bound is the following, where terms $O(N^{-1})$ and $O(\varepsilon)$ come from the bounds of triangles of the second type.

$$N^{-2} \log Z(\Gamma, B_N|\mathfrak{h}, \delta) \leq \sum_j (-\sigma_{\mathbb{Z}^2}(s^j, t^j))\mathcal{A}(T^j) + o(N^{-1}) + O(\varepsilon^{1/2} \log \varepsilon) + O(\varepsilon). \tag{2.8.7}$$

Taking into account that $\int_\Omega \sigma_{\mathbb{Z}^2}(\nabla h_\ell) dxdy = \sum_j \sigma_{\mathbb{Z}^2}(s_j, t_j)\mathcal{A}(t^j)$, one can see that both bounds after dividing by the area of Ω are equal to $\mathcal{F}(h_\ell) + o(N^{-1}) + O(\varepsilon^{1/2} \log \varepsilon)$ that differs from $\mathcal{F}(\mathfrak{h})$ by $o_\delta(1)$ by Lemma 2.3 from [CKP00]. □

2.9 Final remarks

As mentioned in [Gor21], there are two approaches in studying random domino tilings of a multiply-connected domain Γ that are equivalent for a simply-connected domain.

The first approach is looking at domino tilings of Γ with the uniform measure $\mathbb{P}$ defined on them. In this framework, one might be interested in fluctuations either of a height function or a height change. For instance, in [BGG17] the authors showed Gaussian fluctuation of normalized height change $\frac{1}{N}R_N$ using the method of log-gaze.

The second option is fixing a boundary height function B^R with the height change R and looking at uniformly random height functions that extend B^R to Γ. Denote $\mathbb{P}_N^R$ the uniform measure on such extensions, which is just $\mathbb{P}_N$ conditioned to have the fixed height change R. This approach suits a random surface point of view on tilings, where we look at a plot of a height function as a random stepped surface. Computer simulation of domino tilings with different height change in 2.9.4 shows that this parameter is extremely important. Results in this direction include the first description of a non-simply-connected domain in [BF08]. The authors proved a law of large numbers and a central limit theorem for domino tilings of so-called holey Aztec diamond. Up to our knowledge [BG19] is the only work that deals with multivalued height functions, yet the authors do not find $\mathfrak{h}^\star$ explicitly or characterize it besides the law of large numbers. Other works focused on a problem of random lozenge tilings of multiply-connected domains with monodromy-free height functions. In [KO05] the analysis using the complex Burgers equation was done with an example of a frozen(Arctic) curve in a non-simply-connected region. In recent years there also appeared combinatorial works with enumerating results by M. Ciucu et al. for example see [CL19]. Further results are obtained using the tangent method by P.Di Francesco et al. in [DDG20], where the authors have found the frozen curve for quarter-turn symmetric domino tilings of a holey Aztec square, which is a multiply-connected domain with a hole of a finite size.

Also, the idea of defining a height function on $\tilde{\Omega}$ in a different notation is already known, for instance [BLR19].

2.9.1

The case of a hole of a finite size, as in [DDG20], can be, probably, analyzed in our framework as follows. Since the hole converges with respect to Hausdorff distance to a point (x_0, y_0) as $N \to \infty$, we left with one parameter that encodes the height of (x_0, y_0). So, we need to modify the space of function by fixing the value of height functions at (x_0, y_0). As the result, one would expect conic singularities of the limit shape as it is approaching the point (x_0, y_0), as in a similar example noted in [KO05].

2.9.2

Let us recall that a flip of a domino tiling is a replacement of two adjacent vertical dominoes by two adjacent horizontal dominoes. The property of domino tilings of a simply-connected region Γ is that any two domino tilings are related by a sequence of flips [Thu90; STCR95]. In other words, the set of domino tilings forms one orbit under the action of flips. This property is in the core of computer simulations of random domino tilings [PW96]. Thus, the simulation algorithm of uniformly random domino tilings should include an extra move that change R. This move is a cyclic rotation of dominoes along the non-trivial loop. See details in [DDG20].

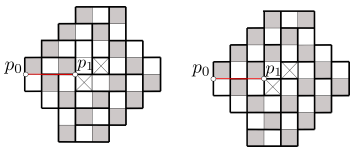

Figure 2.7: Two domino tilings of $\mathcal{AD}_1$ with height change $R_1 = 3$ on the right figure and $R_1 = 7$ on the left. The crossed squares are missing from the domain.

2.9.3

Let us define our main example, the modified Aztec diamond $\mathcal{AD}_N$. Also, we explain certain features of $\mathcal{AD}_N$ and possible ways to analyzing it.

Recall that the Aztec diamond of order N is the union of unit squares on $\mathbb{Z}^2$ whose centers (x, y) satisfy $|x| + |y| \leq N$. Let $N = 4k, k \in \mathbb{N}$ and introduce the Aztec diamond with a modified constraint AD_N°, $N/4 \leq |x| + |y| \leq N$. The boundary of AD_N° consists of two connected components, the external boundary and the internal one. For our main example we make four defects to the latter boundaries, that is consider AD_N° and add $N/4$ squares in the following four locations, right upper and left bottom external boundaries(resp. left upper and right bottom internal boundaries). See an example of $\mathcal{AD}_1$ on Figure (2.7). A height function on this domain has monodromy $M = 8$. It is not hard to check using a checkerboard coloring that $\mathcal{AD}_N$ is tillable for arbitrary $N = 4k, k \in \mathbb{N}$.

One interesting property of $\mathcal{AD}_N$ is an emergence of two paths on the top and on the bottom of it that can be clearly seen on Figure (2.2). These paths exist in all the domino tilings of $\mathcal{AD}_N$, which can be seen from the parametrization of domino tilings by non-intersections paths via bijection with non-intersecting line ensemble as in Figure 2.8.

Recall that a frozen region is the set of points of Ω where fluctuation of H_N disappears as $N \to \infty$, the boundary of the frozen region is called a frozen(arctic) curve. The paths mentioned above approximate the tangent lines to the arctic curve. This property is in the core of the heuristics of the tangent method [CS16], which reconstructs the arctic curve from its tangent lines. Recently, this method was proved for a particular case of the six-vertex model, the ice-model on a three-bundle domain [Agg19]. We think that this technique can be used to determine the Arctic curve in our situation. We leave it for future work.

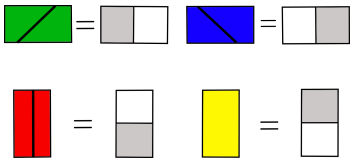

Figure 2.8: Bijection between domino tilings and non-intersecting line paths

More interestingly, one can modify the definition of $\mathcal{AD}_N$ by changing the size of the defects and obtain a one-parameter family of domains and frozen curves. See Section 2.9.4 for simulations of $\mathcal{AD}_{N,M}$ with different defects.

2.9.4 Computer simulations of the modified Aztec diamond.

Here, we present simulations of random domino tilings of $\mathcal{AD}_N$ made for a randomly-chosen height change r. The simulations are obtained using the following Markov chains, where the main difficulty is to generate a random height change, which cannot be done using local moves i.e., flips. First, we create an initial tiling of the multiply-connected region by Kuhn's algorithm. Second, we find tilings with the maximal, and minimal height change. Third, we superimpose our initial tiling with the maximal/minimal one, which consist of cycles. Then,

we rotate randomly along these cycles to generate a random height change. The probability whether to rotate or not along a cycle C is proportional to $\exp(-L(C))$, where $L(C)$ is the length of C. We introduced this weight because otherwise the algorithms does not stabilize due to rotations along big cycles. After it, we perform flips to generate a random tiling with the height change obtained before.

Also, we used another, yet similar, algorithm. In this earlier version, we begin with an initial tiling obtained by Kuhn's algorithm. Then, we perform flips until the picture becomes uniform, and then we delete the inner Aztec diamond from the graph. Then, we apply Kuhn's algorithm again to compete the tiling, and flip it once again until the configuration becomes uniform. This way we were able to generate random tilings with monodromy. The previous algorithm requires existence of the highest and lowest configurations, which do not exist for the domain with monodromy.

We did not prove that the resulting distribution is uniform. However, we expect that it is almost uniform, since the only stationary(i.e., invariant) distribution under action of flips is the uniform distribution.

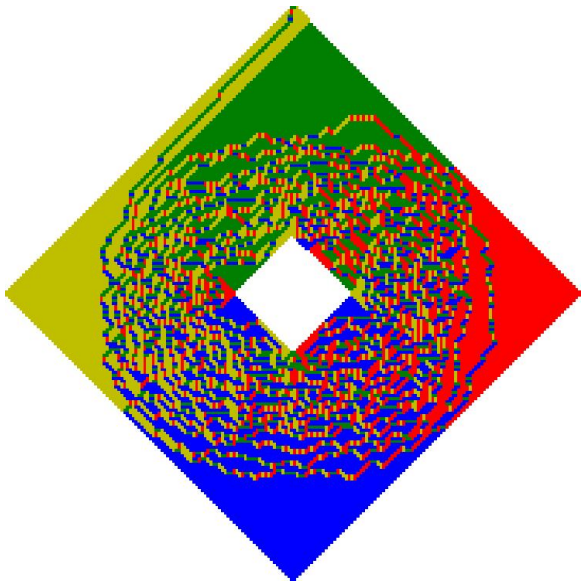

Figure 2.9: A domino tiling of $\mathcal{AD}_{50}$ with $M = 50$ and $R = 88$.

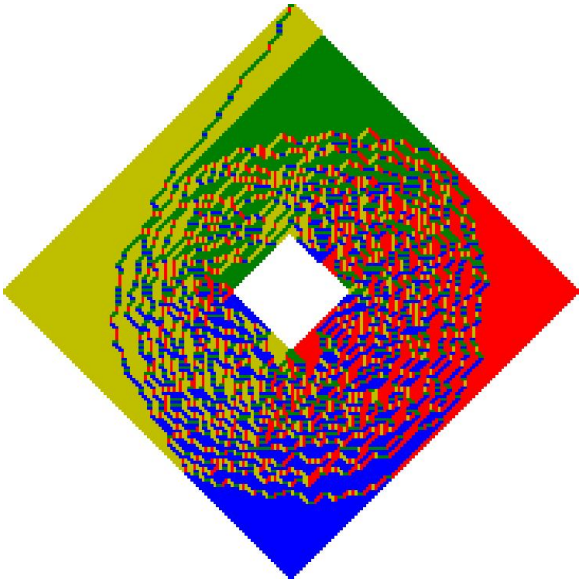

Figure 2.10: A domino tiling of $\mathcal{AD}_{50}$ with $M = 100$ and $R = 72$

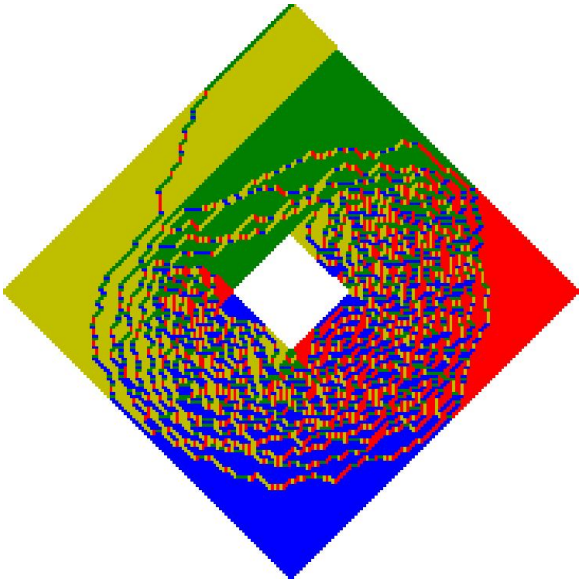

Figure 2.11: A domino tiling of $\mathcal{AD}_{50}$ with $M = 150$ and $R = 76$

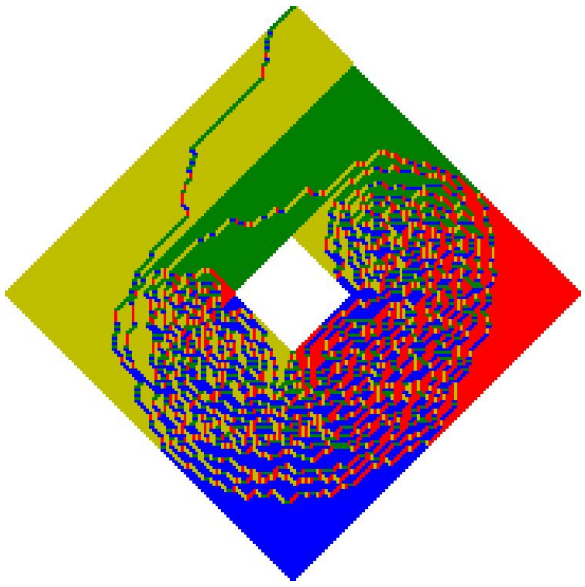

Figure 2.12: A domino tiling of $\mathcal{AD}_{50}$ with $M = 200$ and $R = 88$

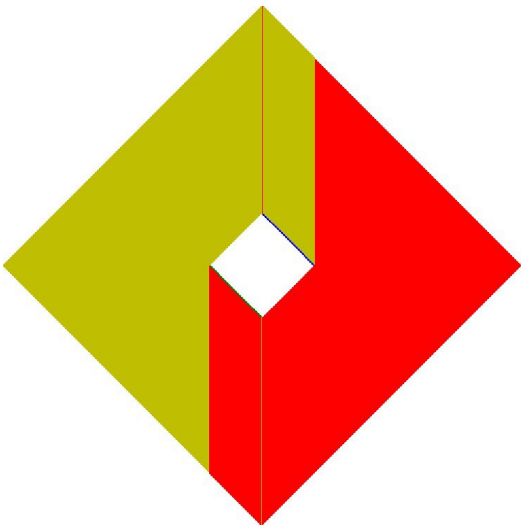

Figure 2.13: A domino tiling with the minimal height change $R = -300$. Almost all the dominoes are vertical.

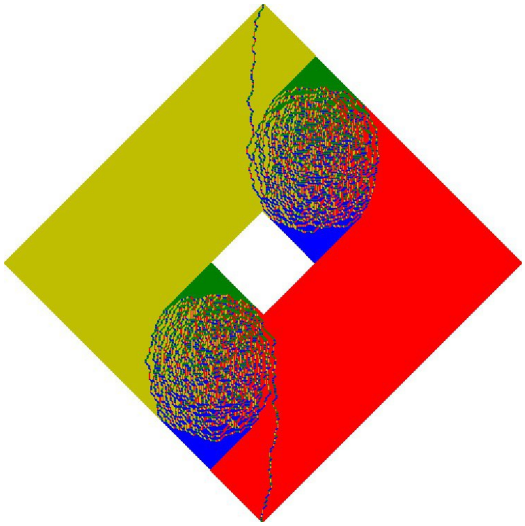

Figure 2.14: A typical domino tiling with the minimal height change $R = -300$.

Chapter 3

A variational principle for the dimer model in multiply-connected domains

Abstract

We study random dimer covers of a large multiply-connected domain of a doubly-periodic lattice with arbitrary positive weights. We encode such a dimer cover by the discrete height function defined on a universal cover of the domain. It allows us to prove that in the limit as the domain grows, the random normalized height function converges to a deterministic continuous Lipschitz function $\mathfrak{h}^\star$. Moreover, this function can be found as a unique minimizer of a certain convex functional.

3.1 Introduction to the dimer model on generic lattice

In this Chapter, we extend results from Chapter 2 for generic lattice. The main strategy remains the same, but some key players need to be changed. The main difference is that we work with the dual graph to the one in Chapter 2, and instead of the lattice $\mathbb{Z}^2$, we work with $\mathbb{Z}^2$-periodic lattice Λ. It means that instead of domino tilings, we are dealing with the perfect matching of the dual graph. It also requires a change in notations for the height function, which becomes a function on the faces of the dual graph. These changes, however, still allows formulation of the thermodynamic limit as the mesh of the lattice goes to 0. In asymptotic description, we, basically, repeat the same steps. The main difference is that here we prove the concentration inequality since we cannot apply them directly from [CKP00], as we did in Chapter 2.

3.1.1 Dimer covers

In this subsection we recall basic facts of the dimer model on a planar bipartite graph for further details see [Ken09; KOS06].

Let Γ be a finite bipartite planar graph with the set of vertices $\mathbf{V}(\Gamma)$ and set of edges $\mathbf{E}(\Gamma)$. A *dimer configuration*, also known as a *dimer cover*, on Γ is a subset of edges called dimers $D \subset \mathbf{E}(\Gamma)$ such that each vertex of Γ is adjacent to exactly one dimer from D. Denote the set of dimer configurations on Γ by $\mathfrak{Conf}(\Gamma)$. One can orient edges from white vertices to black ones, call this orientation *the bipartite orientation*.

One of the basic operations over dimer covers is rotation along a cycle, see 2.3.2 in [KOS06]. Suppose $\gamma := (b_1.w_1, b_2, w_2, \cdots, b_k, w_k, b_{k+1})$ is a cycle on Γ with b_i being black

vertices, and w_i being white ones with $b_{k+1} = b_1$. There are two dimer covers of γ, D_γ consisting of edges $\{(b_i, w_i)\}_{i=1}^k$, and the other one formed by the edges $\{(w_i, b_{i+1})\}_{i=1}^k$. Once we take a dimer cover D that includes D_γ, we can always get another dimer cover that coincides with D everywhere except on γ, which we cover by the second dimer configuration of γ. The resulting dimer cover is called the rotation of D along cycle γ and denoted $D\Delta\gamma$.

Having two dimer configurations D and D' on Γ define their symmetric difference $C(D, D') := D \cup D' / D \cap D'$. Connected components of $C(D, D')$ are called *composition cycles* of dimer configurations D and D'. Also note that one can orient D' in the opposite direction to the bipartite orientation, which orient composition cycles of D and D' compatibly with orientation of D, see Figure 3.1. Clearly, definitions of composition cycle and rotation along cycle allow us to express the dimer configuration D' in terms of dimer configuration D and their composition cycles $C(D, D')$, $D\Delta(C(D, D')) = D'$, see example on Figure3.1.

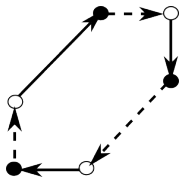

Figure 3.1: Example of dimer covers D in bold, and D' in dashed. Their symmetric difference $C(D, D')$ is the hexagon with one composition cycle, the clockwise oriented hexagon.

3.1.2 Boundary condition of dimer cover

We also need dimer covers with a given boundary condition, and prior to that define boundary $\partial\Gamma$ to be the subgraph of Γ that consists of one-valent vertices (boundary vertices) $\mathbf{V}(\partial\Gamma)$, one-valent edges (boundary edges) $\mathbf{E}(\partial\Gamma)$ and boundary faces $\mathbf{F}(\partial\Gamma)$, which are adjacent to $\mathbf{E}(\partial\Gamma)$ and $\mathbf{V}(\partial\Gamma)$. We call vertices $\mathbf{V}(\Gamma) \setminus \mathbf{V}(\partial\Gamma)$ internal vertices, similarly for edges and faces.

A dimer configuration D on Γ induces a partition of $\mathbf{V}(\partial\Gamma)$ into a subset of vertices occupied by dimers and the other ones. Let us denote the set of occupied boundary vertices by $\alpha \subset \mathbf{V}(\partial\Gamma)$. Now, a dimer cover with a boundary condition α is a set of edges of Γ that are adjacent to all internal vertices of Γ, and to all vertices of α. See example on Figure 3.2. Here,

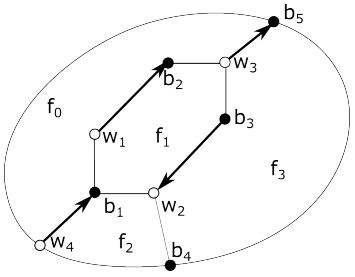

Figure 3.2: Example of Γ non-trivial boundary. See description in Discussion (3.1.2)

the boundary vertices $\mathbf{V}(\partial\Gamma) = \{w_4, b_4, b_5\}$, boundary edges $\mathbf{E}(\partial\Gamma) = \{(w_4, b_1).(w_3, b_5)\}$ and the boundary faces $\mathbf{F}(\partial\Gamma) = \{f_0, f_2, f_3\}$. It is important that the graph Γ itself does not admit any dimer configurations, we simply have 5 black vertices and 4 white ones. However, if we look at dimer configurations with $\alpha = (w_4, b_4)$, there is a dimer configuration with this boundary condition α(we could also choose b_5 instead of b_4).

3.1.3 Height function

A common way of encoding a dimer cover D is through a discrete function, so-called the height function H_D. This parametrization is suitable for the scaling limit, where the height function is going to approximate a continuous Lipschitz function.

In order to define H_D, recall that symmetric difference between two dimer covers D, D' consists of oriented loops denoted by $C(D, D')$. Also, note that D and D' are related by a rotation along $C(D, D')$.

Each dimer cover D defines a white to black flow $\varphi(D)$ on edges of Γ, which takes the value $+1$ for an edge with a dimer oriented with respect to bipartite orientation. Once we have two such flows $\varphi(D), \varphi(D')$ their difference $\varphi(D) - \varphi(D')$ is divergence-free flow, at each vertex of Γ two flows either coincide and cancel each other, or one goes to the vertex, whereas the other goes from the vertex.

The total flux of it between two faces, a fixed reference face f_0, and f along a path γ is defined as follows. The path intersects $C(D, D_0)$ at edges e_i where $(\varphi(D) - \varphi(D_0))(e_i) \neq 0$. Let us denote the set of such edges as $e_i \in \gamma \cap C(D, D_0)$. Then, using the bipartite orientation, we can attach a sign $+1$ for each intersection in a positive direction, and -1 otherwise, denote this sign $\langle (\varphi(D) - \varphi(D_0))(e_i), \gamma \rangle$. Now we can write an expression for the height function as a sum of signs of the intersections along γ.

Definition 3.1.1. The height function is a map $H_{D,D_0} : \tilde{\Gamma}^\star \to \mathbb{Z}$ defined by the following two conditions,

1. $H_{D,D_0}(f_0, \gamma_0) = 0$ for fixed $(f_0, \gamma_0) \in \mathcal{D}(\Gamma)$
2. Value at a face f can be computed as following,

$$H_{D,D_0}(f, \gamma) = \sum_{e_i \in \gamma \cap C(D,D_0)} \langle (\varphi(D) - \varphi(D_0))(e_i), \gamma \rangle \tag{3.1.1}$$

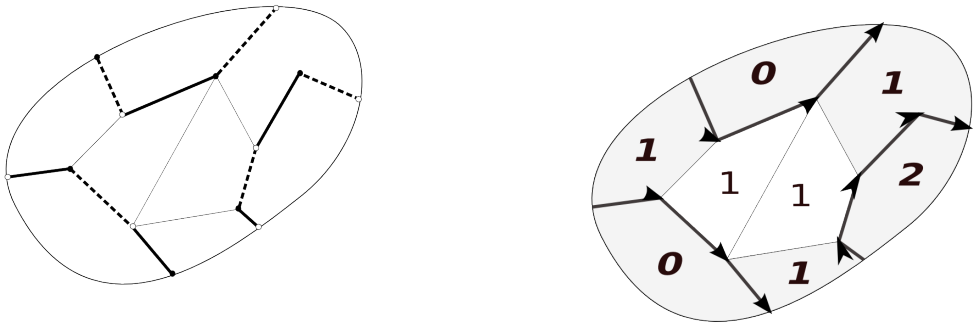

Figure 3.3: Example of two dimer covers, D with fat edges, and D' with dashed ones on the left, and the corresponding height function on the right. Boundary faces are colored in gray. The reference face f_0 is the bottom left one.

This way the level sets of this function are precisely the composition cycles $C(D, D')$, see Figure 3.3, Figure 3.4.

For a simply-connected Γ, i.e., without non-trivial loops, the height function does not depend on γ, and has two important properties.

Proposition 3.1.2. *1. A reference face f_0 with the value $H_{D,D_0}(f_0)$ uniquely determines the function H_{D,D_0} for given D and D_0.*

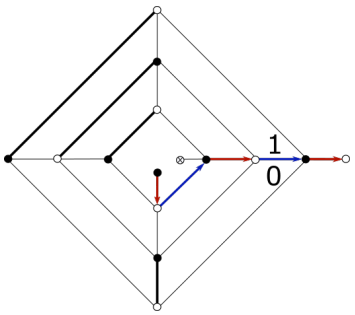

Figure 3.4: Two dimer covers D_1, D_2 that agree at fat black edges, while disagree on the red and on the blue edges(they form composition cycle $C(D_1, D_2)$). Height function H_{D_1,D_2} gets increment ± 1 after going around the center. Here, the boundary of Γ is empty.

2. Boundary height function $H_{D,D_0}|_{\partial\Gamma}$ is fixed for given D_0, f_0.

Proof. Indeed, let us take two different paths γ_1 and γ_2. By the assumption, they are related by a continuous transformation. Thus, this transformation will respect intersections of the paths with composition cycles with their parity, and the values $H_{D,D_0}(f, \gamma_1)$, $H_{D,D_0}(f, \gamma_2)$ differ by a rearrangement of the terms. □

However, in graphs with non-trivial loops, these properties typically fail. A value $H_{D,D_0}(f)$ now may depend on the path γ, as we see on Figure 3.4. Dimer covers D and D_0 from the figure have different boundary conditions, and their composition cycle goes from one connected boundary component to the other one, which creates the monodromy after going around the center.

Note that after going around a loop ψ, the value $H_D(f)$ changes by an additive monodromy $M(\psi)$.

$$H_D(f, \psi \circ \gamma) = H_D(f, \gamma) + M(\psi). \tag{3.1.2}$$

Later we assume that γ is such a path that $(p, \gamma) \in \mathcal{D}(\Gamma)$. This way, we define functions on $\mathcal{D}(\Omega)$, which determine them uniquely by Proposition 2.2.2.

After such a modification, we can recover the dimer cover D from H_{D,D_0} and D_0 even on a multiply-connected graph. From the height function we know its level sets $C'(H_{D,D_0})$, thus we can get D from D_0 by rotation of D_0 along each $C'(H_{D,D_0})$. This clearly recovers the original dimer cover, this can be formulated as the following proposition,

Proposition 3.1.3 (Proposition 5.1 [CR08])**.** *Elements of $\mathfrak{Conf}(\Gamma)$ for a fixed reference face f_0 with a reference dimer cover D_0 are in bijection with height functions $H_{D_0,D}$ on Γ.*

3.1.4 Height change and boundary heights

Once the composition cycle of two dimer covers D_1 and D_2 have a loop around a hole, boundary conditions of $H_{D_1,D_0}|_{\partial\Gamma_i}$ and $H_{D_2,D_0}|_{\partial\Gamma_i}$ differ by 1, where Γ_i is connected boundary component around that hole. Therefore, boundary condition splits into two parts.

Let us define the boundary condition of H_{D,D_0} in a multiply-connected domain as a fixed function on each connected boundary component $\{B_i\}_{i=1}^g$ that does not depend on D called boundary heights, and additive shifts $\{R_i\}_{i=1}^g$ called the height change, which depend on D.

Due to the above reasons, a boundary condition is a family of boundary heights B_i on each connected boundary component $\partial\Gamma_i$ such that $H_{D,D_0}(f, \gamma)|_{\Gamma_i} - H_{D,D_0}(f_i, \gamma) = B_i(f)$ for a base face $f_i \in \mathbf{F}(\Gamma_i)$. One can further fix $H_{D,D_0}(f_i, \gamma_i) = R_i(D)$ for an integer constants

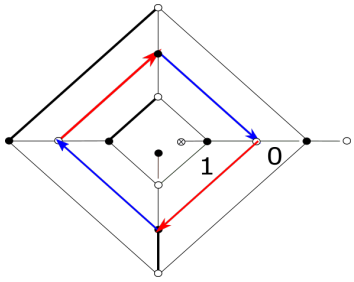

Figure 3.5: Example of two dimer covers(their composition cycle consists of colored edges) with different boundary heights.

$R_i(D)$ called the height change of dimer cover D and a family of paths γ_i that stays inside $\mathcal{D}(\Omega)$. We also call a set of integers $\{R_i\}_{i=1}^g$ an admissible height change if there is a dimer cover this with height change.

Therefore, a boundary condition of the height function H_{D,D_0} splits into boundary heights $\{B_i\}_{i=1}^g$ independent of D, and height change $\{R_i\}_{i=1}^g$ that depend on D.

3.1.5 Pointwise maximum and minimum of height function, co-cycle identity

One of the important property of the height function is co-cycle identity, which follows immediately from Definition 3.1.1, see also section 5.2 [CR08],

$$H_{D,D_1} + H_{D_1,D_2} = H_{D,D_2} \tag{3.1.3}$$

With this identity, it is easy to see that the pointwise maximum of two height functions with a given reference dimer cover is again a height function.

Proposition 3.1.4. *For any two given dimer covers D, D_0 there exists such a dimer cover $\check{D}$ that the pointwise maximum (minimum) of two height functions H_{D,D_0} and H_{D',D_0} is a height function of $\check{D}$*

$$\max\{H_{D,D_0}, H_{D',D_0}\} = H_{\check{D},D_0} \tag{3.1.4}$$

In fact, this is a generalization of the fact for the square grid. There, in a simply-connected region any two domino tilings are linked by a sequence of flips. And to obtain the pointwise maximum, we need to flip each square in case it increases the height.

Proof. Height functions of two dimer covers D and D' differ by $H_{D,D'}$ by the identity (3.1.3), therefore their pointwise maximum $\check{H}_{\check{D}}$ corresponds to the dimer cover $\check{D}$ that can be obtained from D after rotation along cycles $C(D, D')$ which increase the value of height function. Height change of $H_{\check{D},D_0}$ is maximum between those of H_{D,D_0} and H_{D',D_0}. Similarly, one sees the analogous statement for pointwise minimum.

$$\min\{H_{D,D_0}, H_{D',D_0}\} = H_{\check{D},D_0} \tag{3.1.5}$$

where $\check{D}$ is obtained from D after rotation along composition cycles $C(D', D)$ with the opposite orientation compared with the situation with the pointwise maximum. □

3.1.6 Weight system and Boltzmann distribution on dimer configurations

Let us introduce a probability distribution on the set of dimer covers.

A *weight system* on Γ is a map from the set of dimer covers $\mathfrak{Conf}(\Gamma)$ to positive numbers $\mathbb{R}_{>0}$. A weight system w defines a Boltzmann distribution on the set of dimer covers. For a $D \in \mathfrak{Conf}(\Gamma)$ let us define its probability by (3.1.6),

$$\mathbb{P}(D) := \frac{w(D)}{Z(\Gamma)} \tag{3.1.6}$$

where $D \in \mathfrak{D}(\Gamma)$ and $Z(w;\Gamma)$ is a normalization constant called the partition function:

$$Z(\Gamma) = \sum_{D \in \mathfrak{Conf}(\Gamma)} w(D). \tag{3.1.7}$$

We shall focus on a particular type of weight systems called *edge weight systems*. Let us assign to each edge e of Γ a positive real number $w(e)$ called the weight of the edge e. The associated edge weight system on $\mathfrak{Conf}(\Gamma)$ is given by

$$w(D) = \prod_{e \in D} w(e) \tag{3.1.8}$$

where the product goes over all edges contained in D.

In statistical mechanics, these weights are called Boltzmann weights. Their physical meaning can be expressed by the following formula:

$$w(e) = \exp\left(\frac{-E(e)}{kT}\right), \tag{3.1.9}$$

where $E(e)$ is the energy of the dimer occupying the edge e, T is the absolute temperature and k is the Boltzmann constant.

3.2 Doubly-periodic dimer model

Although the dimer model on generic graphs has lots of interesting features, we are mostly interested in doubly-periodic graphs, which allow us to study asymptotic behavior of dimer covers. Let Λ be a $\mathbb{Z}^2$-periodic bipartite planar graph. By this, we mean that Λ is a bipartite graph embedded into the plane $\mathbb{R}^2$ so that translations of $\mathbb{Z}^2$ act by color-preserving isomorphisms of Λ – isomorphisms which preserve the color of vertices.

Later on we will need finite sub-graphs of Λ, call them *lattice regions*. Λ is fixed in all the following discussion. Two typical examples of such an Λ are a square lattice and a honeycomb lattice.

We also need in the fundamental domain of Λ defined as $\Lambda_1 := \Lambda/\mathbb{Z}^2$ and a torus made of $N \times N$ Λ fundamental domains, $\Lambda_N := \Lambda/N\mathbb{Z}^2$. Let us fix D_0 to be a dimer cover of Λ_1 extended to a dimer cover of Λ by periodicity.

3.2.1 Doubly-periodic weight systems and Boltzmann distribution

We will be interested in height functions defined on Λ, thus let us mention some of their properties, which follow directly from the definition.

3.2.2 Newton polygon

Let us recall the next ingredient from section 3 in [KOS06], characteristic polynomial of Λ_1 and its Newton polygon. Let us modify weight system on Λ_1 by multiplying weights by $z^{\pm}1$ and $w^{\pm 1}$ depending on intersection of edges that cross horizontal γ_x and vertical γ_y. If an edge intersects γ_x such that the black vertex is on the left, we multiply the weight of the edge by z, and by z^{-1} otherwise. Similarly, for γ_y and w. Then, the characteristic polynomial of Λ_1 is the partition function of the fundamental domain Λ_1 with such weight system $P(z,w) := Z(\Lambda_1)$. For more details, see 3.1.3 in [KOS06]. The Newton polygon of $P(z,w)$ is defined as follows,

$$\mathcal{N}_\Lambda := \text{Convex hull}\{(i,j) \in \mathbb{Z}^2 | z^i w^j \text{ is a monomial in } P(z,w)\} \tag{3.2.1}$$

A different change of D_0 shifts $\mathcal{N}_\Lambda$ by a constant integer vector. The important property of $\mathcal{N}_{\Lambda_1}$ is that it is the set of allowed slopes of the height function: for each point of the Newton polygon, there is a height function on Λ_N with this slope, maybe asymptotically for large N, see Proposition 3.2 in [KOS06].

3.2.3 Surface tension

For fixed $(s,t) \in \mathbb{R}^2$ we denote by $\mathfrak{Conf}_{s,t}(\Lambda_N)$ the set of dimer covers on Λ_N, that have a height change $(\lfloor Ns \rfloor, \lfloor Nt \rfloor)$.

Consider the normalized partition function of dimer covers with the fixed slope $(\lfloor Ns \rfloor, \lfloor Nt \rfloor)$ of Λ_N, denote the set of such dimer covers $\mathfrak{Conf}_{s,t}(\Lambda_N)$, the normalized partition function $Z_{s,t}(\Lambda_N)$ is defined as

$$Z_{s,t}(\Lambda_N) = N^{-2} \log \sum_{D \in \mathfrak{Conf}_{s,t}(\Lambda_N)} w(D). \tag{3.2.2}$$

This expression admits a limit as $N \to \infty$ and the answer is

$$\lim_{N\to\infty} Z_{s,t}(\Lambda_N) = -\sigma(s,t) \tag{3.2.3}$$

Here σ is minus Legendre transform of Ronkin function of $P(z,w)$,

$$R(B_x, B_y) := \frac{1}{(2\pi i)^2} \iint_{|z|=e^{B_x}, |w|=e^{B_y}} \log P(z,w) \frac{dzdw}{zw} \tag{3.2.4}$$

From the corollary 3.7 from [KOS06], σ is a convex function on $\mathcal{N}$ and strictly convex in the interior of the Newton polygon $\mathcal{N}$ [1].

3.3 Properties of the height functions

3.3.1 Lattice Lipschitz condition for the height function

In this subsection, we are dealing with a finite connected subset of $\Gamma \subset \Lambda$ called a lattice domain. Let $\mathcal{X}(f - f')$ be pointwise maximum over all height functions whose value at a face $f' \in \mathbf{F}(\Gamma)$ is zero, and call it the support height function based at face f. The motivation of the term will be seen later in the paper, in the scaling limit $\mathcal{X}(f)$ converges to the support function of a convex polygon, the Newton polygon $\mathcal{N}$.

The difference between values of a height functions H_{D,D_0} at faces f and f' is always bounded by the value of the support height function based at face f'.

[1] In our notations of σ we follow [KOS06], so they differ from the notations in [CKP00] by the sign of σ.

Proposition 3.3.1. *Values of a height function H_{D,D_0} at faces f, f' satisfy the following inequality*

$$H_{D,D_0}(f,\delta) - H_{D,D_0}(f',\delta') \le \mathcal{X}(f-f') + M(\delta^{-1}\delta'). \tag{3.3.1}$$

Proof. Let us shift the height function H_{D,D_0} by its value at (f',δ'),

$$H_{D,D_0} \mapsto H_{D,D_0}(f,\delta) - H_{D,D_0}(f',\delta). \tag{3.3.2}$$

We get a height function that vanishes at f', and thus, is bounded by $\mathcal{X}(f-f')$ by definition. The factor $M(\delta^{-1}\delta')$ keeps on whether we make a non-trivial loop by computing the difference. □

3.3.2 Criterion of extension and maximal extension

Recall a simple property of Lipschitz function on a compact domain. Suppose that $\Omega \in \mathbb{R}^2$ is a compact planar set, and g is a function on $\partial\Omega$ that satisfies $|g(x)-g(y)| \le |x-y|$ for $x, y \in \partial\Omega$. Then, it extends to Ω by the function $f_g(x) := \max_{y\in\partial\Omega}\{g(y) - |x-y|\}$. and it is the minimal extension of g.

The aim of this subsection is to mimic the property above for the height function, and to deduce the criterion of extension of boundary height function B from the boundary $\partial\Gamma$ to lattice domain Γ.

Proposition 3.3.2. *Suppose that f and f' are boundary faces of Γ and boundary height function B satisfies the lattice Lipschitz condition*

$$B(f) - B(f') \le \mathcal{X}(f-f'). \tag{3.3.3}$$

Then, there is a height function H_{D,D_0} on Γ that extends B.

Proof. Let us define the maximal height function $H^{\max}(f)$ that extends B,

$$H^{\max}(f) := \min_{f'\in\partial\Gamma}\{B(f') + \mathcal{X}(f-f')\}. \tag{3.3.4}$$

Each $B(f') + \mathcal{X}(f-f')$ is a height function for fixed f', and pointwise minimum is, as well, a height function by Proposition (3.1.4). It is easy to check that it has boundary conditions B from the lattice Lipschitz condition and definition of H. $H(f)$ □

There is analogues formula for the maximal extension of boundary height function,

$$H^{\max}(f) := \max_{f'\in\partial\Gamma}\{B(f') - \mathcal{X}(f-f')\}. \tag{3.3.5}$$

Let us discuss example of the support function, which we already saw in the Chapter 2. We follow exposition from example 29.4(b) [RLa92]. Let K be the square in $\mathbb{R}^2$ with vertices at $(0,\pm1)$ and $(\pm1,0)$. For a given vector $u = (2,1)$ we want to maximize the linear form $\langle k, u\rangle$ where $k \in K$. The maximum is archived on the vector $(1,0)$, $\langle (1,0),(2,1)\rangle = 2$. In general, $\theta_K(u) = \max u_1, u_2$ where $u = (u_1, u_2)$.

3.4 Scaling limit of the dimer model

For the later purposes, it is worth giving notations in more general context. Suppose that $\mathcal{K} \subset \mathbb{R}^2$ is a compact convex set and let $<\cdot,\cdot>$ be the standard scalar product on $\mathbb{R}^2$. In the dimer model $\mathcal{K} = \mathcal{N}_\Lambda$, and in Chapter 2 we had used it in the definition of asymptotic height functions, $\nabla\mathfrak{h} \in \mathcal{N}_\Lambda$, or more explicitly $|\mathfrak{h}_x| + |\mathfrak{h}_y| \le 2$. The relation between the Newton polygon and the inequality is the following.

Suppose we have a linear map $\ell(x) = \ell(x_1, x_2) := ax_1 + bx_2$ defined on $\mathbb{R}^2$ with $(a, b) \in \mathcal{K}$. The value of $\ell(x)$ is bounded by the supremum of the values of linear functionals k with slope in $\mathcal{K}$ over $\mathcal{K}$,

$$\ell(x) \le \theta_{\mathcal{K}}(x) := \sup_{k \in \mathcal{K}} \{\langle k, x\rangle\}. \tag{3.4.1}$$

. The function $\theta_{\mathcal{K}}$ is called *the support* function of $\mathcal{K}$. Also define the *polar set* of $\mathcal{K}$, $\mathring{\mathcal{K}} := \{x \in \mathbb{R}^2 | \langle x, k\rangle \le 1 \forall k \in \mathcal{K}\}$. This set is also a convex compact set. It is easy to check an alternative definition, $\theta_{\mathcal{K}}(x) = \min\{\lambda \ge 0 | \frac{x}{\lambda} \in \mathcal{K}\}$. From it, we see that $\theta_{\mathcal{K}}(x) \le 1$ implies $x \in \mathcal{K}$. Furthermore, the support function is positively homogeneous, $\theta_{\mathcal{K}}(\alpha x) = \alpha \theta_{\mathcal{K}}(x)$ and $\theta_{\mathcal{K}}(\alpha x)$ is a convex function. Therefore, it defines a norm. However, this norm might be non-symmetric if $\mathcal{K}$ is not centrally symmetric. The most important property is that a linear function with gradient (slope) $\nabla f \in \mathcal{K}$ is by definition bounded from above by the value of the support function θ_K, whose value at a point is the maximal value of the linear function with slope in $\mathcal{K}$. Therefore, a continuous function $\mathfrak{h}$ with $\nabla \mathfrak{h} \in \mathcal{K}$ satisfy the Lipschitz property $\mathfrak{h}(x) - \mathfrak{h}(y) \le \theta_{\mathcal{K}}(x - y)$.

It is useful to keep in mind three examples, 1-Lipschitz functions, where $\mathcal{K}$ is just a unit disk and $\theta_{\mathcal{K}}(x) = |x|$. In the Chapter 2, however, have a more complicated situation. For the Newton polygon of the square grid, the rhombus $\mathcal{N}_{\mathbb{Z}^2} = \{(s, t) \in \mathbb{R}^2 | |s| + |t| \le 2\}$, while the norm we used is twice the ∞-norm $2|(x, y)|_\infty := 2\max\{|x|, |y|\}$. The unit ball in this norm is a square $B_1 := \{(x, y) \in \mathbb{R}^2 | \max\{|x|, |y|\} \le 2\}$. The relation between these two sets is that they are polar dual of each other.

The unit ball in this norm is the set of points v such that $1 = \theta_\Lambda(v) = \sup_{a \in \mathcal{N}_\Lambda} \langle v, a\rangle$, which is by definition the boundary of $\mathring{N}_\Lambda$, the polar dual of $\mathcal{N}_\Lambda$.

The support function is clearly a Lipschitz function and thus, it has a gradient almost everywhere by the Rademacher theorem, and further, the slope of the support function lies on $\partial\mathcal{K}$. This is due to the fact that in time 1 it reaches ∂K. Its value at $x = (0, 0)$ is 0 and it is the maximal function among continuous functions with the value 0 at $(0, 0)$. Therefore, we obtain the following Lipschitz condition

$$\mathfrak{h}(x) - \mathfrak{h}(y) \le \theta_\Lambda(x - y). \tag{3.4.2}$$

Simply because the function $x \mapsto \mathfrak{h}(x) - \mathfrak{h}(y)$ for a fixed y, is an asymptotic height function, which vanishes at $x = y$. Therefore, its value is bounded by the maximal such function θ. Let us call it the *Support Lipschitz condition*.

With the help of θ_Λ, this definition can be rewritten as

$$\mathscr{H}(\Omega) := \{\mathfrak{h} : \Omega \to \mathbb{R} \mid \mathfrak{h}(x) - \mathfrak{h}(y) \le \theta_\Lambda(x - y)\}, \tag{3.4.3}$$

3.4.1 Asymptotic height functions

Following the literature [KOS06; CKP00] let us define a set of asymptotic height functions on planar domain $\Omega \subset \mathbb{R}^2$ as a subspace of the space of Lipschitz functions on Ω, $Lip(\Omega)$ with the constraint on their gradient,

$$\mathscr{H}(\Omega) := \{\mathfrak{h} \in Lip(\Omega) \mid \nabla \mathfrak{h} \in \mathcal{N}_\Lambda \text{ almost everywhere}\}. \tag{3.4.4}$$

An equivalent way to encode asymptotic height functions is saying that they are Lipschitz functions in the norm induced by the Newton polygon. The norm is given by the support function of the Newton polygon $\mathcal{N}_\Lambda$. Abusing notations, we denote the support function of the Newton polygon $\mathcal{N}_\Lambda$ by θ_Λ.

As the example of the square grid shows (2.6), one should change this norm to the intrinsic one,

$$\|x-y\|_\infty^\Omega := \inf_\gamma \int_0^1 \theta_\Lambda(\gamma'(t))dt. \tag{3.4.5}$$

Important fact of asymptotic height functions is compactness of the space of asymptotic height functions with a given boundary conditions $\mathfrak{b}$, call this space $\mathscr{H}(\Omega,\mathfrak{b})$. Further introduce its close subset of asymptotic height functions with a given boundary conditions and a given asymptotic height change $\mathfrak{r} := \{r_i\}_{i=1}^g$, $(\Omega,\mathfrak{b},\mathfrak{r})$.

Both spaces trivially extend to the universal covering space $\tilde{\Omega}$, and their compactness still holds.

Fix a set of points $\{(x_i,\gamma) \in \mathcal{D}(\Omega) | x_i \in \partial\Omega_i\}$ and a monodromy data, i.e., a map $\mathfrak{m} : \pi_1 \to \mathbb{R}$ such that $\mathfrak{m}(\gamma\cdot\gamma') = \mathfrak{m}(\gamma)+\mathfrak{m}(\gamma')$ and $\mathfrak{m}(\gamma^{-1}) = -\mathfrak{m}(\gamma)$. Also, let $r := \{r_i\}_{i=0}^g$ be a sequence of real numbers and denote point $z = (z_1,z_2) \in \Omega$. A function $\mathfrak{h}$ is an asymptotic height function with height change $r = \{r_i\}_{i=1}^g$ and monodromy $\mathfrak{m}$ if the following holds,

- $\mathfrak{h}\big|_{\partial\Omega_i}(x) - \mathfrak{h}(x_i) = \mathfrak{b}_i(x)$
- $\mathfrak{h}(x_i,\gamma_i) = r_i$,
- $\mathfrak{h}$ satisfy the intrinsic support Lipschitz on Ω, that is $|\mathfrak{h}(x,\delta) - \mathfrak{h}(y,\delta')| \le \|x-y\|_\infty^\Omega + \mathfrak{m}(\delta^{-1}\delta')$ and $\nabla\mathfrak{h} : \Omega \to \mathcal{N}_\Lambda$
- after going around a loop δ', values of $\mathfrak{h}$ changes as follows: $\mathfrak{h}(x,\delta'\cdot\delta) = \mathfrak{h}(x,\delta)+\mathfrak{m}(\delta')$.

It is important to mention that numbers r_i for asymptotic height function take their values in intervals due to the Lipschitz constraint, $-\|x_i-x_0\|_\infty^\Omega \le r_i \le \|x_i-x_0\|_\infty^\Omega$.

Let $\mathscr{H}(\Omega,\mathfrak{m},\mathfrak{b}_r)$ be the space of asymptotic height functions with monodromy $\mathfrak{m}$ and boundary condition $\mathfrak{b}_r$. Also define a union of $\mathscr{H}(\Omega,\mathfrak{m},\mathfrak{b}_r)$ over all possible height changes r, $\mathscr{H}(\Omega,\mathfrak{m},\mathfrak{b}) := \bigcup_r \mathscr{H}(\Omega,\mathfrak{m},\mathfrak{b}_r)$.

Theorem 3.4.1. *The spaces $\mathscr{H}(\Omega,\mathfrak{b},\mathfrak{m})$ and $\mathscr{H}(\Omega,\mathfrak{b}_r,\mathfrak{m},r)$ are compact spaces with respect to the intrinsic norm.*

Proof. The idea of the proof is to show compactness of the space of functions on the fundamental domain that will lead us to compactness of $\mathscr{H}(\Omega,\mathfrak{b},\mathfrak{m})$. Then, $\mathscr{H}(\Omega,\mathfrak{b}_r,\mathfrak{m},r)$ is compact as a closed subset of $\mathscr{H}(\Omega,\mathfrak{b},\mathfrak{m})$.

Recall that by Proposition 2.2.2, the behavior of these functions is determined by their values on $\mathcal{D}(\Omega)$. Thus, it is sufficient to show compactness of $\mathscr{H}(\mathcal{D}(\Omega),\mathfrak{b})$. In order to show it, one can apply Arzela-Ascoli theorem. The first requirement, the existence of a uniform bound for the functions $f \in \mathscr{H}(\mathcal{D}(\Omega),\mathfrak{b})$, is satisfied because of the boundary condition $\mathfrak{b}$ that is fixed on $\partial\Omega_0$. The equicontinuous follows directly from the Lipschitz condition. Then, these function with a given monodromy data $\mathfrak{m}$ form a closed subspace of $\mathscr{H}(\mathcal{D}(\Omega),\mathfrak{b})$. Thus, it is a compact space. The same works for the subspace with a given height change r and a fixed monodromy data $\mathfrak{m}$, $\mathscr{H}(\Omega,\mathfrak{b}_r,\mathfrak{m},r)$. The latter is, again, a compact space as a closed subset of $\mathscr{H}(\Omega,\mathfrak{b},\mathfrak{m})$. □

Theorem 3.4.2. *Spaces of asymptotic height functions $\mathscr{H}(\tilde{\Omega},\mathfrak{b})$ and $\mathscr{H}(\tilde{\Omega},\mathfrak{b}.\mathfrak{r})$ are compact with respect to the intrinsic norm given by $\mathcal{N}_\Lambda$.*

Proof. Let us use Arzela–Ascoli theorem to obtain compactness of the $\mathscr{H}(\mathcal{D}(\Omega),\mathfrak{b})$. Since asymptotic height functions satisfy the Lipschitz condition, they are equicontinuous, and they are also uniformly bounded because of the boundary condition $\mathfrak{b}$ fixed on the external

boundary of Ω. The last detail is that condition $\nabla\mathfrak{h} \in \mathcal{N}_\Lambda$ is a closed constraint. Therefore, we have compactness of $\mathscr{H}(\mathcal{D}(\Omega), \mathfrak{b})$, which is isomorphic to $\mathscr{H}(\tilde{\Omega}, \mathfrak{b})$ by Proposition **??**. Here the compactness is with respect to sup norm, and applying a partition of unity that vanishes outside Ω, we obtain compactness with respect to the intrinsic norm. The space $\mathscr{H}(\tilde{\Omega}, \mathfrak{b}.\mathfrak{r})$ is compact as a closed subset of $\mathscr{H}(\tilde{\Omega}, \mathfrak{b})$ □

Immediately from the compactness we obtain existence and uniqueness of the minimizer of $\mathcal{F}$ over these spaces. Recall the expression of function $\mathcal{F} : \mathfrak{h} \mapsto \iint_\Omega \sigma(\nabla\mathfrak{h})dxdy$.

Corollary 3.4.2.1. *There exists a unique minimizer $\mathfrak{h}^\star$ of functional $\mathcal{F}$ over the space $\mathscr{H}(\tilde{\Omega}, \mathfrak{b})$.*

There is a unique minimizer $\mathfrak{h}^\star_r$ of $\mathcal{F}$ over the space $\mathscr{H}(\tilde{\Omega}, \mathfrak{b}.\mathfrak{r})$.

Proof. The proof is the same as for the case of $\Lambda = \mathbb{Z}^2$ in Theorem 2.7.1.

Consider a fundamental domain $\mathcal{D}(\Omega)$ for action of $\pi_1(\Omega)$ on the universal covering space of Ω. Recall that by Proposition **??**, it is sufficient to find a minimizer of $\mathcal{F}$ on $\mathcal{D}(\Omega)$.

The boundary $\partial\mathcal{D}(\Omega)$ consists of two parts, $\partial\mathcal{D}(\Omega) = \partial\Omega \bigsqcup \partial\mathcal{D}^1(\Omega)$, the first one is supplemented with boundary condition $\mathfrak{b}$ and the other one is the union of $2g$ curves $\{\upsilon_i\}_{i=1}^{2g}$ matched in pairs υ_i, υ' with free boundary conditions subject to periodicity across the pairs so that the values on υ_i coincide with the values on υ_i'(recall that υ_i and υ_i' were obtained by the cut along the curve γ_i)

The space $\mathscr{H}(\Omega, \mathfrak{m}, \mathfrak{b})$(resp. $\mathscr{H}(\Omega, \mathfrak{m}, \mathfrak{b}_r, r)$) is compact by Theorem 2.4.4. Then, $\mathcal{F}$ is upper semi-continuous on spaces $\mathscr{H}(\Omega, \mathfrak{m}, \mathfrak{b}_r, r)$ and $\mathscr{H}(\Omega, \mathfrak{m}, \mathfrak{b})$. This follows from Lemma 2.1 from [CKP00], which uses only the convexity of σ and the Lipschitz condition, and thus, trivially extends to partially free periodic boundary conditions.

Therefore, there exists the minimizer $\mathfrak{h}^\star$ of $\mathcal{F}$ on $\mathscr{H}(\Omega, \mathfrak{m}, \mathfrak{b})$ (resp. there exists the minimizer $\mathfrak{h}^\star_r$ on $\mathscr{H}(\Omega, \mathfrak{m}, \mathfrak{b}_r, r)$). By the same convexity argument as in Lemma 2.4 from [CKP00], this minimizer is unique.

A priori $\mathfrak{h}^\star$ and $\mathfrak{h}^\star_r$ depend on a particular choice of the fundamental domain $\mathcal{D}(\Omega)$. However, since gradients of functions from $\mathscr{H}(\tilde{\Omega}, \mathfrak{b})$ are well-defined objects on Ω by Lemma 2.2.1 and σ is strictly convex everywhere in the interior of the domain of definition [CKP00; KOS06], we can use Proposition 4.5 from [DS08] to show uniqueness. See also the discussion in Section 5.6 in [ADPZ20].

□

Later on we will prove that asymptotic height function are natural limits of height functions in the scaling limit, see Proposition 3.4.5. In all those statements, we will need that support height function approximates θ_Λ after normalization. By Theorem 2.1 [KOS06], for each point $(s,t) \in \mathcal{N}_\Lambda$ there is a sequence of dimer covers D_N of Λ_N with height change $(\lfloor Ns \rfloor, \lfloor Nt \rfloor)$. Therefore, after normalization by $\frac{1}{N}$ we have a sequence of height functions of $\frac{1}{N}\Lambda$ with the value 0 at the point p, and the slope that converges to (s,t). This further implies the convergence of $\frac{1}{N}\mathcal{X}_p$ to the support function θ_Λ.

3.4.2 Approximation of lattice regions

We call a sequence of lattice regions with boundary conditions $\{\Gamma_N, B_N\}$ *an approximation* of $(\Omega, \{\mathfrak{b}_i\}_{i=1}^g)$ if

1. $\Gamma_N \subset \frac{1}{N}\Lambda \cap \Omega$, where $\frac{1}{N}\Lambda$ is Λ with mesh $\frac{1}{N}$.

2. each Γ_N admits at least 1 dimer cover with normalized boundary condition $B_N^{R_N}$ for each non-trivial $R_N = \{R_N^i\}_{i=1}^g$.

3. for every admissible asymptotic height change r, there exists a sequence of admissible normalized height changes $\{R_N\}$ that converges to r, $R_N^i \to r^i$ as $N \to \infty$.

4. Γ tends to Ω with respect to the Hausdorff distance d_H, i.e., for sufficiently large N $d_H(\Omega, \Gamma_N) = O(N^{-1})$.

5. Further, $|B_N^{R_N}(x_N) - \mathfrak{b}^r(x)| \leq O(N^{-1})$ for the standard Euclid distance for sufficiently large N with $x_N \in \partial\Gamma_N, x \in \partial\Omega$ such that $|x_N - x| \leq O(N^{-1})$ (the existence of such points is guaranteed by the previous assumption).

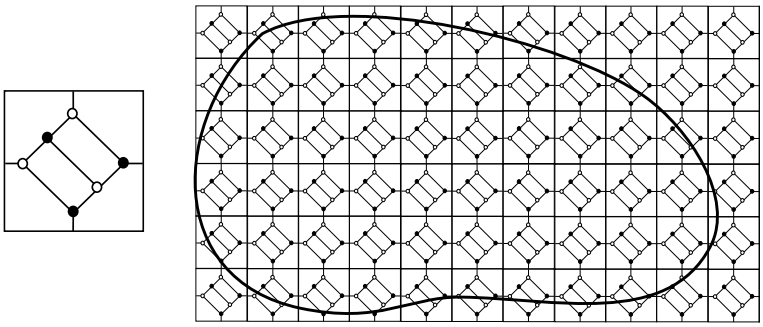

Figure 3.6: Fundamental domain of for dimer city lattice on the left, and approximation Ω_N of region Ω by the dimer city lattice on the right.

3.4.3 Convergence of maximal extensions and the density lemma

In this subsection, we are going to show consecutively three lemmas. The first of them is about asymptotic behavior of the support height function suitably normalized, which approximates the continuous support function θ.

Lemma 3.4.3. *Suppose we have faces $f, f_0 \in \Lambda_N$ and points $x, x_0 \in \mathbb{R}^2$ such that $x \in f$ and $f_0 \in \mathfrak{f}_0$. Then, for sufficiently large N we have*

$$N^{-1}(\mathcal{X}(f - f_0)) - \theta(x - x_0) = O(N^{-1}). \tag{3.4.6}$$

Proof. Without loss of generality, suppose that $x_0 = 0$, thus the term with θ vanishes at 0, $\theta(0) = 0$. Then, $\theta(x)$ is the maximal possible value of the asymptotic height functions whose value at 0 is zero. Then, the value of $\mathcal{X}(f)$ is also zero at f_0 due to our normalization. Therefore, we have agreement of the values at 0 and f_0. Now, by [KOS06, Theorem 3, 2], the Newton polygon is the set of allowed slopes for dimer covers. Therefore, since the slope of $\nabla\theta \in \partial\mathcal{N}_\Lambda$, it can also be archived, that is there exists a sequence of dimer covers D_N of Λ_N whose slope converges to the slope of θ (more precisely, slope of D_N is already $O(N^{-1})$-close to $\nabla\theta$). Therefore, the value of θ at point x is $O(N^{-1})$-close to the value of $\frac{1}{N}\mathcal{X}(f)$. □

We know Thus, let us derive from it the converge of the maximal lattice extension to the continuous counterpart. Suppose Ω is a domain with boundary condition $\mathfrak{b}$, and (Γ_N, B_N) its approximation. Further, let H_N^{max} be the normalized maximal extension of a B_N, and $\mathfrak{h}$ be the maximal extension of $\mathfrak{b}$. Then,

Proposition 3.4.4. *For sufficiently large N, we have the following estimate,*

$$\|H_N^{\max} - \mathfrak{h}_{\max}\|_\infty = O(N^{-1}) \tag{3.4.7}$$

Proof. Recall expressions for both extensions,

$$H_N^{\max}(f,\gamma) = N^{-1} \min_{f' \in \partial\mathcal{D}(\Gamma)} \{B(f') + \mathcal{X}_f(f')\}, \tag{3.4.8}$$

$$\mathfrak{h}^{\max}(x,\gamma) := \min_{y \in \partial\mathcal{D}(\Omega)} \{\mathfrak{b}(y,\gamma) + \theta(x,y)\}. \tag{3.4.9}$$

These expressions look similar, however the minimums are taken over different sets. To fix this, let us define a lattice approximation of $\mathfrak{h}_{\#,N} : \mathbf{F}(\Gamma) \to \mathbb{R}$. It is the restriction of $\mathfrak{h}$ to a point of every face of Γ_N. In fact, it does not matter which internal point we take, a different choice would a value with an error of order $o(N^{-1})$ due to the Lipschitz condition of $\mathfrak{h}$. We fix this point to be the center of each face for the sake of reducing ambiguity. In other words, we have that $|\mathfrak{h} - \mathfrak{h}_{\#,N}| < o(N^{-1})$. Now, let us compare expressions for $H_N^{\max}$ and $\mathfrak{h}_{\#,N}$, the minimum is taken over the same set $\mathcal{D}(\Gamma_N)$. Thus, we only need to compare the expressions themselves. But the boundary conditions are $O(N^{-1})$ close due to the assumption that (Γ_N, B_N) is an approximation of $(\Omega, \mathfrak{b})$, and the other terms are close due to 3.4.3.

□

Theorem 3.4.5. *For every asymptotic height function $\mathfrak{h}$ there is a sequence of normalized height functions $\{\frac{1}{N}H_N\}$ that converges to $\mathfrak{h}$ with respect to intrinsic sup norm. And wise versa, around each height function H_N there is an asymptotic height function $\mathfrak{h}'$ such that $\|H_N - \mathfrak{h}'\|_\infty^\Omega \leq O(N^{-1})$*

Proof. A key ingredient of the proof is a lattice approximation of asymptotic height functions. Suppose that $\mathfrak{h}$ is an asymptotic height function on a domain Ω that has its approximation $\{\Gamma_N\}$. Since a height function H is a map $\mathbf{F}(\Gamma_N) \to \mathbb{Z}$, we can make it a map $\Omega \to \mathbb{R}$ after declaring the value of H at a point x to be its value at the face F_x containing x. Analogously, we can think of the function $\mathfrak{h} : \mathbf{F}(\Gamma_N) \to \mathbb{R}$ after declaring the value $\mathfrak{h}(f)$ to be the value $\mathfrak{h}(x_F)$ for the center point of the face F, where the precise definition of the central point is irrelevant, it can be any internal point. Different choices differ by an error $O(N^{-1})$.

Then, the height function that approximates $\mathfrak{h}$ from below is

$$\hat{H}_N(x,\gamma) := \min_{y \in \mathcal{D}(\Gamma)} (\lfloor \mathfrak{h}(y,\gamma_y) \rfloor + \beta_N(x,y)), \tag{3.4.10}$$

where $\lfloor \mathfrak{h}(y,\gamma) \rfloor$ stands the integer part of $\mathfrak{h}(y,\gamma)$.

We need to show that this function satisfies three properties:

1. $\left\| \hat{H}_N(x_N,\gamma) - \mathfrak{h}(x,\gamma') \right\|_\infty^\Omega = O(N^{-1})$
2. $\hat{H}_N(x,\gamma)$ is a height function defined on $\tilde{\Gamma}$
3. $\hat{H}_N\Big|_{\partial\Gamma_N}(x,\gamma) = B$

The first property follows from that fact that $\hat{H}_N$ is fit within $O(N^{-1})$ to $\mathfrak{h}_{\#,N}$, which is $O(N^{-1})$ close to $\mathfrak{h}$ itself. The second property follows from the fact that the pointwise minimum of two height functions is a height function. In order to guarantee the third

property, let us squeeze $\hat{H}_N(x,\gamma)$ between the maximal, and the minimal extensions. This operation acts trivially on a height function H with the right boundary conditions as by definition H is bigger or equal than the minimal extension, and it is less or equal than the maximal extension. Thus, we change the function by only terms of order $O(N^{-1})$ near the boundary $\partial\Gamma$ (remember, $\hat{H}_N$ is already is $O(N^{-1})$ close to the right boundary condition due to the first property).

□

3.5 Asymptotic enumeration of dimer covers

One characteristic of the universality phenomenon, which is believed to happen for the dimer model, is independence of precise details conditions. In particular, the partition function of a domain with two nearly equal boundary conditions should be relatively close to each other. In order to justify this sentence, we are going to prove several propositions. The first of them is the computation of the partition function of a square with approximately linear boundary conditions.

3.5.1 Independence of precise boundary condition

In this subsection we give two proofs of the fact that the partition function of a convex lattice domain with nearly linear boundary conditions B is independent of precise details of B up to a small error negligible in the scaling limit as $N \to \infty$. The first proof mimics the original proof for the square grid in Lemma 3.5 [CKP00] and also [Gor21].

First, let us fix two positive reals, ϵ and k. Let (Γ, B) be a convex lattice domain with normalized boundary condition B that are fit to within ϵ to a linear function S of slope (s,t). We further assume that Γ fits into a rectangle of $K \times L$ fundamental domains, and $L > \epsilon^{-1}$.

Proposition 3.5.1. *Then, the normalized partition function $Z(\Gamma, B)$ is independent of precise choice of B_N, keeping (s,t) fixed, up to an additive error of order $\epsilon^{\frac{1}{2}} \log \frac{1}{\epsilon}$.*

Proof. Let us consider separately two cases, (s,t) that is separated by $\epsilon^{\frac{1}{2}}$ from $\partial\mathcal{N}_\Lambda$, and the case where it is close to the boundary of Newton polygon to within $\epsilon^{\frac{1}{2}}$.

In the first case, take another boundary condition B' that is fit within ϵL the linear function of slope (s,t). We will show that $Z(\Gamma, B)$ differs from $Z(\Gamma, B')$ by at most $\epsilon^{\frac{1}{2}} \log \frac{1}{\epsilon}$, or in other words, the weighted number of extension of B, roughly, equals to the weighted sum of extensions of B'.

Assume that $B \leq B'$ (we can always path from B to $B'' := \min\{B, B'\}$ so that $B \leq B''$. And let $H^\star$ and $H_r^\star$ be the minimal extension of B, and the maximal extension of B'. Then, our goal is to define two maps F and G on the set of height functions on Γ, if H extends B, then $F(H) := \max\{H^\star, H\}$ which now extends B'. The second map G is defined similarly, it takes an extension of B' and produces an extension of B,

$$G(H) := \min\{H_r^\star, H\}. \tag{3.5.1}$$

Note that $F(G(H)) = H$ at points where $H^\star \leq H \leq H_r^\star$. Further, recall the formula for $H^\star$(the formula for $H_r^\star$ is similar),

$$H^\star(f) := \max_{f' in \partial\Gamma} \{B(f') + \mathcal{X}(f - f'))\}. \tag{3.5.2}$$

Due to convexity of Γ and Proposition 3.4.4, $H^\star(f')$ and $H_r^\star(f')$ differ by a constant from $\theta(f - f')$. Thus, both extensions differ from the value of $S(x)$ by at least $\epsilon^{\frac{1}{2}} \max_{y \in \partial\Gamma} \theta(x,y)$ since the slope of S is separated from $\partial\mathcal{N}_\Lambda$ by $\epsilon^{\frac{1}{2}}$.

Our goal is to show that this map is a bijection with probability tending to 1 for a large N. Let us show that a typical extension B is close to S. We embed Γ into torus T_N with the weights that are alternated by the magnetic fields (B_x, B_y) in such a way that the slope of dimer covers of T_N converges to the slope of S as $N \to \infty$. From Proposition 3.7.3 we know that a random height function on T_N is close to S with high probability, in particular on $\partial\Gamma$. It means that we have two boundary conditions on $\partial\Gamma$ both of which converge to S. Thus, by results of 3.7.3 we conclude that with the high probability, a random extension of B is fit to within ϵN to S. Thus, we know that $H(F(H)) = H$ at all the points at least at distance $\epsilon^{1/2}\log(\frac{1}{\epsilon})N$ from $\partial\Gamma$.

What remains in the first case, is to deal with the points at most at distance $\epsilon^{1/2}\log(\frac{1}{\epsilon})N$ from $\partial\Gamma$. Let us estimate the number of extensions of B that close to $\partial\Gamma$. At each step from the boundary, the height function could take two possible values. Thus, the number of extensions can be bound by 2^A, where $A(\epsilon)$ is the number of points at the distance at most $\epsilon^{1/2}\log(\frac{1}{\epsilon})N$. This number is $A = O(\epsilon^{1/2}\log(\frac{1}{\epsilon})N^2)$, which is a rough estimate of entropy that we needed.

Now, let us deal with the second case, when (s,t) are ϵ-close to $\partial\mathcal{N}_\Lambda$. By convexity of $\mathcal{N}_\Lambda$, (s,t) is ϵ-close to a point $(s^\star, t^\star) \in \partial\mathcal{N}_\Lambda$, and (s',t') should be a convex combination of two point vertexes, denote them (s_1,t_1) and (s_2,t_2). Further, recall that each of those points correspond to a dimer cover of the fundamental domain $\mathcal{D}(\Lambda)$ with such a slope, call them D_1 and D_2. The only way to obtain a slope (s,t) for a dimer cover is to cover the vast majority of fundamental domains with either D_1 or D_2.

This results in estimate order of $O(\binom{N^2}{\epsilon N^2})$. Define $A := N^2$ for convention,

$$\binom{A}{c\epsilon N^2} \le \frac{A^{c\epsilon^{1/2}N^2}}{\left(\frac{c\epsilon^{1/2}N^2}{e}\right)^{c\epsilon^{1/2}L^2}} \le \left(\frac{N^2}{c\epsilon^{1/2}N^2}\right)^{c\epsilon^{1/2}N^2} = \left(\frac{e}{c\epsilon^{1/2}}\right)^{c\epsilon^{1/2}N^2} = \exp\left(N^2 O(\epsilon^2\log\frac{1}{\epsilon})\right) \tag{3.5.3}$$

Thus, after taking log and dividing by N^2, we get the desired. The second way to arrive to this result is to compare the partition function $Z(\Gamma)$ with two partition functions, $Z(\Gamma_{\min}, N)$ from below and $Z(\Gamma_{\max}, N)$ from above in such a way that $Z(\Gamma_{\min}, N) + \epsilon\log(\epsilon) < Z(\Gamma) < Z(\Gamma_{\max}, N) + \epsilon\log(\epsilon)$, where lattice region $\Gamma_{\min}$ is contained in Γ such that it is close to Γ $Dist(\partial\Gamma, \partial\Gamma_{\min}) < CN$, and the boundary conditions on $\Gamma_{\min}$ are taken from restriction of dimer configuration from torus. Similarly, for the upper bound, we take a lattice region $\Gamma_{\max}$ such that $Dist(\partial\Gamma, \partial\Gamma_{\max}) < C'N$ with periodic boundary conditions obtained from torus. Then, we can use the criterion of extension for the height function from a smaller region to a larger one. This way we obtain a bijection between dimer configurations on a torus and on a square up to a partition function of $\Gamma \setminus \Gamma_{\min}$ (or $\Gamma_{\max} \setminus \Gamma$). Those partition functions can be estimated by area, which gives the same answer as in the previous proof. □

The straightforward corollary is the partition function of the square.

Proposition 3.5.2 (The square lemma)**.** *Let $(\mathcal{S}, \mathfrak{b})$ be a continuous domain with a boundary condition, where $\mathcal{S}$ is a unit square and $\mathfrak{b}$ is δ-close to a linear function with the slope (s,t).*

Suppose that $(\Gamma N, B_N)$ is an approximation of $(\mathcal{S}, \mathfrak{b})$ and let B_N be δ-close to a linear function with the slope (s,t). Then, the partition function of (Γ_N, B_N) is independent of B_N up to an additive error of order $O(\delta^{\frac{1}{2}}\log(\frac{1}{\delta}))$.

$$N^{-2}\log Z(\Gamma_N, B_N) = -\sigma(s,t) + O(\delta^{\frac{1}{2}}\log(\frac{1}{\delta})) \tag{3.5.4}$$

3.5.2 Triangular lemma

Here, we prove an estimate for the partition function of a triangle based on the computation for the square. Further, we need an axillary statement, the cutting rule.

Suppose that we have a domain with a boundary condition $(\Gamma, \mathfrak{b})$ and a subset ρ on the dual lattice from the boundary of Γ to itself (thus, Γ/ρ consists of several components, let us denote them Γ^i). We want to calculate the partition function of Γ and one way to do it is to calculate partition functions $Z(H(\rho))$ with the given height function $H(\rho)$ along ρ. Then to sum up $Z(H(\rho))$ over all $H(\rho)$. The result is the original partition function because we just permute terms in a finite sum.

Then, we can interpret each $Z(H(\rho))$ as the product of the partition functions saying that ρ cuts Γ.

$$Z(\Gamma, \kappa) = \sum_{B_\rho} \prod_i Z(\Gamma^i, B^i_\rho) \tag{3.5.5}$$

where B^i_ρ is the boundary height function on Γ^i that coincide with the original boundary height function B and B_ρ where it is possible.

Now we are ready to for the computation of the partition function of the triangle.

Claim 2. *Let Ω be an equilateral triangle in $\mathbb{R}^2$ and $\mathfrak{b} : \Omega \to \mathbb{R}$ extends to a function in $\mathscr{H}(\Omega)$. Let $\mathfrak{h} \in \mathscr{H}(\Omega, \mathfrak{b})$ be an asymptotic height function δ-close to a linear with the slope (s, t) and let (Ω_N, B_N) be an approximation of $(\Omega, \mathfrak{b})$.*

$$\lim_{\delta \to 0} \lim_{N \to \infty} N^{-2} \log Z(\mathfrak{h}, \delta \mid \Omega_N, B_N) = -\sigma(s, t) \tag{3.5.6}$$

Proof. Let us take a square lattice with the mesh ℓ [2] and use the cutting rule for the curve ρ obtained from the intersection of the square lattice and Ω.

$$Z(\Omega_N, B_N) = \sum_{B_\rho} Z(B_\rho) = \sum_{B_\rho} \prod_j Z(\mathcal{S}^j, B^j_\rho), \tag{3.5.7}$$

where $\mathcal{S}_j$ is the square from the Square lattice with the boundary height function B^j_ρ.

We have two types of squares: included squares that do not intersect $\partial(\Omega)$ and excluded squares that intersect $\partial(\Omega)$. We want to build an upper and a lower bound of the partition function of $(\Omega_N, B_n | \mathfrak{h}, \delta)$, let us denote the upper bound by $Z_L(\Omega_N)$ and the lower bound by $Z_U(\Omega_N)$. We estimate included squares using the Square lemma and make a rough bound for the excluded squares.

The lower bound.

We want to make a lower bound of sum from the cutting rule, let us take only one summand corresponding to a boundary height function B_N.[3]

Here we estimate the excluded squares by the minimal weight of an edge (let us denote it by $w_{\min}$) to the power of number of edges in these squares.

$$\log Z(\Omega_N, B_N) \geq \log Z_L(\Omega_N) := \log w_{\min} S_{ex} + \sum_k \log Z^k_N(s, t), \tag{3.5.8}$$

where S_{ex} is the total number of edges in the excluded squares that we estimate by $o(\ell)$. And $Z^k_n(s, t)$ is the partition function of the square S^k. After the normalization, we have

[2] Where we take $\ell \leq \delta$ such that $\ell = o(\delta)$

[3] Existence of such height function follows from the density lemma applied to $\mathfrak{h}$. A boundary height function is a restriction of the height function that approximates $\mathfrak{h}$.

$\lim_{n\to\infty} N^{-2}\log Z_N^k(s,t) = -\sigma(s,t)\times\mathcal{A}(S_k) + o(\delta)$ from the square lemma and remark 1. Finally, the lower bound is,

$$N^{-2}\log Z_L(\Omega_N) = \sum_k N^{-2}\log Z_N^k(s,t) + o(\delta). \tag{3.5.9}$$

The upper bound.

In the upper bound we estimate the sum in the Cutting Rule by taking the maximal summand times the number of summands, which is the number of the all boundary height functions.

We bound the excluded squares by the maximal weight of the edge to the power of the total number of edges. For the included squares we estimate the same way as for the lower bound. Let us bound the number of boundary height function by $2^{o(N)}$

$$Z(\Omega_N, B_N) \le Z_U(\Omega_N) := w_{\max}^{o(\ell)} \times 2^{o(N)} \times \sum_j N^{-2}\log Z_N^j(s,t) \tag{3.5.10}$$

Finally, after taking the limit as $N\to\infty$ the first summands differ from each other by $o(\delta)$. Thus, both estimates differ from $-\sigma(s,t)\times$ Area of the triangle by $o(\ell)$. So after taking limit as $\ell\to 0$ and $\delta\to 0$ we have the proposition. □

3.5.3 Surface tension theorem

Theorem 3.5.3. *Let Ω be a compact, connected, multiply-connected domain in $\mathbb{R}^2$. Then let $(\Omega.\mathfrak{b})$ be the domain with a boundary condition $\mathfrak{h}\in\mathscr{H}(\Omega,\mathfrak{b}$ and (Ω_N, B_N) be an approximation of $(\Omega,\mathfrak{b})$. We recall that $Z(\mathfrak{h},\delta\,|\,\Omega_N,B_N)$ is a partition function of configurations with height functions δ-close to $\mathfrak{h}$. Then*

$$\lim_{\delta\to 0}\lim_{N\to\infty} N^{-2}\log Z(g,\delta\ |\Omega_N,B_N) = -\int_\Omega \sigma(\nabla g)dxdy \tag{3.5.11}$$

Proof. Fix a fundamental domain $\mathcal{D}(\Omega)$ with branch-cuts made along curves $\{\gamma_i\}_{i=1}^g$.

For the proof we need a triangular mesh a side length ℓ and piecewise linear approximations of Lipschitz functions from Claim 1. Consider a triangular mesh of length size ℓ that triangulates $\mathcal{D}(\Omega)$ into triangles T^j of the standard area $\mathcal{A}(T^j)$. Let also $\mathfrak{h}_\ell$ be the piecewise linear approximation of $\mathfrak{h}$ that is linear on each triangle and coincides with the values of $\mathfrak{h}$ at the vertices of the triangles.

Then, we choose small ε and take ℓ such that $\ell\varepsilon<\delta$, and on at least at $1-\epsilon$ fraction of points of a triangle in measure we have two properties: first, $|\mathfrak{h}_\ell-\mathfrak{h}|\le\ell\varepsilon$, and second, the gradient of $\mathfrak{h}$ exists and fit within ε to the gradient of $\mathfrak{h}_\ell$ in ℓ_2 norm, which is possible by Lemma 2.2 [CKP00]. We need these properties in order to write $\mathcal{F}(\mathfrak{h}_\ell)=\mathcal{F}(\mathfrak{h})+o_\delta(1)$ as $\varepsilon\to 0$.

Let us use the (3.5.5) for a subset ρ obtained from the intersection of the triangular mesh with the domain. Note that the subset ρ cuts Γ_N into triangles with boundary conditions along ρ. Denote the triangles by $\{T^j\}$ and their boundary height functions by $\{B_\rho^j\}$.

$$Z(\Gamma_N,B_N|\mathfrak{h},\delta) = \sum_{\mathfrak{b}_\rho} Z(\Gamma_N,B_\rho|\mathfrak{h},\delta) = \sum_{\mathfrak{b}_\rho}\prod_j Z(T^j,B_\rho^j|\mathfrak{h},\delta), \tag{3.5.12}$$

There are two types of triangles $\{T^j\}$. The included triangles (the first type) that do not intersect the boundary of the fundamental domain and where $\mathfrak{h}_\ell$ is fit to within $\ell\varepsilon$ to $\mathfrak{h}$.

The excluded triangles (the second type) intersect the boundary of the fundamental domain or where $\mathfrak{h}_\ell$ does not approximate $\mathfrak{h}$.

We make an upper and a lower bound for the normalized partition function $N^{-2}\log Z(\Gamma_N, B_N|\mathfrak{h}, \delta)$. In both cases, we can estimate the two types of triangles separately. For the included triangles we use Corollary 4.2 from [CKP00], and for the excluded we make a rough estimate. Then, after taking limit as $N \to \infty$, the normalized estimates differ from each other by $o_\delta(1)$.

3.5.4 The lower bound.

In the lower bound, it is sufficient to include some height functions that are δ-close to $\mathfrak{h}$. To do this, we can take only one term from (3.5.12) corresponding to one boundary height function B_ρ (for instance, we can take B_ρ obtained from the restriction of H'_N) (Theorem 3.4.5 gives us a sequence of normalized height functions $\{H'_N\}$ that converges to $\mathfrak{h}$ as $N \to \infty$).

Let us estimate the triangles of the first type by the product that includes only triangles of this type.

$$Z(\Gamma_N, B_N|\mathfrak{h}, \delta) \geq \prod_{T_j \text{of 1st type}} Z(T^j, B^j_\rho|\mathfrak{h}_\ell, \delta) \tag{3.5.13}$$

The bound for the included triangles obtained by using Corollary 4.2 [CKP00] to count δ-close height functions to make sure that we include only height functions δ-close to h. Thus, for triangles of the first type, we have the following,

$$N^{-2}\log \prod_{T_j \text{of 1st type}} Z(T^j, B^j_\rho|\mathfrak{h}_\ell, \delta) = \sum_{T_j \text{of 1st type}} (-\sigma(s^j, t^j))\times \mathcal{A}(T^j) + o(N^{-1}) + O(\varepsilon^{1/2}\log\varepsilon), \tag{3.5.14}$$

where (s^j, t^j) is a slope of $\mathfrak{h}_\ell$ on the triangle T^j and $\mathcal{A}(T^j)$ is the area of the triangle T^j. Finally, for sufficiently large, N the lower bound is the following,

$$N^{-2}\log Z(\Gamma_N, B_N|\mathfrak{h}, \delta) \geq \sum_j (-\sigma(s^j, t^j))\mathcal{A}(T^j) + o(N^{-1}) + O(\varepsilon^{1/2}\log\varepsilon), \tag{3.5.15}$$

where we fixed a height function on the excluded triangles to be H'_N.

3.5.5 The upper bound.

We can use almost the same strategy to make an upper bound. First, we have to include all height function δ-close to $\mathfrak{h}$. Let us estimate the included triangles the same way as for the lower bound to count height functions δ-close to $\mathfrak{h}$. For the excluded triangles we make a rough estimate since the area of those triangles is proportional to ε, the number of configurations is bounded from above by $\exp(\varepsilon)$ times the number of terms in the cutting rule, which is $2^{O(N)}$ since it is the number of configurations of a line of size N.

$$Z(\Gamma, B_N|\mathfrak{h}, \delta) \leq \prod_{T_j \text{of 1st type}} Z(T^j, B^j_\rho|\mathfrak{h}_\ell, \delta))2^{O(N)} + N^2\varepsilon \tag{3.5.16}$$

And after taking limit as $N \to \infty$, the normalized upper bound is the following, where terms $O(N^{-1})$ and $O(\varepsilon)$ come from the bounds of triangles of the second type.

$$N^{-2}\log Z(\Gamma, B_N|\mathfrak{h},\delta) \le -\sum_j \sigma(s^j,t^j)\mathcal{A}(T^j) + o(N^{-1}) + O(\varepsilon^{1/2}\log\varepsilon) + O(\varepsilon). \quad (3.5.17)$$

Taking into account that $\int_\Omega \sigma(\nabla h_\ell)dxdy = \sum_j \sigma(s_j,t_j)\mathcal{A}(t^j)$, one can see that both bounds after dividing by the area of Ω are equal to $\mathcal{F}(h_\ell) + o(N^{-1}) + O(\varepsilon^{1/2}\log\varepsilon)$ that differs from $\mathcal{F}(\mathfrak{h})$ by $o_\delta(1)$ by Lemma 2.3 from [CKP00]. □

3.6 Variational principle

Theorem 3.6.1. *Let $(\Omega,\mathfrak{b})$ be a domain with a boundary condition and (Ω_N, B_N) be an approximation of $(\Omega,\mathfrak{b})$, then*

$$\lim_{N\to\infty} N^{-2}\log Z\left(\Omega_N, B_N\right) = -\iint_\Omega \sigma(\nabla\mathfrak{h}^\star)dxdy$$

where $\mathfrak{h}^\star$ is the minimizer of the functional $\mathcal{F}(\mathfrak{h}) := \iint_\Omega \sigma(\nabla\mathfrak{h})dxdy$ on the set $\mathcal{H}(\Omega,\mathfrak{b})$.

Moreover, let H_N be a random height function on (Ω_N, B_N). Then we have the convergence in probability for H_N to $\mathfrak{h}^\star$, that is for each $\delta > 0$

$$\mathbb{P}\left(\|H_N - \mathfrak{h}^\star\|_\infty^\Omega > \delta\right) \to 0 \text{ as } N\to\infty.$$

So a random height function converges to $\mathfrak{h}^\star$ in probability with respect to the intrinsic norm.

3.6.1 Convergence of height functions to the limit shape

Here, we give a proof of a law of large numbers for height function. More precisely, we show that a normalized height function converges in both regimes to its expected value that is approximately the unique solution to the variational problem. We write it for an arbitrary height change, and later discuss the modifications for a fixed height change.

Consider a sequence $\{\overline{H}_N\}$ of expectation values of normalized height functions on (Γ_N, B_N). We know that by Theorem 3.4.5 there exists a sequence of asymptotic height functions $\{\mathfrak{h}_N\}$, such that $\left\|\mathfrak{h}_N - \overline{H}_N\right\|_\infty^\Omega \le \frac{C}{N}$. By Proposition 2.4.4 $\{\mathfrak{h}_N\}$ has a convergent subsequence, denote its limit by $\mathfrak{h}$. Without loss of generality, we suppose that the convergent subsequence is $\{\mathfrak{h}_N\}$ itself. We will see later that $\mathfrak{h} = \mathfrak{h}^\star$

Lemma 3.6.2. *One can find such an ℓ' that for $\forall\delta > 0$ and for sufficiently large N*

$$\mathbb{P}(\|H_N - \mathfrak{h}\|_\infty^\Omega > \delta) \le \exp(-N\delta^2/\ell'). \quad (3.6.1)$$

Proof. We deduce it from a combination of Lemma 3.7.3 applied to H_N and convergence of h_N to $\mathfrak{h}$. The goal is to show that the inequality $\|H_N - \mathfrak{h}\|_\infty^\Omega \le \delta$ holds for sufficiently large N with probability exponentially close to 1.

By the triangle inequality we have

$$\|H_N - \mathfrak{h}\|_\infty^\Omega \le \left\|\bar{H}_N - \mathfrak{h}_N\right\|_\infty^\Omega + \|\mathfrak{h}_N - \mathfrak{h}\|_\infty^\Omega + \left\|H_N - \bar{H}_N\right\|_\infty^\Omega. \quad (3.6.2)$$

The first term in the right-hand side of (3.6.2) is smaller than $\delta/3$ for sufficiently large N by definition of $\mathfrak{h}_N$, that is by Lemma 3.4.5 we have $C > 0$ such that $\left\|\mathfrak{h}_N - \bar{H}_N\right\|_\infty^\Omega < \frac{C}{N}$, which is smaller than $\delta/3$ for sufficiently large N. The second terms of (3.6.2) is smaller

than $\delta/3$ for sufficiently large N due to convergence of $\mathfrak{h}_N$ to $\mathfrak{h}$, which holds by definition of $\mathfrak{h}$.

The third term (3.6.2) is smaller than $\delta/3$ with the probability $1-\exp(-\frac{\delta^2 N}{\ell})$, where we defined $\ell = 3\ell'$ for ℓ' from Lemma 3.7.3. Therefore, we have $\|H_N - \mathfrak{h}\|_\infty^\Omega > \delta$ with probability bounded by $\exp(-N\delta^2/\ell')$.

□

So far, we know that up to extracting a subsequence, normalized height functions converge with respect to the uniform norm in probability to $\mathfrak{h}$ and the contribution of height functions that are far away from $\mathfrak{h}$ are exponentially suppressed. Thus, $\mathfrak{h}$ is the limit shape. Since height change R_N is a continuous function of H_N, it converges to the height change of the limit shape, which is r. Later, we prove that $\mathfrak{h} = \mathfrak{h}^\star$.

3.6.2 Convergence of partition function

Let us show that one can find an asymptotic expression of the partition function, which is a straightforward corollary of the convergence of height functions to the limit shape. The following proof holds for a fixed height change r after replacing $\mathfrak{h}$ by $\mathfrak{h}_r$ and $Z(\Gamma_N, B_N)$ by $Z(\Gamma_N, B_N, R_N)$.

Define $U_\delta^N(\mathfrak{h}^\star)$ to be the set of height functions on Γ_N that are fit to within δ to $\mathfrak{h}^\star$, $\|H_N - \mathfrak{h}^\star\|_\infty^\Omega \le \delta$.

Then, the following holds due to the concentration inequality above,

$$\mathbb{P}_N \|H_N - \mathfrak{h}^\star\|_\infty^\Omega \le \delta) = 1 - \mathbb{P}_N(\|H_N - \mathfrak{h}^\star\|_\infty^\Omega > \delta). \tag{3.6.3}$$

Or more precisely,

$$\frac{Z(\Gamma_N, B_N|\mathfrak{h}^\star, \delta)}{Z(\Gamma, B_N)} = 1 + O(\exp(-\delta^2 N/\ell)). \tag{3.6.4}$$

Now, let us take the logarithm of both sides and normalize them by N^{-2}. Also introduce the notation $S(N,\delta) := 1 + O(\exp(-\delta^2 N/\ell))$ for the simplicity.

$$N^{-2}\log Z(\Gamma_N, B_N) = N^{-2}\log(Z(\Gamma_N, B_N|\mathfrak{h}^\star, \delta)) + N^{-2}\log(S(N,\delta)). \tag{3.6.5}$$

Now we can take limit as $N \to \infty$ to make $\log S(N,\delta)$ converge to zero. Finally, we obtain the desired expression by Theorem 3.5.3,

$$N^{-2}\log Z(\Gamma_N, B_N) \xrightarrow[N\to\infty]{} -\mathcal{F}(\mathfrak{h}^\star). \tag{3.6.6}$$

3.6.3 The Surface tension functional and the limit shape

We still need to show that h minimizes $\mathcal{F}$, that is $h = \mathfrak{h}^\star$. Again, it follows easily from the concentration of height functions around $\mathfrak{h}$.

Assume that $\mathfrak{h} \neq \mathfrak{h}^\star$. We need to show that $\mathcal{F}(\mathfrak{h}) \ge \mathcal{F}(\mathfrak{h}^\star)$. Suppose the opposite, that is $\mathcal{F}(\mathfrak{h}) < \mathcal{F}(\mathfrak{h}^\star)$. By Theorem 2.8.1, $\mathcal{F}(\mathfrak{h}^\star)$ (resp.$\mathcal{F}(\mathfrak{h})$) is the limit of the normalized number of domino tilings whose normalized height functions are fit within δ to $\mathfrak{h}^\star$ (resp.$\mathfrak{h}$) for $\delta \to 0$. Then, we can use that normalized height functions H_N concentrate around $\mathfrak{h}$, which can be separated from $\mathfrak{h}^\star$ by the choice of a smaller $\delta > 0$. The contradiction follows from the fact that the overwhelming majority of domino tilings are δ-close to $\mathfrak{h}$, but not to $\mathfrak{h}^\star$ and thus, we are done.

The proof for the fixed asymptotic height change r works the same way after replacing of $\mathfrak{h}$ by $\mathfrak{h}_r$.

3.7 Probability estimates and concentration lemma

In this section we follow section «6.2. Robustness.» from [CEP96] to conclude the Density Lemma. We begin with the properties that are based on locality of the height function (the value $H(v)$ determines the sets of possible values at faces adjacent to v), and the Markov property of the distribution.

3.7.1 Auxiliary estimates

First, we need to understand that partition functions with two close boundary conditions B_1, B_2, $Z(\Gamma, B_1)$ and $Z(\Gamma, B_2)$ are close to each other as well. Further, the expectation values of height functions extending B_1 and B_2 are also close. This is used in the core of enumeration of dimer configurations.

Theorem 3.7.1. *Let B_1 and B_2 be two extendable boundary heights such that $B_1 \leq B_2$. Then, let H_1 be a random extension of B_1 and similarly H_2 be a random extension of B_2. Then, we can sample H_1 and H_2 such that $\mathbb{E}(H_1(w)) \leq \mathbb{E}(H_1(w))$ for $w \in \Gamma$.*

Proof. Let us prove it by induction with respect to cardinality of $\mathbf{F}(\Gamma/\partial\Gamma)$. The base is the case of $\Gamma = \partial\Gamma$.

Since $B_1 \leq B_2$, there exists a boundary face $v \in \mathbf{F}(\Gamma)$ where $B_1(v) \leq B_2(v)$ (if it does not exist, then we are done since we can sample in such a way that $H_1 = H_2$). Let us take a face w adjacent to v, and sample first the values at w and then sample the rest. Note that, necessary, faces v and w have one edge in common, call e. Assume, without loss of generality, that if we go from v to w, we intersect e in a positive direction.

Then, for a dimer cover D there are four possible outcomes for the values of the height of w that can be summarized as follows,

1. Edge e belongs to both the reference dimer configuration D_0 and to D.
2. Edge e belongs to the reference dimer configuration D_0, but not to D.
3. Edge e does not belong either to the reference dimer configuration D_0, or to D.
4. Edge e does not belong to the reference dimer configuration D_0, but it belongs to dimer cover D.

Then, in principle, we have to consider eight possible outcomes for $D = D_1$, and, independently, for $D = D_2$. However, the first and the second cases results in the same height of w, which equals to $H(v)$.

Therefore, we can note that in either case of e belongs to D_0, or does not, the possible outcomes for the extensions $H_1(w)$ and $H_2(w)$ differ no more than by 1, $|H_1(w) - H_2(w)| \leq 1$. After it, we can apply the induction hypothesis to sample on $\Gamma \setminus \{w\}$.

□

Notice that this theorem implies that we also have $\mathbb{E}(H_1) \leq \mathbb{E}(H_2)$. We can also deduce a similar result for two "close" lattice regions Γ_1 and Γ_2 with "close" boundary conditions B_1 and B_2. By "close" we mean the discrete Hausdorff distance, more precisely it means the following. Suppose that every face $f_1 \in \mathbf{F}(\partial\Gamma_1)$ could be connected with $\mathbf{F}(\partial\Gamma_2)$ by a path of length d_1, and wise-versa, each for every $f_2 \in \mathbf{F}(\partial\Gamma_2)$. Further, assume that values $|H(f_1) - H(f_2)| \leq d_2$. Then, we have the following.

Theorem 3.7.2. *There exists a constant $C > 0$ such that for every $v \in \mathbf{F}(\Gamma_1 \cap \Gamma_2)$ we have*

$$|\mathbb{E}(H_1(v)) - \mathbb{E}(H_2(v))| \leq C(d_1 + d_2), \tag{3.7.1}$$

where H_1 is a random extension of boundary condition B_1, and H_2 is a random extension of boundary condition B_2.

Proof. Let us follow the argument from [CEP96; Gor21], let $\tilde{H}_1$ be the minimal extension of B_1 and $\tilde{H}_2$ be the maximal extension of B_2. Then, we have $\tilde{H}_1(v) \geq \tilde{H}_2(v) - C(d_2 + d_1)$ for $v \in \partial\Gamma_1 \cap \partial\Gamma_2$, for some constant $C > 0$. Since the inequality holds for the minimal extension $\tilde{H}_1$, it holds for any other extension. A repetition of those arguments for $\tilde{H}_2$ implies that for any extensions H_1, H_2. With the help of the discussion in the previous theorem, we have the desired. □

3.7.2 Coupling lemma

Claim 3. *Let $(\Gamma, \partial\Gamma)$ be a graph with a boundary and let f and g be two boundary height functions on Γ. We denote by $\bar{H}_g$ an average height function on (Γ, g), $\bar{H}_f$ on (Γ, f). We suppose that $f \leq g$, then $\bar{H}_f \leq \bar{H}_g$ pointwise.*

Proof. Let $\mathcal{H}(\Gamma, g)$ and $\mathcal{H}(\Gamma, f)$ be sets of height functions on Γ with boundary height functions f and g. Denote induced probability measures by μ_f, μ_g.

Let us prove condition $f \leq g$ implies that $\bar{H}_f \leq \bar{H}_g$. To do this we need to build a *coupling* of measures μ_f and μ_g. It is a probability measure π on $H(\Gamma, g) \times H(\Gamma, f)$, such that its projection on $H(\Gamma, g)$ gives μ_g and the same is true respectively for f. The most important constraint is that $\mathbb{P}_\pi(H_1, H_2) = 1$ for only pairs of height functions such that $H_1 \leq H_2$. In case we have such a measure, we get $\bar{H}_f \leq \bar{H}_g$ pointwise, because $\bar{H}_f$ and $\bar{H}_g$ can be obtained as projections of π.

Let us prove it using induction by number of internal vertices of Γ. The base of induction where the set of internal vertices is empty is trivial. Moreover, the case of $f = g$ is trivial as well. Thus, it is sufficient to prove for $f < g$ at a boundary face v. Note that $H_f(v) \leq H_g(v) + 1$. Let us pick an internal face w adjacent to v. There are two possible values for $H_g(w)$, namely H and $H - 1$ for some H (respectively H' and $H' - 1$ for $H_f(w)$ for some H'). Therefore, the probability distributions μ_f and μ_g are the convex combinations of measures $mu_f^{\pm}$ and $\mu_g^{\pm}$ corresponding each outcome(in other words, to each extra boundary condition at face w),

$$\mu_f = \alpha\mu_f^+ + (1 - \alpha)\mu_f^- \tag{3.7.2}$$

$$\mu_g = \beta\mu_g^+ + (1 - \beta)\mu_g^- \tag{3.7.3}$$

where α is proportional to the partition function of the dimer covers with the extra boundary condition f^+ at face w, and β is proportional to the partition function with the extra boundary condition f^- at w. Thus, we can use our induction hypothesis to conclude that the coupling exists for any pair measures with an extra boundary condition at w, and it is given by a convex combination of couplings, which exist by the induction hypothesis.

□

Now, recall Azuma–Hoeffding inequality for values of a martingale with bounded difference. Suppose M_k, $\{k = 0, 1, \cdots\}$ is a martingale such that $|M_k - M_{k-1}| \leq c_k$,

$$\mathbb{P}(|M_N - M_0| \geq \epsilon) \leq 2\exp\left(-\frac{\epsilon^2}{2\sum_{k=1}^N c_k^2}\right) \tag{3.7.4}$$

We mimic theorem 21 from [CEP96]

Proposition 3.7.3. *There exists a constant $\ell(\Omega) > 0$ such that for all $C > 0$ and for sufficiently large N the following inequality holds,*

$$\mathbb{P}_N(\left\|H_N - \bar{H}_N\right\|_\infty^\Omega > c) < \exp\left(-\frac{NC^2}{\ell(\Omega)}\right). \tag{3.7.5}$$

Proof. Let us fix a path $(f_0, \dots, f_m)$ with $m+1$ points from the boundary faces $\mathbf{F}(\partial\Gamma)$ to an internal face $f \in \mathbf{F}(\Gamma)$. Then, consider a filtration of σ algebras $\mathcal{F}_k$ generated by outcomes of $H(f_i)$ for $i \le k$ ($H(f_0)$ is fixed since $f_0 \in \mathbf{F}(\partial\Gamma)$). Then, took the conditional expectation value at a face f with respect to $\mathcal{F}_k$, $M_k = \mathbb{E}(H(f)|\mathcal{F}_k)$.

By the tower property for conditional expectations, $M_k = \mathbb{E}(H(f)|\mathcal{F}_k)$ forms a martingale with bounded increments, that is $\mathbb{E}(M_{k+1}|\mathcal{F}_k) = M_k$. Now recall that Azuma's inequality for a martingale X_k with bounded increment $|X_k - X_{k-1}| \le c_k$ is

$$\mathbb{P}(|M_N - M_0| \ge \epsilon) \le 2\exp\left(-\frac{\epsilon^2}{2\sum_{k=1}^N c_k^2}\right) \tag{3.7.6}$$

Therefore, application of Azuma's inequality to M_k gives the concentration inequality.

$$\mathbb{P}_N^\Gamma(|H_N(f) - \overline{H}_N(f)| > N^{-1}a\cdot\sqrt{m}) < 2\exp(-a^2/2). \tag{3.7.7}$$

One can renormalize this concentration inequality exactly as we did it for the square lattice in 2.5.2, and the resulting inequality for normalized height functions is the following.

Choose a such that $C = N^{-1}a\sqrt{m}$. The length of a path m behaves for large N as $m \approx \ell'(\Omega, f)N$. The quantity $\ell'(\Omega, f)$ is approximately the length of the shortest path inside Ω from the face $f \in \mathbf{F}(\Omega)$ to $\partial\Omega$. Let us define $\ell'(\Omega) := \max_f \ell(\Omega, f)$, which is finite due to compactness of Ω.

The resulting concentration inequality so far is the following,

$$\mathbb{P}_N^\Gamma(|H_N(f) - \overline{H}_N(f)| > C) < 2\exp\left(-\frac{NC^2}{2\ell'(\Omega)}\right), \tag{3.7.8}$$

To obtain the probability $\mathbb{P}_N^\Gamma(\left\|H_N - \overline{H}_N\right\|_\infty^\Omega \ge C)$, we need to sum over all faces $f \in \mathbf{F}(\Gamma)$ probabilities that $|H_N(f) - \overline{H}_N(f)| \ge C$,

$$\mathbb{P}_N^\Gamma\left\|H_N - \overline{H}_N\right\|_\infty^\Omega > C) = \sum_{f\in\mathbf{F}(\Gamma)} \mathbb{P}(|H_N(f) - \overline{H}_N(f)| \ge C) \tag{3.7.9}$$

The number of terms in the letter expression is bounded from above by $N^2|\Omega|$, where $|\Omega|$ is the area of Ω, which is due to the fact that the number of faces of Γ_N is approximately $|\Omega| \times N^2$,

$$\mathbb{P}_N^\Gamma\left(\left\|H_N - \overline{H}_N\right\|_\infty^\Omega > C\right) < 2|\Omega|N^2\exp\left(-\frac{C^2N}{2\ell'(\Omega)}\right). \tag{3.7.10}$$

One can further choose an $\ell(\Omega) < 32\ell'(\Omega))$ to absorb the prefactor $12|\Omega|N^2$ for sufficiently large N, and factor 2 in front of ℓ'

$$\mathbb{P}_N^\Gamma\left(\left\|H_N - \overline{H}_N\right\|_\infty^\Omega > C\right) < \exp\left(-\frac{C^2N}{\ell(\Omega)}\right). \tag{3.7.11}$$

□

Appendix: Absolute height functions

3.7.3 Absolute height functions

Due to the dependence of H_{D,D_0} and N_Λ on D_0, sometimes it is more convenient to define an analogue of D_0 which a priori does not come from a single dimer configuration. One way to do it is to take a canonical flow of divergence 1 at each vertex.

It can be done for every bipartite graph without self-intersections, see Theorem 3.3 in [GK11]. We will focus on regular graphs, i.e., graphs with the same valence N for all vertices.

In this case, one can define $\varphi(v) = \frac{1}{N}$ Obtained height functions are called *absolute height functions*. However, the absolute height function takes values at $\mathbb{Q}$ instead of $\mathbb{Z}$ or to multiply coefficients by N to make them integers.

One can notice that absolute height functions obey the local rule. It states that around each vertex they increase with the respect to cyclic order around this vertex: around black vertices they increase in clock-wise direction and around white vertices in counter-clock-wise direction. See an example on Figure 3.7 .

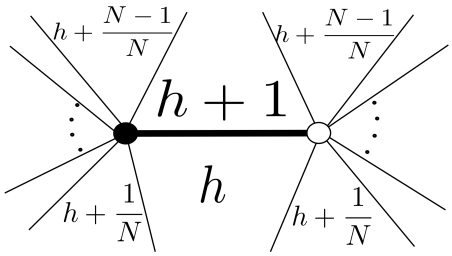

Figure 3.7: The local rule for an absolute height function

Moreover, it is not hard to check that every function on faces that satisfy the local rule is an absolute height function of some dimer cover.

Proposition 3.7.4. *There is a bijection between absolute height functions and functions on faces that satisfy the local rule.*

Also note that absolute height functions are Lipschitz functions in a sense described below, which is a consequence of the local rule.

Let $\pi(f_1, f_2)$ be the length of the shortest oriented path on dual graph of Γ that connects faces f_1 and f_2.

Proposition 3.7.5. *Every absolute height function satisfies modified Lipschitz condition:*

$$H_D(f_1) - H_D(f_2) \leq \frac{1}{\mathcal{N}}\pi(f_1, f_2) \tag{3.7.12}$$

Chapter 4

The Tangent plane method

Abstract

The aim of this chapter is to give an introduction to the *Tangent plane method*, which gives an explicit parametrization of the arctic curve for the wide range of models. It was proposed by Richard Kenyon and Istvan Prause in their work [KP22]. We discuss it on the example of random domino tilings of Aztec diamond, and Aztec diamond with a hole.

4.1 Introduction

Variational problems we see in the large deviation principle for the dimer model and random domino tilings have a long story. They arise in the physical description of formation of the equilibrium shape of crystals, where we are interested in the shape minimizing the total surface free energy with a fixed volume. The Wulff construction [Wul01] gives a phenomenological description of the minimizer's graph as an envelope of its tangent planes. This description was known in physical literature, for instance §140 in [LL58], without a mathematically rigorous proof. However, such a proof appeared for two-dimensional Ising model in [RRS92], where the shape is the interface separating the two phases of the system. Later, the rigorous construction for the three-dimensional Ising model in a low temperature limit appeared in [CK01], where the limiting interface was identified with the limit shape of the plane partitions.

Another parallel story to crystal formation is soap filming, where the shape minimizes *the surface tension* of the soap film. This analogy gives the name for the function σ and the functional $\mathcal{F}$ in the dimer model. Moreover, a soap film is the realization of a *minimal surface*, which is a surface that locally minimizes the area. The latter given by functional $\mathfrak{h} \mapsto \int \sqrt{1+\nabla\mathfrak{h}^2}dxdy$, thus we arrive at another variational problem. However, how to analyze such a problem? The first idea is to look at the corresponding Euler-Lagrange equations, or in physical terms, equations of motion.

The usual Laplace equation $\Delta u = 0$ is nothing but the Euler-Lagrange equation for the functional $\int_\Omega \|\nabla u\|^2 \, dxdy$. What is more important, one can obtain a solution to the Laplace equation out of an analytic function f defined on a simply-connected domain Ω simply by taking the real or imaginary part of the function f. In this chapter, we are going to apply a similar strategy to analyze Euler-Lagrange equations corresponding to the variational problems coming from the dimer model. These variational problems fit into a

particular class of problems, the so-called *gradient variational problems*. Unlike the classical functional $\int_\Omega \|\nabla u\|^2 \, dxdy$, in the dimer model we deal with a functional $\int_\Omega \sigma(\nabla \mathfrak{h}) dxdy$ with non-smooth σ, which makes their analysis more difficult. Also, in this chapter we are using a different notation for the Newton polygon for the square lattice turned by 45 degrees so that the characteristic polynomial is $P(z,w) = 1 + z + w - zw$ and the Newton polygon is the unit square with vertices $(0,0), (1,0), (0,1), (1,1)$.

4.2 Gradient variational problems

Solving a gradient variational problem in $\mathbb{R}^2$ means finding a function $\mathfrak{h} : \Omega \to \mathbb{R}$ that minimizes a certain functional $I(\mathfrak{h})$ that depends only on $\nabla \mathfrak{h}$ over a suitable functional space $\mathscr{H}(\Omega)$. We further assume that the functional $I(\mathfrak{h})$ can be written as,

$$I(\mathfrak{h}) = \int_\Omega \sigma(\nabla \mathfrak{h}) dxdy \tag{4.2.1}$$

for a given convex function $\sigma : \mathcal{N} \to \mathbb{R}$, which is bounded and strictly convex in interior of a convex polygon $\mathcal{N}$ and extended to $+\infty$ outside $\mathcal{N}$. Strict convexity of σ implies existence and uniqueness of the minimizer $\mathfrak{h}^\star$ over the space of functions with prescribed boundary conditions and the gradient constraint $\nabla \mathfrak{h} \in \mathcal{N}$ by [DS08]. In the dimer models, $\mathcal{N}$ is the Newton polygon $\mathcal{N}_\Lambda$ from 1.4.1. However, we can formulate the gradient variational problem without connection to the dimer model.

Such a variational problem also arises in the study of minimal surfaces in $\mathbb{R}^3$, which are surfaces of locally minimal area for given boundary conditions. The variational characterization of a minimal surface given by $(x, y, \mathfrak{h}(x,y))$ is that $\mathfrak{h}$ is a critical point of the functional $I(\mathfrak{h}) = \int_\Omega \sqrt{1 + |\nabla \mathfrak{h}|^2} dxdy$. The famous Weierstrass-Enneper parameterization encodes such a surface in terms of two arbitrary holomorphic functions. One example of a minimal surface is the helicoid (see Figure 4.1), a surface defined parametrically in Cartesian coordinates as

$$x = \rho \cos(\alpha\theta), \quad y = \rho \sin(\alpha\theta), \quad z = \theta. \tag{4.2.2}$$

The *Costa surface*, discovered in [Cos84], is another example. It is a surface of genus 1 embedded into $\mathbb{R}^3$ without self-intersections, see Figure 4.1. An explicit parametrization of this surface in terms of Weierstrass elliptic functions was obtained in [FGM95].

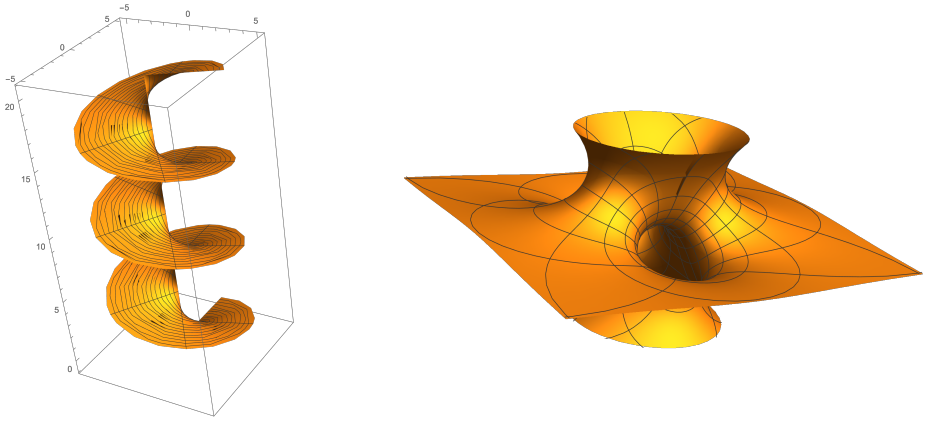

Figure 4.1: Plots of the helicoid on the left, and of the Costa surface on the right obtained by Mathematica.

In the dimer model, we deal with a particular example of gradient variational problem, and the situation is similar to the minimal surfaces. An asymptotic description of the model

is given by the continuous height function $\mathfrak{h}$, which solves the gradient variational problem. The *tangent plane method* is a method that help us in reconstructing the minimizer $\mathfrak{h}$ out of three harmonic functions, two components of the gradient $(s,t) := \nabla\mathfrak{h}$, and a third function called *the intercept* c.

Other gradient variational problems recently appeared, for instance in studies of the six-vertex model, and the five-vertex model [RS17; KP22; KP24]. The main difference is that while for the dimer models the main functions are harmonic, in the five-vertex model they are ratios of harmonic functions with a common denominator.

The functional space on which the functional is minimized is composed of Lipschitz functions, whose gradient is well defined almost surely by Rademacher's theorem. The fact that σ takes finite values only inside $\mathcal{N}$ implies that the gradient of the solution $\mathfrak{h}$ belongs to $\mathcal{N}$ almost everywhere. Let us introduce several technical definitions. In this discussion, we assume that $\mathcal{L}, \mathcal{F}, \mathcal{G}, \mathcal{Q}$ are open subsets of Ω, and the points in the definition 4.2.1 belong to $\mathbb{Z}^2$.

Definition 4.2.1.

- $\mathscr{P} = (p_1, \dots, p_k)$ are the vertices (corners) of $\mathcal{N}$.
- $\mathscr{G} = (q_1, \dots, q_l)$, $q_i \in \mathring{\mathcal{N}}$ are the gas points.
- $\mathscr{Q} = (p_{k+1}, \dots, p_{k+m})$ are the quasifrozen points, points on $p_i \in \partial\mathcal{N} \setminus \mathscr{P}$.

With the help of these notations, we define four regions on Ω from Definition 2.7 from [ADPZ20],

Definition 4.2.2. The *liquid region* of $\mathfrak{h}$ is

$$\mathcal{L} := \mathrm{Int}\{z \in \Omega : \mathfrak{h} \text{ is } C^1 \text{ in a neigbourhood of } z,\ \nabla\mathfrak{h}(z) \in \mathring{\mathcal{N}} \setminus \mathscr{G}\}. \tag{4.2.3}$$

The *frozen region* of $\mathfrak{h}$ is

$$\mathcal{C} := \mathrm{Int}\{z \in \Omega : \mathfrak{h} \text{ is } C^1 \text{ in a neighborhood of } z,\ \nabla\mathfrak{h}(z) \in \mathscr{P}\}. \tag{4.2.4}$$

The *gas region* of $\mathfrak{h}$ is defined as

$$\mathcal{G} := \mathrm{Int}\{z \in \Omega : \mathfrak{h} \text{ is } C^1 \text{ in a neighborhood of } z,\ \nabla\mathfrak{h}(z) \in \mathscr{G}\}. \tag{4.2.5}$$

The gas phase is discussed in the context of the doubly-periodic Aztec diamond, where there is a unique point $q \in \mathscr{G}$.

Moreover, $\mathfrak{h}$ is C^∞ smooth in the liquid region $\mathcal{L}$ by results from [DS08], see also discussion on page 29 in [ADPZ20].

The Euler-Lagrange equation for (4.2.1), defined in the liquid region $\mathcal{L}$ is:

$$\mathrm{div}(\nabla\sigma \circ \nabla\mathfrak{h}) = 0. \tag{4.2.6}$$

This equation itself, follows from a standard calculus in variations, see [Eva10, Chapter 8]: simply take a test function h, which is a smooth function supported strictly inside $\mathcal{L}$ and look at the expansion in ε of $I(\mathfrak{h}^\star + \varepsilon h)$, where we assume that $\mathfrak{h}^\star + \varepsilon h$ has a gradient strictly inside $\mathcal{N}$ (we can choose a small enough ε for this). A sufficient and necessary condition for $\mathfrak{h}^\star$ to be the minimizer of the convex functional I is vanishing of the linear order in ε in expansion of $I(\mathfrak{h}^\star + \varepsilon h)$ for any choice of function h. Or in other words, one needs to check vanishing of the Gâteaux derivative of I at $\mathfrak{h}^\star$ in any direction h. After expanding $\sigma(\mathfrak{h} + \varepsilon h)$ up to the first order, we get

$$\int_\Omega \sigma(\nabla\mathfrak{h}(x,y)+\varepsilon\nabla h(x,y))dxdy = \int_\Omega \sigma(\nabla\mathfrak{h}(x,y))dxdy+ \varepsilon\int_\Omega (\nabla\sigma\circ\nabla\mathfrak{h}(x,y)\cdot\nabla h(x,y))\,dxdy + o(\varepsilon) \quad (4.2.7)$$

Then, after applying the Stokes theorem (note $h\big|_{\partial\Omega}=0$), we obtain the following expression for coefficient of the linear term in ε,

$$-\int_\Omega h(x,y)\,\mathrm{div}(\nabla\sigma\circ\nabla\mathfrak{h}(x,y))dxdy. \quad (4.2.8)$$

Since (4.2.8) should vanish for any function h, we necessarily have $\mathrm{div}(\nabla\sigma\circ\nabla\mathfrak{h}^\star)=0$ for the minimizer $\mathfrak{h}^\star$. We would also need to check that the second order expansion is positively defined, but it holds automatically due to convexity of the functional I.

4.2.1 Brief summary of analytic properties of limit shape

In the article [ADPZ20], the authors establish analytic properties of the minimizers coming from the dimer models. Let us mention some of them. The paper discusses the generic dimer model with periodic weights. However, we will focus on the case of random domino tilings, or lattice $\Lambda=\mathbb{Z}^2$ with uniform weights (all the weights equal to 1).

We need to restrict ourselves to a particular class of domains called *natural domains* with *natural boundary heights (boundary conditions)*. First, let us orient the sides of the Newton polygon $\mathcal{N}_{\mathbb{Z}^2}$ in the counterclockwise direction, and denote them $\mathcal{P}_N,\mathcal{P}_W,\mathcal{P}_S,\mathcal{P}_E$. A natural domain $\Omega\in\mathbb{R}^2$ is a polygon with edges $\{\ell_i\}_{i=1}^{i=k}$ such that for each pair of adjacent edges ℓ_k,ℓ_{k+1} we can find a pair of adjacent edges l_m,l_{m+1} of the Newton polygon $\mathcal{N}_{\mathbb{Z}^2}$ such that $\langle\ell_k,l_m\rangle=0$ and $\langle\ell_{k+1},l_{m+1}\rangle=0$ or $\langle\ell_{k+1},l_m\rangle=0$ and $\langle\ell_k,l_{m+1}\rangle=0$.

More precisely, for the square lattice, it means that the sides are parallel to the directions of the square lattice, with an angle of ± 90 degrees between two consecutive sides. Therefore, the natural domains look similarly to the Aztec diamond, for example Aztec rectangles.

A natural domain admits various boundary conditions, and we call $\mathfrak{b}$ a *natural boundary condition* if on every edge ℓ_i connecting consecutive vertices z_j, z_{j+1} of Ω with z being a point on ℓ_i,

$$\mathfrak{b}(z)=\langle p_n, z-z_j\rangle+\mathfrak{b}(z_j). \quad (4.2.9)$$

In practice, it means that the asymptotic height function $\mathfrak{h}$ has $\nabla\mathfrak{h}\in\partial\mathcal{N}$ and the function is affine on the components of the boundary in the continuous picture, while on the discrete picture each side of the domain consists of brick-wall patterns like sides of an Aztec diamond.

We may expect a situation similar to the Aztec diamond with a liquid region in the center of the domain, and frozen phases near the corners. Let us define them once again, starting from minimizer $\mathfrak{h}$. Let us follow notations from [ADPZ20]. First, define three sets

Let us explain the quasifrozen regions on the following computer simulation on Figure 4.2, where we have two types of boundary behavior near $\partial\mathcal{L}$. The two connected components of the liquid region are separated from each other by the quasifrozen region, which in the discrete picture consists of two types of lozenges in contrast to the frozen regions, which consists of exactly one type. Furthermore, the boundary conditions do not fix the picture completely, for example on the Figure 4.2, there are two different simulations done for the same boundary conditions.

Theorem 5.15 from [ADPZ20] summarizes boundary regularity,

Figure 4.2: Quasifrozen domain for a lozenge tiling model with the same boundary conditions, but with different functions σ, computer simulations by M.Duits [ADPZ20]

Theorem 4.2.3 ([ADPZ20])**.**

1. *The boundary $\partial\mathcal{L}$ is the real locus of an algebraic curve.*
2. *Each connected component of $\partial\mathcal{L}$ is isomorphic to $\partial\mathbb{D}$, $\partial\mathcal{L}_k = f_k(\partial\mathbb{D})$, where f_k is holomorphic inside the disk.*
3. *$\partial\mathcal{L}$ is locally smooth and convex except at a finite number of points.*
4. *The only singularities of $\partial\mathcal{L}$ are cusps and tacnodes, see Figure 4.3.*

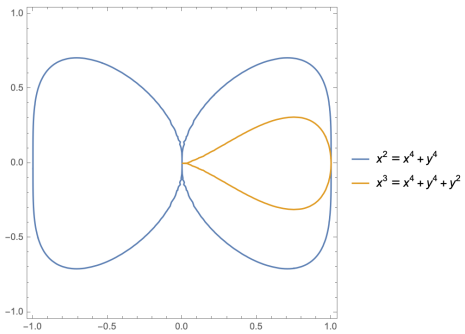

Figure 4.3: Examples of curves having a singularity at the origin: a *cusp* for the curve in yellow, and a *tacnode* for the curve in blue.

Therefore, we have the following picture going from the boundary of the region to the bulk: near the boundary $\partial\Omega$, we have frozen and quasifrozen regions, where $\mathfrak{h}$ is linear with the maximal possible slope, $\mathfrak{h} \in \partial\mathcal{N}$. The boundary of this part is the arctic curve $\mathcal{C}$, which is smooth except at finitely many points. After crossing the boundary, we end up in the liquid region, where $\nabla\mathfrak{h} \in \mathring{\mathcal{N}}$. There, we might have another connected component of the arctic curve $\mathcal{C}$, which bounds a gas phase where the gradient is constant $\nabla\mathfrak{h} = q$. Now, we know enough properties of $\partial\mathcal{L}$ to perform some computations, and the main tool are isothermal coordinates, which help to simplify the analysis of the Euler-Lagrange equations for the dimer model.

4.2.2 The tangent plane method and the complex Burgers equation

Here we discuss a novel method of computation of the arctic curves, the *tangent plane method* proposed by Kenyon and Prause in [KP22]. The method can be applied to a generic

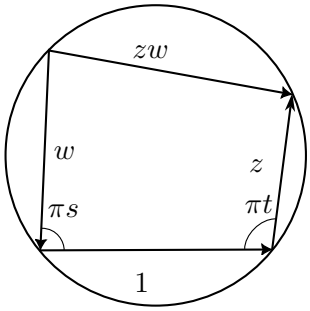

Figure 4.4: Relation between coordinates (s,t) and (z,w)

gradient variational problem. However, we are going to give the description for the situation for random domino tilings. For generic situation, see [KP22; KP24].

The idea is that we start with the liquid region $\mathcal{L}$, and then assuming that $\mathfrak{h}$ is the minimizer, we map the liquid region to the Newton polygon, $(x,y) \mapsto (s,t) := \nabla\mathfrak{h}(x,y) \in \mathcal{N}$. Moreover, in the paper [KP22], the authors look at $\mathcal{N}$ as a Riemann surface with the metric g given by the Hessian of surface tension σ:

$$g = \sigma_{ss} ds^2 + 2\sigma_{st} ds dt + \sigma_{tt} dt^2. \tag{4.2.10}$$

Convexity of σ implies that the Hessian is positive definite, and thus corresponds to a (non-degenerate) metric.

Then, they perform the main trick of the method, that is a specific change of coordinates, $(s,t) \mapsto z$, for complex variables z on the spectral curve $P(z,w) = 0$. The relation between (s,t) and (z,w) can be formulated graphically as on Figure 4.4. We justify this figure in Theorem 4.2.4 below.

Such z is an example of an isothermal/conformal coordinate, which diagonalizes metric g, as we are going to show. More generally, call a map ζ that completes the following commutative diagram the *intrinsic coordinate*,

$$\begin{array}{ccc} \mathcal{L} & \xrightarrow{\nabla\mathfrak{h}} & \mathcal{N} \\ \downarrow 1{:}1 & & \downarrow 1{:}1 \\ \Sigma^+ & \xrightarrow{\deg\, d} & \mathcal{C}^+ \\ \cap & & \cap \\ \Sigma & \xrightarrow{\pi} & \mathcal{C} \end{array}$$

There is always a choice of orientation of such an intrinsic coordinate ζ, and we fix it so that it is an orientation-reversing map to the upper half plane, such an intrinsic coordinate is z. (The upper half plane is the upper half of the spectral curve, which is in this case the Riemann sphere).

Theorem 4.2.4. *In the liquid region $\mathcal{L}$, there are defined two functions $z(x,y)$, $w(x,y)$ satisfying the following properties,*

1. $\nabla\mathfrak{h} = \frac{1}{\pi}(\arg w, -\arg z)$,
2. *Ampère's equation* $\frac{z_x}{z} + \frac{w_y}{w} = 0$,
3. *spectral curve equation* $P(z,w) = 0$.

Proof. We start with a point (z_0, w_0) on the spectral curve $\{P(z,w)=0\}$. Then, we know that the real part of its image under the logarithm map $(\log|z_0|, \log|w_0|)$ defines a point in the amoeba $(X,Y) := (\log|z_0|, \log|w_0|) \in \mathcal{A}$. Here, we assume that (z_0, w_0) is a generic point, so that $(X,Y) = (\log|z_0|, \log|w_0|)$ is in the interior of $\mathcal{A}$. We further assume that $z_0 \in \mathbb{H}$ (so that w_0 has a negative imaginary part. In fact, we know from the Harnack property of the spectral curve that there is exactly another root of P, which is sent to the same point of the amoeba, given by $(\bar{z_0}, \bar{w_0})$. We write

$$z_0 = e^{X+i\theta_0}, \qquad w_0 = e^{Y+i\omega_0},$$

with $\theta_0 \in (0,\pi)$ and $\omega_0 \in (\pi, 2\pi)$.

The gradient of the Ronkin function $\mathcal{R}$ evaluated at this point defines the corresponding slope (s,t). More precisely, we have the following equation,

$$(s,t) := \nabla\mathcal{R}(\log|z|, \log|w|). \tag{4.2.11}$$

Let us compute the derivatives of the $\mathcal{R}$ by its definition,

$$\begin{aligned} s = \frac{\partial}{\partial X}\frac{1}{(2\pi i)^2}\iint_{\mathbb{T}^2}\log P(e^X z, e^Y w)\frac{dzdw}{zw} &= \frac{1}{(2\pi i)^2}\int_{|w|=e^Y}\left(\int_{|z|=e^X}\frac{\partial_X P(e^X z, e^Y w)}{P(e^X z, e^Y w)}\frac{dzdw}{zw}\right) \\ &= \frac{1}{2\pi i}\int_{|w|=e^Y}\frac{dw}{w}\left(\frac{1}{2\pi i}\int_{|z|=e^X} d\log P\right), \end{aligned} \tag{4.2.12}$$

where we look at $\left(\frac{1}{2\pi i}\int_{|z|=e^X} d\log P\right)$ as a function of w, which is fixed, and then integrate it over the circle $\{|w| = e^Y\}$. For a given value of w, there is a unique value of $z = z(w) = \frac{w+1}{w-1}$ such that $P(z(w), w) = 0$. It turns out that when w moves counterclockwise around the circle of radius e^Y, the root $z(w)$ is inside the disc of radius e^X when w is on the arc from $\bar{w_0}$ to w_0, and outside when w is on the arc from w_0 to $\bar{w_0}$. As a consequence, the function $w \mapsto \int_{|z|=e^X} d\log P(\cdot, w)$ is a the indicator function of the arc $(\bar{w_0}, w_0)$.

Therefore, the remaining integral is

$$s = \int_{\bar{w_0}}^{w_0}\frac{1}{2\pi i}\frac{dw}{w} = \frac{1}{2\pi i}(\log w_0 - \log\bar{w_0}) = \frac{1}{2i\pi}(\log(e^{Y+i\omega_0}) - \log(e^{Y+i(2\pi-\omega_0)})) = \frac{\omega_0}{\pi} - 1.$$

The computation for the other coordinate of the gradient corresponding to t is the same except that the integral $\frac{1}{2i\pi}\int_{|w|=e^Y} d\log P(z,\cdot)$ is the indicator function of the oriented arc from z_0 to $\bar{z_0}$. This means that when we integrate the result over z, we get

$$t = \int_{z_0}^{\bar{z_0}}\frac{1}{2\pi i}\frac{dz}{z} = \frac{1}{2\pi i}(\log\bar{z_0} - \log z_0) = \frac{1}{2i\pi}(\log(e^{X+i(2\pi-\theta_0)}) - \log(e^{X+i\theta_0})) = 1 - \frac{\theta_0}{\pi}.$$

As a result, we have that

$$\log z_0 = X + \pi i(1-t), \qquad \log w_0 = Y + \pi i(1+s). \tag{4.2.13}$$

By a global translation of the set of slopes by the vector $(1,-1)$ (or by replacing z by $-z$ and w by $-w$), we can assume that the following relation holds

$$\log z_0 = X - i\pi t, \qquad \log w_0 = Y + i\pi s. \tag{4.2.14}$$

We now associate to each point (x,y) of the liquid region a pair (z,w), in such a way that the arguments of $z(x,y) = z_0$ and $w(x,y) = w_0$ match the (translated) slopes $-t$ and s respectively, times π according to (4.2.14).

Now, we substitute X, Y from (4.2.14) to the intrinsic Euler Lagrange equation, which can be rewritten as $X_x + Y_y = 0$ and see that it becomes $\mathrm{Re}(\frac{z_x}{z} + \frac{w_y}{w}) = 0$. This is one real equation, which should be supplemented with a consistency condition $\frac{\partial s}{\partial y} = \frac{\partial t}{\partial x} = \frac{\partial^2 \mathfrak{h}}{\partial y \partial x}$ or $-\frac{\partial s}{\partial y} + \frac{\partial t}{\partial x} = 0$, which by (4.2.11) can be written as $\langle(-\frac{\partial}{\partial y}, \frac{\partial}{\partial x}), \nabla\mathcal{R}(\log|z|, \log|w|)\rangle = 0$, since $\nabla\mathcal{R}(\log|z|, \log|w|) = \frac{1}{\pi}(+\arg w, -\arg z)$. Thus, we end up with the second real equation $\mathrm{Im}(\frac{z_x}{z} + \frac{w_y}{w}) = 0$. It completes the derivation of the Ampère's equation. □

It turns out that the coordinate z itself defines isothermal coordinates $(U, V) := (\mathrm{Re}z, \mathrm{Im}z)$. In fact, let us look at (4.2.14). Since logarithm is a holomorphic map, it satisfies the Cauchy-Riemann equations, and so does the right-hand side. For example, for $Y + i\pi s$ we have two equations,

$$Y_U = \pi s_V, \qquad Y_V = -\pi s_U. \tag{4.2.15}$$

and for $X - i\pi t$.

$$X_U = -\pi t_V, \qquad X_V = \pi t_U. \tag{4.2.16}$$

These equations are combined into complex equations with the help of Wirtinger derivatives,

$$X_z = \frac{1}{2}(X_U - iX_V) = \frac{1}{2}(-i\pi(s_U - is_V)) = -i\pi s_z,$$
$$Y_z = i\pi t_z. \tag{4.2.17}$$

We also see that $\frac{Y_z}{s_z} = i\pi = -\frac{X_z}{t_z}$, therefore, we have $\frac{X_z}{t_z} + \frac{Y_z}{s_z} = 0$. It is the first criterion for z being an intrinsic variable from proposition 2.1 from [KP24].

Then, recall that $X = \sigma_s(s,t), Y = \sigma_t(s,t)$, which enables us writing

$$\pi s_V = Y_U = \sigma_{st}s_U + \sigma_{tt}t_U, \pi t_V = -X_U = -\sigma_{ss}s_U - \sigma_{st}t_U. \tag{4.2.18}$$

This is nothing but the real Beltrami equation, a sufficient condition for the coordinates (U, V) to be isothermal/conformal. Thus, $z = U + iV$ is the intrinsic coordinate according to the definition of [KP22]. The authors there propose a criterion for a coordinate ζ to be an intrinsic one, that we formulate in the following Proposition:

Proposition 4.2.5 ([KP22], Proposition 2.1)**.** *The following two equations are each equivalent to ζ being an intrinsic coordinate*

$$\frac{X_\zeta}{s_\zeta} + \frac{Y_\zeta}{t_\zeta} = 0 \tag{4.2.19}$$

$$\frac{s_\zeta}{t_\zeta} = \frac{-\sigma_{st} - i\sqrt{\det H_\sigma}}{\sigma_{ss}} \tag{4.2.20}$$

And in the case the above equations hold, we have

$$\frac{X_\zeta}{t_\zeta} = -i\det H_\sigma = -\frac{Y_\zeta}{s_\zeta}. \tag{4.2.21}$$

Note also that the last relation from Proposition 4.2.5 together with (4.2.17) implies that $\det H_\sigma = \pi^2$.

Proof. Let us define $\gamma := \frac{s_\zeta}{t_\zeta}$. Then, due to $X_\zeta = (\sigma_s)_\zeta = \sigma_{ss} s_\zeta + \sigma_{st} t_\zeta$, we write $\frac{X_\zeta}{t_\zeta} = \sigma_{ss}\gamma + \sigma_{st}$. Rewriting this computation for Y, we see $\frac{Y_\zeta}{s_\zeta} = \sigma_{tt}\frac{1}{\gamma} + \sigma_{st}$. Therefore, the first condition of Proposition 4.2.19 is nothing but

$$\sigma_{ss}\gamma^2 + 2\sigma_{st}\gamma + \sigma_{tt} = 0. \tag{4.2.22}$$

The two roots are

$$\gamma = \frac{-\sigma_{st} \pm i\sqrt{\det H_\sigma}\sigma_{ss}}{\sigma_{ss}}. \tag{4.2.23}$$

Since in our convention, ζ is assumed to be orientation-reversing map, $\operatorname{Im}(\gamma) < 0$ and we have the minus sign. Furthermore, $\frac{X_\zeta}{t_\zeta} = -i\sqrt{\det H_\sigma} = \frac{Y_\zeta}{s_\zeta}$. □

Now, with the help of Proposition 4.2.5 we can prove the intrinsic Euler-Lagrange equation in two forms,

Proposition 4.2.6. *For $(x, y) \in \mathcal{L}$ we have*

$$X_\zeta \zeta_x + Y_\zeta \zeta_y = 0, \tag{4.2.24}$$

$$\frac{\zeta_x}{\zeta_y} = \frac{s_\zeta}{t_\zeta} = \gamma. \tag{4.2.25}$$

Proof. The last expression of the proof of Proposition 4.2.5 implies that (we are using the chain rule for $X_x = X_\zeta \zeta_x + X_{\bar\zeta}\bar\zeta_x$ and $\bar f(\bar z) = \overline{f(z)}$) ,

$$X_x - i\sqrt{\det H_\sigma} t_x = X_\zeta \zeta_x + X_{\bar\zeta}\bar\zeta_x - i\sqrt{\det H_\sigma}(t_\zeta \zeta_x + t_{\bar\zeta}\bar\zeta_x) = \tag{4.2.26}$$

$$= (X_\zeta - i\sqrt{\det H_\sigma} t_\zeta)\zeta_x + \overline{(X_\zeta + i\sqrt{\det H_\sigma} t_\zeta)\zeta_x} = 2X_\zeta \zeta_x. \tag{4.2.27}$$

Similarly for Y,

$$Y_y + i\sqrt{\det H_\sigma} s_y = 2Y_\zeta \zeta_y. \tag{4.2.28}$$

Therefore, since $t_x = s_y$ we have the following intrinsic Euler-Lagrange equation

$$X_\zeta \zeta_x + Y_\zeta \zeta_y = 0. \tag{4.2.29}$$

Let us look at (4.2.14), the left-hand side $X - i\pi t$ is a holomorphic function of ζ, as well as $Y + i\pi s$. Therefore, they satisfy the Cauchy-Riemann equation, which tells us that

$$X_\zeta = i\pi t_\zeta, \tag{4.2.30}$$

$$Y_\zeta = -i\pi s_\zeta. \tag{4.2.31}$$

Which in combination with $X_\zeta \zeta_x + Y_\zeta \zeta_y = 0$ gives us that $t_\zeta \zeta_x - s_\zeta \zeta_y = 0$ or $\frac{t_\zeta}{s_\zeta} = \frac{\zeta_y}{\zeta_x} = \frac{1}{\gamma}$.

Then, apply the Proposition 4.2.6 combined with the relation $-\frac{y_{\bar z}}{x_{\bar z}} = \frac{z_x}{z_y}$. It follows from $z = z(x, y)$, where we take the derivative with respect to $\bar z$ and obtain $0 = z_x x_{\bar z} + z_y y_{\bar z}$. Finally, we get $-\frac{y_{\bar z}}{x_{\bar z}} = \frac{z_x}{z_y} = \frac{s_z}{t_z}$, and we are done. □

However, one can see that z is a conformal coordinate directly from the equation we already have. Let us show that the metric g in coordinates (U, V) is diagonal, i.e., that the scalar product $g(\frac{\partial}{\partial U}, \frac{\partial}{\partial V}) = 0$ and $g(\frac{\partial}{\partial U}, \frac{\partial}{\partial U}) = g(\frac{\partial}{\partial V}, \frac{\partial}{\partial V})$. For this, let us note the expressions for the vector fields in coordinates (s, t).

$$\frac{\partial}{\partial U} = s_U \frac{\partial}{\partial s} + t_U \frac{\partial}{\partial t}, \qquad \frac{\partial}{\partial V} = s_V \frac{\partial}{\partial s} + t_V \frac{\partial}{\partial t}.$$

Now, the scalar product $g(\frac{\partial}{\partial U}, \frac{\partial}{\partial V})$ equals to

$$\sigma_{ss} s_U s_V + \sigma_{st}(s_V t_U + s_U t_V) + \sigma_{tt} t_U t_V. \tag{4.2.32}$$

Then, using (4.2.14) we have

$$\pi s_V = Y_U = \sigma_{st} s_U + \sigma_{tt} t_U, \pi t_V = -X_U = -\sigma_{ss} s_U - \sigma_{st} t_U. \tag{4.2.33}$$

It helps us to express the derivatives with respect to V through derivatives with respect to U in (4.2.32), let us write each term of (4.2.32) and mark by the same color the terms which cancel each other in the sum (4.2.32).

$$\begin{aligned}
\pi\sigma_{st} t_U s_V &= \sigma_{st}^2 s_U t_U + \sigma_{st}\sigma_{tt} t_U^2, \\
\pi\sigma_{st} s_U t_V &= -\sigma_{ss}\sigma st s_U^2 - \sigma_{st}^2 s_U t_U \\
\pi\sigma_{ss} s_U s_V &= \sigma_{ss}\sigma_{st} s_U^2 + \sigma_{ss}\sigma_{tt} t_U s_U \\
\pi\sigma_{tt} t_U t_V &= -\sigma_{ss}\sigma_{tt} t_U s_U - \sigma_{st}\sigma_{tt} t_U^2
\end{aligned}$$

As for the diagonal elements of the metric, we have

$$g(\frac{\partial}{\partial U}, \frac{\partial}{\partial U}) = \sigma_{ss} s_U^2 + 2 s_U t_U \sigma_{st} + \sigma_{tt} t_U^2, \tag{4.2.34}$$

$$g(\frac{\partial}{\partial V}, \frac{\partial}{\partial V}) = \sigma_{ss} s_V^2 + 2 s_V t_V \sigma_{st} + \sigma_{tt} t_V^2. \tag{4.2.35}$$

Let us repeat the same steps and express derivatives with respect to V, (note that we have an extra multiple π in (4.2.33), which appear each time we transform derivative with respect to V into derivative with respect to U)

$$\begin{aligned}
\frac{1}{\pi^2}(\sigma_{ss}(\sigma_{st} s_U + \sigma_{tt} t_U)^2 \\
+ 2\sigma_{st}(\sigma_{st} s_U + \sigma_{tt} t_U)(-\sigma_{ss} s_U - \sigma_{st} t_U) \\
+ \sigma_{tt}(\sigma_{ss} s_U + \sigma_{st} t_U)^2).
\end{aligned} \tag{4.2.36}$$

Then, comparison of coefficients in front of s_U^2 shows that in (4.2.34) we have σ_{ss}, while in (4.2.36) we have

$$\frac{1}{\pi^2}\sigma_{ss}(\sigma_{st}^2 - 2\sigma_{st}^2 + \sigma_{tt}\sigma_{ss}) = \sigma_{ss}\frac{\sigma_{ss}\sigma_{tt} - \sigma_{st}^2}{\pi^2} = \sigma_{ss} \tag{4.2.37}$$

(terms which contribute to the coefficient are in the olive color). A similar computation done for coefficients in front of t_U^2 shows that (the terms are in the red color), on one hand, we get σ_{tt}, while on the other hand

$$\frac{1}{\pi^2}\sigma_{tt}(\sigma_{ss}\sigma_{tt} - \sigma_{st}^2) = \sigma_{tt}. \tag{4.2.38}$$

Finally, the same computation shows agreement for the coefficient in front of $s_U t_U$, $2\sigma_{s,t}$ on one hand, and $\frac{1}{\pi^2}(2\sigma_{s,t}(\sigma_{s,s}\sigma_{t,t} - \sigma_{s,t}^2 - \sigma_{t,t}\sigma_{s,s} + \sigma_{t,t}\sigma_{s,s})) = 2\sigma_{s,t}$ on the other.

4.2.3 An intermediate parameterization

It may happen that there are several points in the liquid region with the same slope $(s,t) \in \mathring{\mathcal{N}} \setminus \mathscr{G}$. In that case it is not possible to parameterize the liquid region by the slope, and thus by the coordinate z. However, the degree d of $\nabla\mathfrak{h}\colon \mathcal{L} \to \mathring{\mathcal{N}} \setminus \mathscr{G}$ is constant except many at a finite number of points. We can therefore introduce a ramified covering Σ of degree d over the spectral curve $\{P(z,w)=0\}$ such that the variables z and w are now meromorphic functions of the variable $u \in \Sigma$. Let Σ^+ the preimage by z of the upper-half plane. This gives a diffeomorphism from Σ^+ to the liquid region.

The functions s and t, considered before as functions of z, can be now seen also as functions of $u \in \Sigma^+$.

4.2.4 The intercept function

Let us look at the graph of the minimizer $\mathfrak{h}^\star$. More precisely, take the tangent plane $\mathcal{P}_{x_0,y_0}$ to it at a given point (x_0,y_0). It has a slope given by $\nabla\mathfrak{h}^\star(x_0,y_0) = (s(x_0,y_0), t(x_0,y_0))$. It also intersects the vertical axis at the ordinate $(\mathfrak{h}^\star - (sx+ty))$. The function $c := \mathfrak{h}^\star - sx - ty$ is called *the intercept*. With its help, we can parametrize the tangent planes to the plot of $\mathfrak{h}^\star$ as follows,

$$\mathcal{P}_{x_0,y_0} = \{(x,y,z) \in \mathbb{R}^3 | \{s(x_0,y_0)x + t(x_0,y_0)y + c(x_0,y_0) = z\}. \tag{4.2.39}$$

The important properties of c for us are first, it is constant on every frozen region since on each frozen region $\mathfrak{h}^\star$ is linear with a fixed slope, and so is its tangent plane. Thus, after subtracting the linear part of $\mathfrak{h}^\star$, the difference takes a constant value on each frozen region. Further, the minimizer $\mathfrak{h}^\star$ can be reconstructed from s, t and c as $\mathfrak{h}^\star = sx + ty + c$. After it, the limit shape is obtained as the envelope of planes given by (4.2.39). The main property of these planes is harmonicity of functions s, t and c as functions of the isothermal coordinate, which is discussed in the next section.

4.2.5 Harmonicity of s, t and c

The property of functions s,t and c as functions of isothermal coordinate u is that they are harmonic by Theorem 3.1 from [KP22].

Now, let us re-formulate Proposition 4.2.5 in real terms and prove harmonicity of s,t and c in isothermal coordinates.

Proposition 4.2.7. *The functions s, t and c are harmonic in the variable $u \in \Sigma^+$.*

Proof. Functions s and t are harmonic in the variable u since they are equal to the argument (imaginary part of the logarithm) of z and w, which are holomorphic functions of u in the interior of Σ^+.

Next, consider $c = (\mathfrak{h} - (sx+ty))$, and let us apply to it ∂_u and $\partial_{\bar{u}}$ remembering that

$$\nabla\mathfrak{h} = (\mathfrak{h}_x, \mathfrak{h}_y) = (s,t),$$

$$c_u = (\mathfrak{h} - (sx+ty))_u = \mathfrak{h}_x x_u + \mathfrak{h}_y y_u - (s_u x + t_u y + s x_u + t y_u) = -s_u x - t_u y. \tag{4.2.40}$$

Then, applying $\partial_{\bar{u}}$ we obtain by harmonicity of s,t

$$\partial_{\bar{u}}(s_u x + t_u y) = s_u x_{\bar{u}} + t_u y_{\bar{u}}. \tag{4.2.41}$$

Moreover, taking the derivative of $u = u(x, y)$ with respect to $\bar{u}$ (which gives 0), we get by the chain rule: $0 = u_x x_{\bar{u}} + u_y y_{\bar{u}}$. Since u is locally a holomorphic function of z, it is also an intrinsic coordinate. We can therefore apply Proposition 4.2.6, and get

$$-\frac{y_{\bar{u}}}{x_{\bar{u}}} = \frac{u_x}{u_y} = \frac{s_u}{t_u},$$

from which it follows that

$$\Delta_u c = 4c_{u,\bar{u}} = 0.$$

□

Therefore, we can hope to reconstruct all three functions as long as we are able to perform explicit harmonic extensions of piecewise constant boundary conditions. As a corollary, we can obtain the limit shape $\mathfrak{h}^\star$ as envelope of harmonically moving planes by Theorem (4.2.9), see also [KP22, Theorem 3.2],

4.2.6 Tangent plane equation

Introduce the main equation of the method, Equation (20) from [KP22], which will help us to compute the arctic curve.

Proposition 4.2.8. *Inside the liquid region, parameterized by $u \in \Sigma^+$, the following equation holds:*

$$s_u x + t_u y + c_u = 0 \tag{4.2.42}$$

What is important is that this complex equation is equivalent to two real equations for the real and imaginary parts, which gives for every $u \in \Sigma^+$ a linear system for $(x(u), y(u))$, once we know s, t, and c as functions of u.

Proof. Let us apply the Wirtinger derivative ∂_u to the minimizer $\mathfrak{h}$, remembering that $\nabla\mathfrak{h} = (s, t)$, we have the following equalities

$$\mathfrak{h}_u = sx_u + ty_u = (sx + ty)_u - (s_u x + t_u y) \tag{4.2.43}$$

$$s_u x + t_u y + (\mathfrak{h} - (sx + ty))_u = 0, \tag{4.2.44}$$

which is the same as

$$s_u x + t_u y + c_u = 0. \tag{4.2.45}$$

□

In practice, we deal with harmonic extensions made of linear combinations of $\arg(u)$, the important identities are first $\arg(u) = \operatorname{Im}\log(u)$, which we use to take the Wirtinger derivative as

$$\partial_u \arg(u) = \frac{1}{2i}\frac{1}{u}. \tag{4.2.46}$$

As a corollary of (4.2.7) and (4.2.8), we obtain the plot of the minimizer $\mathfrak{h}^\star$ over Σ^+ can be recovered as an envelope of harmonically moving planes with the slope given by $(s(u), t(u))$, $u \in \Sigma^+$.

Theorem 4.2.9 (Theorem 3.2 [KP22])**.** *The graph of the minimizer $\mathfrak{h}^\star$ over $u \in \Sigma^+$ is the envelope of harmonically moving planes $\mathcal{P}_u$ that satisfy two conditions:*

- $\mathcal{P}_u := \{(x(u), y(u), z(u)) \in \mathbb{R}^3 | s(u) + t(u) + c(u) = z(u)\}$
- $s_u x + t_u y + c_u = 0$

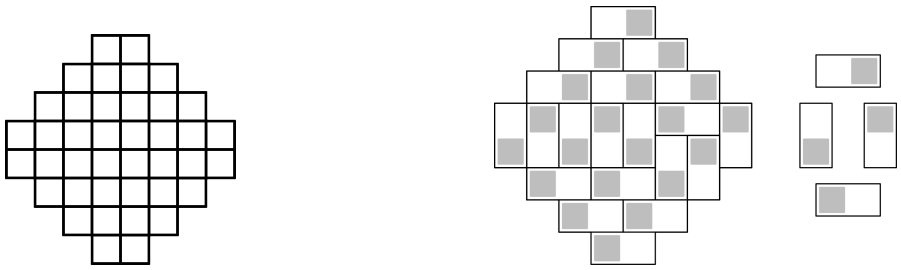

Figure 4.5: Example of the Aztec diamond of order 4 on the left, and a domino tiling of it on the right, with four types of dominoes according to the chess-board coloring.

4.3 Applications for the random domino tilings

In the rest of the chapter, we are going to explain the method applied to a simply-connected domain, the Aztec diamond, and to our main example, the Aztec diamond with a hole. We also need to use assumption for the number of frozen regions of the particular domains, and values of s, t and c there. This data is inferred from discrete boundary conditions and computer simulations.

4.3.1 A case with a simply-connected liquid region: the uniform Aztec diamond

Recall that the Aztec diamond of order N is the union of unit squares $S(m, n)$ of the square lattice whose centers (m, n) satisfy

$$|m - \frac{1}{2}| + |n - \frac{1}{2}| \leq N. \tag{4.3.1}$$

It is also convenient to introduce chess-board coloring on the square grid, this way we obtain 4 types of dominoes, see Figure 4.6.

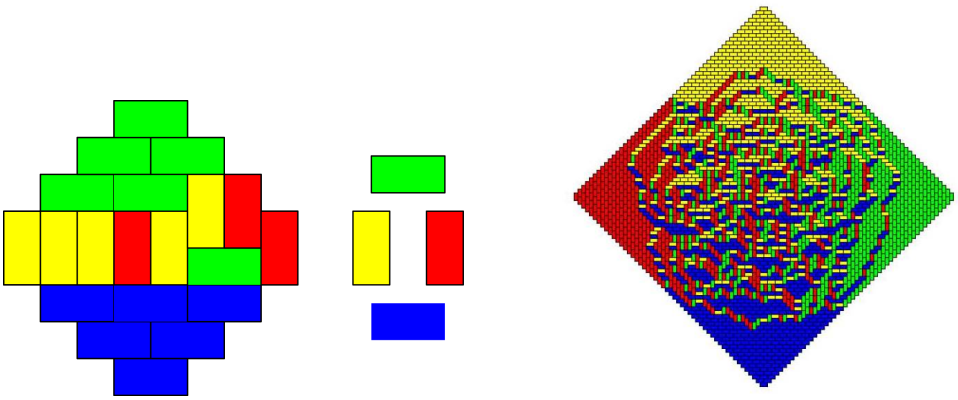

Figure 4.6: Example of the same domino tiling in color notation, and domino tiling of Aztec diamond of order 50 by J.Propp.

We consider in this section the case of the uniform measure on tilings of the Aztec diamond of size N. As N goes to infinity, the height function converges in probability to a deterministic function which is linear in the four regions in the limiting renormalized square deprived from the inscribed disc (the *frozen regions*) and is smooth inside the inscribed disc (the *liquid* region). This statement is due to Jockush, Propp and Shore [JPS98]. The goal of this section is to recover this result using the tangent plane method, described above, following loosely [KP22, Section 6.1],[Section 2.3][KP24].

Applying the tangent plane method

In the case of the uniform Aztec diamond, it is convenient to use a coordinate system (x, y) in the renormalized domain wich is rotated by 45 degrees with respect to the horizontal/vertical discrete coordinate axes, so that the renormalized domain becomes in the limit the unit square $[0, 1] \times [0, 1]$. See Figure 4.8 to see the directions of the two axes for x and y.

In the liquid region $\mathcal{L}$, there is a unique point where the limiting height function has a given slope in the interior of the Newton polygon (the fact that each of the four frozen phases is seen only once on the boundary of $\mathcal{L}$ is a sign that the degree d from u to z or w is 1). This is thus a case when we can take $u = z$: the liquid region can be paramaterized by $z \in \mathbb{H}$. We now determine the values for s, t and c on the boundary of the liquid region (which corresponds to $z \in \mathbb{R} \cup \{\infty\}$, bounded by the four distinct frozen regions.

Each interval $(-\infty, -1)$, $(-1, 0)$, $(0, 1)$, $(1, \infty)$ corresponds to an arc of the arctic curve touching a given frozen phase, with slope (s, t) given respectively (with the convention of the slope given by Equation (4.2.13)) by $(1, 0)$, $(0, 0)$, $(0, 1)$ and $(1, 1)$ respectively.

We form a table consisting of four columns for each frozen region, and three rows for each function s, t and c.

	(1) $z < -1$ $1 > w > 0$	(2) $-1 < z < 0$ $0 > w > -1$	(3) $0 < z < 1$ $-1 > w$	(4) $1 < z$ $w > 1$
s	1	0	0	1
t	0	0	1	1
c	0	1	0	0

The value of c is determined up to some additive constant, fixed here to be zero. Its value in each region is fixed by the condition that the linear parts of the height functions with the given slopes in the table should match at the "turning points", where two frozen regions touch on the boundary of the Aztec diamond. See Figure 4.7 for a picture of those linear pieces.

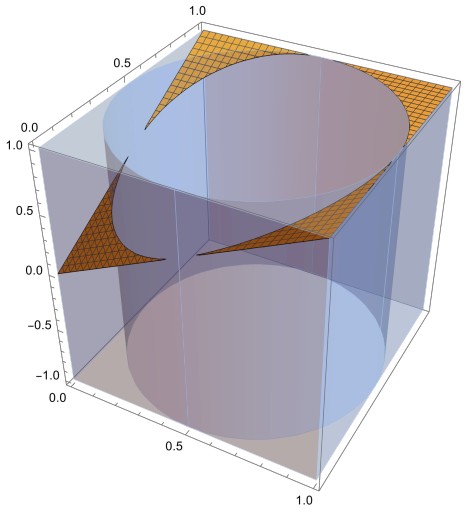

Figure 4.7: Height above the frozen regions of the Aztec diamond, which is a piecewise linear function. The values of c on each arc of the arctic curve reflect the continuity of the height along the boundary of the liquid region.

We represent visually on Figure 4.8 the information of the table, and four specific values of z at the transition between two frozen phases near the arctic curve.

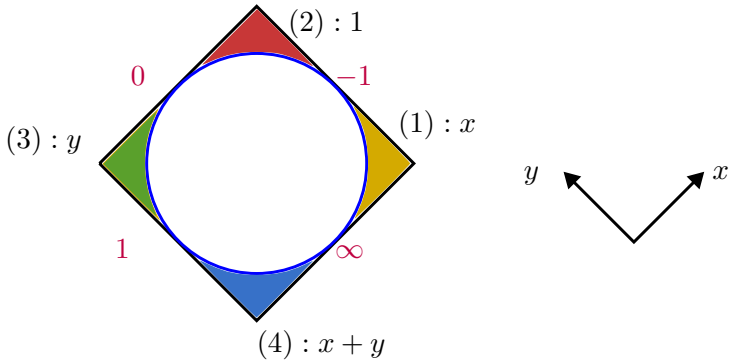

Figure 4.8: The four frozen phases of the Aztec diamond, with colors corresponding to branches of the boundary of the amoeba from Figure 1.18. For each region, we indicate in black the equation for the ordinate as an affine function of x and y. For each "turning point", we indicate in purple the corresponding value of z in the parametrization.

Parametrization of the limit shape of the Aztec diamond

We know that s, t and c are harmonic functions of the variable z. We construct explicit harmonic extensions of the boundary values from the table. For s and t, the answer is given directly by Equation (4.2.13), which can be rewritten as

$$s(z) = \frac{1}{\pi}\arg(-w(z)) = \frac{1}{\pi}\arg\frac{1-z}{1+z}, \qquad t(z) = -\frac{1}{\pi}\arg(-z) = 1 - \frac{1}{\pi}\arg(z).$$

For c, we proceed with the same idea, using building blocks of the form

$$f(z) = \frac{1}{\pi}\arg\frac{z-b}{z-a}$$

which is the harmonic extension of the indicator function of interval $[a, b]$. The corresponding harmonic extensions is:

$$c(z) = \frac{1}{\pi}\arg\frac{z}{z+1}.$$

Another choice of conformal coordinate instead of z which will be useful in connection with the next example is choosing $\zeta = \frac{2}{\pi}\arctan z$, which maps the complex plane to an infinite cylinder $\mathbb{C}/2\mathbb{Z}$. The upper-half plane for z parametrizing the liquid region (respectively the real axis together with the point at infinity parametrizing the arctic curve) is mapped to the upper half of the cylinder (respectively to $\mathbb{R}/2\mathbb{Z}$).

The table of boundary conditions of s, t and c for $\mathcal{AD}$ for the variable ζ is the following (where the intervals for ζ represent a cyclic order, as on the cylinder, $-1 = 1$):

	(1) $-1 < \zeta < -\frac{1}{2}$	(2) $-\frac{1}{2} < \zeta < 0$	(3) $0 < \zeta < \frac{1}{2}$	(4) $\frac{1}{2} < \zeta < 1$
s	1	0	0	1
t	0	0	1	1
c	0	1	0	0

The harmonic extensions in this parametrization are given by the pullback under the map $z \mapsto \frac{2}{\pi}\arctan(z)$, that is, by a composition with the map $\zeta \mapsto \tan(\frac{\pi\zeta}{2})$.

$$s(\zeta) = \frac{1}{\pi}\arg\frac{1-\tan(\frac{\pi\zeta}{2})}{1+\tan(\frac{\pi\zeta}{2})} = \frac{1}{\pi}\arg\tan(\frac{\pi}{2}(\frac{1}{2}-\zeta)),$$
$$t(\zeta) = 1 - \frac{1}{\pi}\arg(\tan(\frac{\pi\zeta}{2})),$$
$$c(\zeta) = \frac{1}{\pi}\arg\frac{\tan(\frac{\pi}{2}\zeta)}{\tan(\frac{\pi}{2}\zeta)+1}.$$

Now, we need to plug them into linear system for (x, y) given by Equation (4.2.8). For it, we need derivatives of s, t and c. Recall that we differentiate the $\arg z$ by applying the Wirtinger derivative using the identity $\arg(z) = \operatorname{Im}\log z$, which gives a factor $\frac{i}{2}$ to each arg, and therefore factorizes. Thus, we present derivatives without this common factor. In the coordinate z after a common multiplication by $2\pi i$, we have

$$2i\pi s_z = \frac{1}{z-1} - \frac{1}{z+1} = \frac{2}{z^2-1},$$
$$2i\pi t_z = \frac{1}{z},$$
$$2i\pi c_z = \frac{1}{z} - \frac{1}{z+1} = \frac{1}{z(z+1)}.$$

With the help of expressions, we can build parametric plots using linear system $s_z x + t_z y + c_z = 0$ for finding $(x(z), y(z))$, which continuously depends on z, and then by inversion, compute for every (x, y) in the liquid region the value of $s(x, y)$, $t(x, y)$, $c(x, y)$, which would give the equation of the tangent plane to the limit shape above the point (x, y). This would finally allow us to reconstruct the limiting height function $\mathfrak{h}$ as the enveloppe of this family of tangent planes.

But before that, there is something simpler we can do: we can look at the image of $\partial\mathbb{H}$ by the map $z \mapsto (x(z), y(z))$ which corresponds exactly to the arctic curve, that is the boundary of the liquid region.

Furthermore, from a computational point of view, it may be hard to give an analytical expression for the solution $(x(z), y(z))$ (except for the uniform Aztec diamond in coordinate z, as we will see). Rather, we can instead for each z compute the linear system and its solution, $(x(z), y(z))$ and plot it by varying z.

In fact, the functions defining the coefficients may not well-defined precisely on the boundary, thus if we try to do it numerically, we add a small positive imaginary part to z. This reflects the fact that gradient $\nabla\mathfrak{h}$ is defined only in the interior of the liquid region, and not on the arctic curve.

$$\operatorname{Re}(s_z)x + \operatorname{Re}(t_z)y + \operatorname{Re}(c_z) = 0, \tag{4.3.2}$$
$$\operatorname{Im}(s_z)x + \operatorname{Im}(t_z)y + \operatorname{Im}(c_z) = 0. \tag{4.3.3}$$

This is the approach we will use for the next examples.

But it turns out, as it is often the case for the Aztec diamond, that computations are quite easy, and we can find $x(z), y(z)$ for every $z \in \mathbb{H}$ by solving the simple linear system,

$$x(z) = \frac{|z-1|^2}{2(|z|^2+1)}, \qquad y(z) = \frac{1}{1+|z|^2}, \tag{4.3.4}$$

or even invert it to find $z(x, y)$. Indeed, the two real equations (4.3.2) and (4.3.3) are equivalent to the degree-2 complex equation in z:

$$2zx + (z^2-1)y - z + 1 = 0,$$

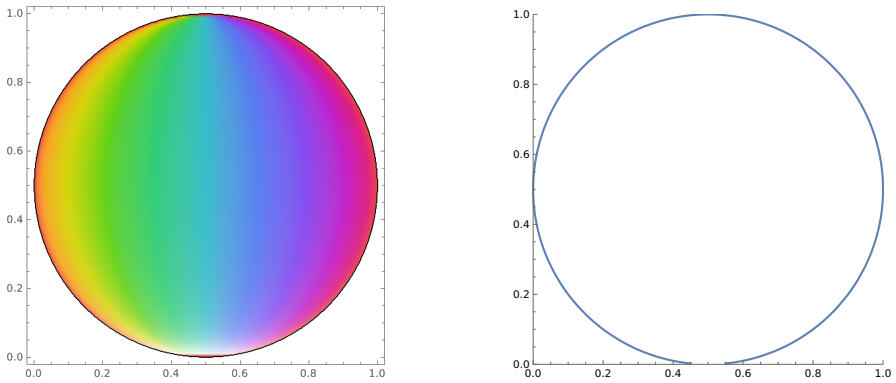

Figure 4.9: Left: the argument of $z(x, y)$ for (x, y) in the liquid region. Cyan means that z is pure imaginary, purple and pink (close to the right boundary) correspond to z near $\mathbb{R}^-$, whereas yellow and orange (on the left) means that z is close to $\mathbb{R}^+$. Right: a large piece of the arctic curve obtained from the parametrization by Equations 4.3.4, for z real between -20, 20. One can see that the bottom of the circle is cropped, meaning that this part corresponds to z in a neigbourhood of ∞.

for which we search the solution with positive (or rather non-negative) root, which is given by:

$$z(x, y) = \frac{1 - 2x + i\sqrt{1 - (2x - 1)^2 - (2y - 1)^2}}{2y},$$

At this point, we already recognize the arctic circle of radius $\frac{1}{2}$ and center $(\frac{1}{2}, \frac{1}{2})$ as the limit of definition of the square root defining z: this corresponds to the boundary of the liquid region. As mentionned before, another way to recover a parametrization of the arctic curve would be to take the solutions from Equation (4.3.4) and plot it for $z \in \mathbb{R} \cup \{\infty\}$. See Figure 4.9 for a plot of the argument of z across the liquid region, and for a parametric plot of the arctic curve.

Remark 2. Instead of taking the smallest fundamental domain with one white and one black vertex, and considering the spectral curve presented in Section 1.4.1, one could have taken a fundamental domain made of two white and two black vertices forming a 2×2-square. See Figure 4.10. The coordinate axes (x, y) are now aligned with the horizontal and vertical axes of the square lattice, so that the renormalized domain is a rotated square $|x| + |y| \leq 1$. If we label with 1 the vertices on the top row, and with 2 those of the second row of the fundamental domain, the modified Kasteley matrix $\mathcal{K}(z, w)$ is given by

$$\mathcal{K}(z, w) = \begin{pmatrix} 1 - w & z - 1 \\ \frac{1}{z} - 1 & \frac{1}{w} - 1 \end{pmatrix} \tag{4.3.5}$$

and the characteristic polynomial can be written as $-4 + z + w + \frac{1}{z} + \frac{1}{w}$. See Figure 4.10, right for the Newton polygon of this characteristic polynomial, and Figure 4.11 for its amoeba, with the indication of the four frozen phases. A similar table for boundary values of s, t and c.

	(1)	(2)	(3)	(4)
s	1	0	-1	0
t	0	-1	0	1
c	$-\frac{1}{2}$	$\frac{1}{2}$	$-\frac{1}{2}$	$\frac{1}{2}$

Note that in that case, z itself does not parametrize the liquid region: for a given value of z, there are two values of w such that (z, w) is on the spectral curve. However, one can

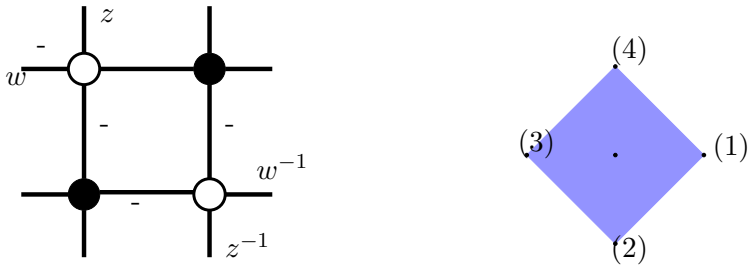

Figure 4.10: Left: a 2×2-fundamental domain for the square lattice. Kasteleyn minus signs are indicated on the edges, as well as the extra factors $z^{\pm 1}$ and $w^{\pm 1}$ for edges crossing the fundamental domain. Right: the Newton polygon of the corresponding characteristic polynomial.

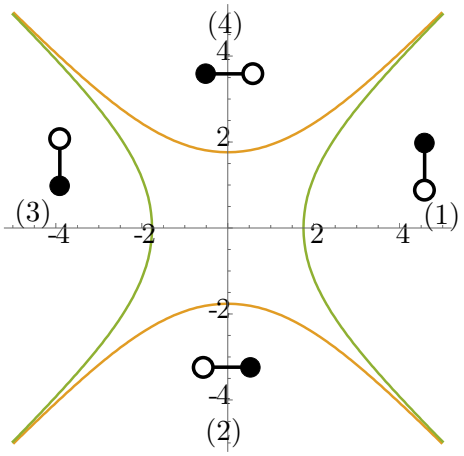

Figure 4.11: Amoeba of the characteristic polynomial $-4 + z + w + \frac{1}{z} + \frac{1}{w}$. The connected components of the complement are labeled with numbers corresponding to frozen phases and vertices of the Newton polygon, together with the corresponding type of edges.

parametrize both z and and w using rational fractions of a variable u living on the Riemann sphere, which could be chosen as the isothermal coordinate.

4.3.2 A case with a multiply-connected liquid region, Aztec diamond with two-periodic weights

We follow loosely the discussion here [KP24, Section 2.3].

Before analysis of a multiply-connected region, let us discuss our example with a multiply-connected liquid region, where the region is the simply-connected, but the liquid region is non simply-connected due to presence of smooth or gas phase, so-called bubble. This can be achieved for non-uniform distribution on the set of dimer configurations, and the most common example of such phenomenon is the *doubly-periodic Aztec diamond*[CJ14; KP24].

This system of weights for the square lattice is related to the dimer model on the square-octagon graph: there is a weight-preserving correspondence between configurations on the two lattices (obtained by performing the so-called *spider move* or *square move*), which maps domino tilings of doubly-periodic square grid to dimer configurations on the square-octagon lattice as long as the weights $a^2 = 2b$ from Figure 4.12.

In that case, the modified Kasteleyn matrix from (4.3.5) becomes

$$\mathcal{K}(z, w) = \begin{pmatrix} b - w & z - b \\ \frac{1}{z} - b & \frac{1}{w} - b \end{pmatrix} \tag{4.3.6}$$

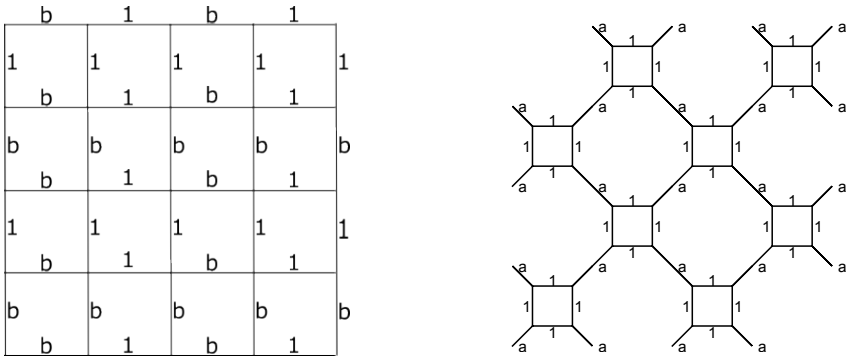

Figure 4.12: Edge weights of the square grid on the left, and the corresponding weights of the octagon lattice on the right, the correspondence between weights is $a^2 = 2b$.

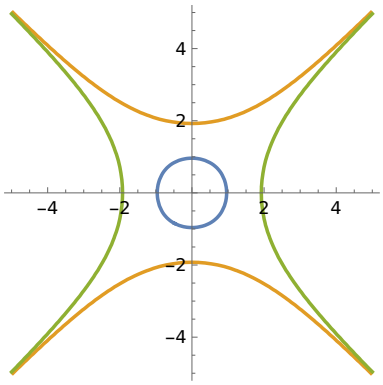

Figure 4.13: Amoeba of the 2-periodic weight function on the square lattice, for $b = 0.5$. The hole in the middle corresponds to the *gas* or *smooth phase* of the corresponding dimer model, which describes the bubble appearing in the middle of the pictures of Figure 4.14.

and the characteristic polynomial is $-2(1+b^2) + b(z + w + \frac{1}{z} + \frac{1}{w})$. See Figure 4.13 for its amoeba. The spectral curve is a genus 1 algebraic curve $\mathcal{C}$ if $b \neq 1$, which is a Harnack curve. It can be uniformized to a rectangular torus $\mathbb{C}/(2\mathbb{Z} + 2\tau\mathbb{Z})$, with $\tau \in i\mathbb{R}_+^*$: there is a birational map

$$\psi : \zeta \in \text{torus} \mapsto (z(\zeta), w(\zeta)) \in \mathcal{C}.$$

See for example [BCT23, Section 5] and [BT24, Proposition 9].

The relation between b and τ (assuming that $b < 1$, there is a symmetry $b \leftrightarrow \frac{1}{b}$) is given by

$$b = \sqrt{k'}, \qquad \text{with } k' = \frac{\theta_4(0|\tau)^2}{\theta_3(0|\tau)^2}.$$

In particular, for $\tau = 1$, $k' = \frac{1}{\sqrt{2}}$, and $b = 2^{-1/4}$.

Based, for example, on computer simulations Figure 4.14 of domino tilings of the doubly-periodic Aztec diamond on Figure 4.14, we see presence of all three phases, frozen, rough and smooth, together with arctic curve with two connected components, the outer curve separating frozen and rough regions, and the inner curve separating rough and smooth phase regions. This is again a situation where there is a unique point in the liquid region for a given slope in the Newton polygon. The restriction of ψ to the annulus $\mathcal{A} = \mathbb{R}/2\mathbb{Z} + (0, \tau)$ parametrizes the upper half of the spectral curve $\mathcal{C}^+$, and thus $\zeta \in \mathcal{A}$ gives a parametrization of the liquid region as an isothermal coordinate. The lower boundary of the annulus is mapped to the outer boundary of the liquid region (the liquid/solid interface): up to a horizontal translation, we may assume that the turning points correspond to $\zeta = -\frac{1}{2}0, \frac{1}{2}, 1$

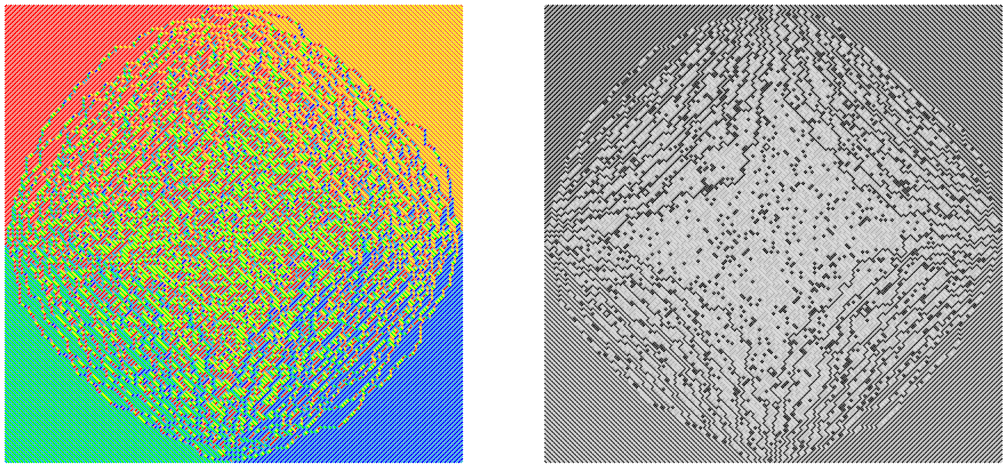

Figure 4.14: Random domino tiling of doubly-periodic Aztec diamond for $b = 0.5$ in two representations, the color representation on the left with eight colors to distinguish rough and smooth phases, and with eight different gray colors on the right.

(mod 2). The upper boundary is mapped to the inner boundary of the liquid region (the liquid/gas interface).

The boundary conditions along the outer boundary are the same as in the uniform case:

	(1) $-\frac{1}{2} < \zeta < 0$	(2) $0 < \zeta < \frac{1}{2}$	(3) $\frac{1}{2} < \zeta < 1$	(4) $1 < \zeta < \frac{3}{2}$
s	1	0	-1	0
t	0	-1	0	1
c	$-\frac{1}{2}$	$\frac{1}{2}$	$-\frac{1}{2}$	$\frac{1}{2}$

In order to perform harmonic extensions in a multiply-connected domain, we need a particular toolbox of special functions. Basically, we are going to apply the same strategy: first write down a basic building block, and then to construct harmonic extensions in terms of these building blocks. Since the spectral curve is a torus, these blocks will be constructed from elliptic functions that we discuss now.

Elliptic functions and their classification by Weierstrass functions

Let Λ be a lattice generated two vectors ω_1 and ω_2 called periods of Λ, $\Lambda := \{n\omega_1 + m\omega_2 : n, m \in \mathbb{Z}\}$. Then, a Λ-elliptic function is a meromorphic function on $\mathbb{C}$ that satisfies $f(z) = f(z + \omega_1) = f(z + \omega_2)$.

The most famous example of elliptic functions is Weierstrass's $\wp$-function, which is defined as

$$\wp(z, \Lambda) := \frac{1}{z^2} + \sum_{\lambda \in \Lambda \setminus \{0\}} \left(\frac{1}{(z-\lambda)^2} - \frac{1}{\lambda^2} \right). \tag{4.3.7}$$

The function $\wp$ clearly has poles of order two at each lattice point. It is an elliptic function, which follows from the definition. For the next subsections, we need two other Weierstrass functions.

The Weierstrass ζ-function is a function fixed by the equation

$$\frac{d\zeta(z, \Lambda)}{dz} = -\wp(z, \Lambda). \tag{4.3.8}$$

This defines it up to an additive constant that we fix in a way that $\lim_{z \to 0} \zeta(z, \Lambda) - \frac{1}{z} = 0$. Using ellipticity of $\wp$ one can derive quasi-periodic properties of ζ Weierstrass function, $\zeta(z + \omega_i) = \zeta(z) + 2\eta_i$, where $\eta_i = \zeta(\omega_i/2)$.

The Weierstrass σ-function is defined by

$$\frac{d\log(\sigma(z,\Lambda)}{dz} = \zeta(z,\Lambda). \tag{4.3.9}$$

Here, we fix an integration constant so that $\lim_{z\to 0}\sigma(z,\Lambda) - z = 0$. by definition of σ and quasi-periodicity of ζ one derives quasi-periodicity of σ,

$$\sigma(z+\omega_i) = e^{-2\eta_i(z+\omega_i/2)}\sigma(z). \tag{4.3.10}$$

Function σ is a suitable building block of elliptic functions, and every elliptic function can be expressed in terms of Weierstrass σ function [NIA90].

Theorem 4.3.1. *Suppose f is an elliptic function with periods ω_1, ω_2 and set of zeroes in a fundamental domain of Λ at points $\{\varkappa_i\}$ of the corresponding orders $\{n_i\}$ and set of poles $\{\varkappa_i'\}$ of the orders $\{n_i'\}$ subject to two conditions:*

- $\sum n_i\varkappa_i = \sum n_i'\varkappa_i'$,
- $\sum n_i = \sum n_i'$.

And let us define a function g as

$$g(z) := \frac{\prod_i \sigma(z-\varkappa_i,\Lambda)^{n_i}}{\prod_i \sigma(z_i-\varkappa_i',\Lambda)^{n_i'}}. \tag{4.3.11}$$

Then, the ratio $\frac{f}{g}$ is constant on $\mathbb{C}$.

Proof. First, g is elliptic by quasi-periodicity of σ recalled in Equation (4.3.10), and by (4.3.11). Moreover, by (4.3.11) it has the same zeroes and poles with the same multiplicities as f. Thus, ratio $\frac{f(z)}{g(z)}$ has no zeroes no poles on $\mathbb{C}$ and thus is is constant by Liouville's theorem. □

In our case, $\Lambda = 2\mathbb{Z} + 2\tau\mathbb{Z}$, so that $\omega_1 = 2$ and $\omega_2 = 2\tau$.

Applying the tangent plane method

The solution from [KP24], adapted to our normalization, is the following,

$$\begin{aligned}
s(\zeta) &= \frac{1}{\pi}\arg\frac{\sigma(\zeta)\sigma(\zeta-\frac{1}{2})}{\sigma(\zeta-1)\sigma(\zeta+\frac{1}{2})},\\
t(\zeta) &= \frac{1}{\pi}\arg\frac{\sigma(\zeta+\frac{1}{2})\sigma(\zeta)}{\sigma(\zeta-\frac{1}{2})\sigma(\zeta+1),},\\
c(\zeta) &= \frac{1}{2} + \frac{1}{\pi}\arg\frac{\sigma(\zeta+\frac{1}{2})\sigma(\zeta-\frac{1}{2})}{\sigma(\zeta-1)\sigma(\zeta)} - \frac{1}{4}\mathrm{Im}(\zeta)
\end{aligned}$$

The functions s and t are arguments of genuine elliptic functions in the variable ζ on the whole torus, by Theorem 4.3.1. For the function c, the zeros and the poles of the fraction in the argument are fixed by the wanted behavior along the outer boundary, but this does not define a proper elliptic function as it is not of the form given by Theorem 4.3.1. We need to add the multiple of the imaginary part of u to guarantee periodicity in the horizontal direction. The coefficient $\frac{1}{4}$ is specific for the choice of $\tau = 1$. For an arbitrary value of τ, it should be replaced by $\frac{\eta_1}{\pi}$ (when $\omega_1 = 2$ and $\omega_2 = 2\tau$, then $\eta_1 = \frac{\pi}{4}$).

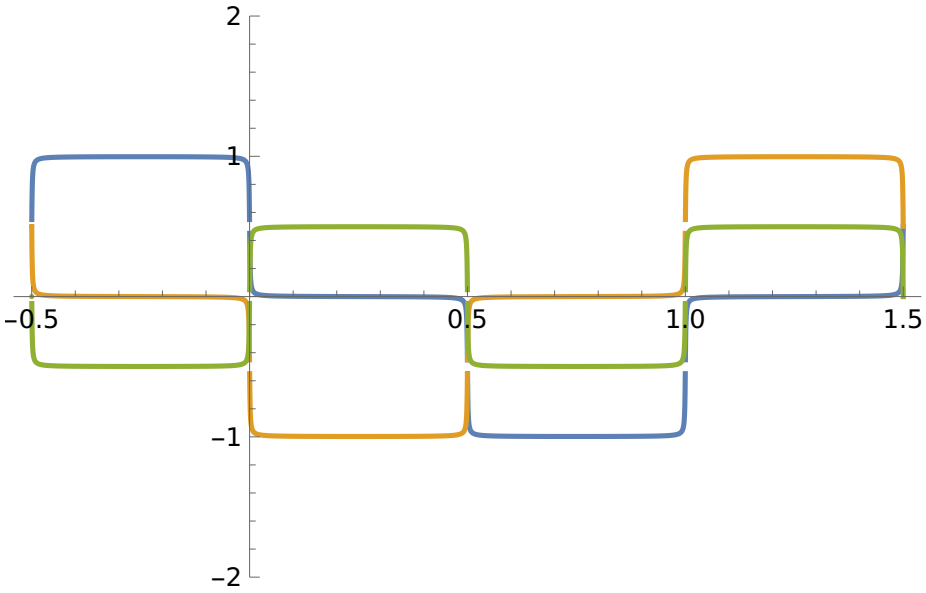

Figure 4.15: Plot of the functions s, t, and c for ζ on (in fact very close to) the lower boundary of the cylinder $\mathcal{A}$, matching the table, in blue, yellow and green respectively.

Writing the master equation for the harmonically moving planes,

$$s_\zeta x + t_\zeta y + c_\zeta = 0,$$

solving for $x = x(\zeta)$ and $y = y(\zeta)$ for each ζ on the boundary of the annulus $\mathcal{A}$ gives a parametrization of the arctic curve. This curve is represented on Figure 4.16: the yellow connected component corresponds to $\mathrm{Im}(\zeta) = 0$, whereas the blue component, delimiting the boundary of the gas bubble, corresponds to $\mathrm{Im}(\zeta) = 1$. We can determine the equation of the tangent plane to the gaz bubble by evaluating s, t and c along the blue boundary, and obtain that with our convention, that plane is the plane $z = 0$.

In the next section, we will reuse these expressions in a more complicated situation.

4.3.3 Formulation of problem for Aztec diamond with a hole

Here, we perform computations for the Aztec diamond with a hole for both constrained and unconstrained cases. Furthermore, instead of letter ζ, we denote the intrinsic coordinate by u to distinguish it from ζ-Weierstrass function. First, using computer simulation Figure 4.17 we can assume that the number of frozen phases equals to 16, 4 phases around the external boundary, and 12 around the internal boundary. Then, we define the uniformization map $u : \mathcal{L} \to \mathcal{A}$, where $\mathcal{A} = [0, 2] \times [0, \tau]/\sim$. Later, we assume a case of $\tau = 1$. The upper connected boundary component of $\partial\mathcal{A}$ consists of 12 intervals (a_i, a_{i+1}), subject to

$a_{i+3} = a_i + 1/2$, where $a_1 = \tau - 1/2 - a, a_2 = \tau - 1/2, a_3 = \tau - 1/2 + a$ for a small parameter a, which we later take as $a = 1/6$. The lower boundary has the same boundary conditions as $\mathcal{AD}$, and it consists of 4 intervals (a_i, a_{i+1}), $13 \le i \le 16$. Thus, for the lower boundary conditions we can use the expression for the ring from the section above (it will not change the behavior on the line $\mathrm{Im}u = \mathrm{Im}\tau$ since those extensions are zero there).

u	(a_1, a_2)	(a_2, a_3)	(a_3, a_4)	(a_4, a_5)	(a_5, a_6)	(a_6, a_7)
s	0	-1	0	1	0	-1
t	1	0	-1	0	1	0
c	$+\varkappa/2$	$-\varkappa/2$	$-3\varkappa/2$	$-\varkappa/2$	$\varkappa/2$	$3\varkappa/2$

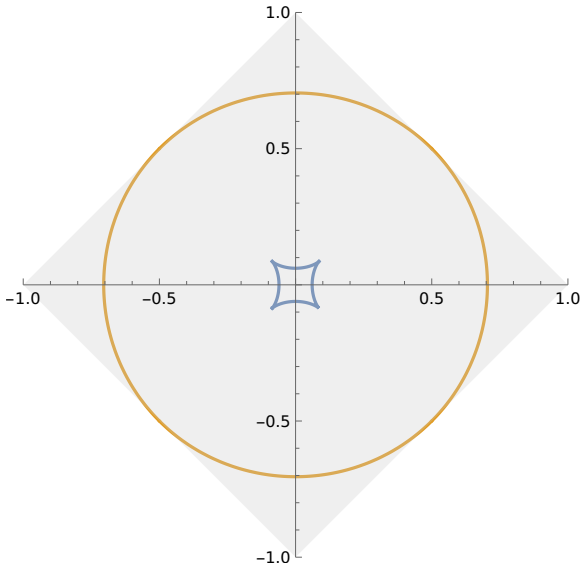

Figure 4.16: Frozen curve for the doubly-periodic Aztec diamond. The grey square is the limiting domain of a renormalized large Aztec diamond. The liquid phase, homeomorphic to an annulus, is bounded on the outside from the four frozen phases by the yellow component, and bounded in the inside from the gas bubble by the blue components. The frozen regions, labeled (1), (2), (3), (4) in the table, appear in the right, top, left, bottom corner respectively. The equation of the corresponding plane can be read from the matching column in the table. The one for the gas bubble is $z = 0$.

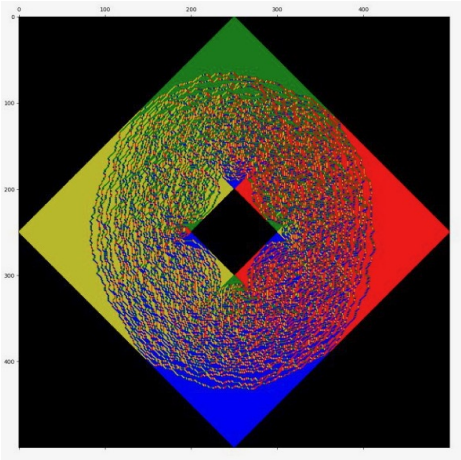

Figure 4.17: Computer simulations of random domino tiling of Aztec diamond with a hole

$\varkappa$ parametrize the size of the hole, $0 < \varkappa < 1$. The boundary data for $c(u)$ is obtained by analogy with the Aztec diamond (4.3.3), $c(u)$ changes by 1 each time we move from one frozen region to the other. Since we removed the Aztec diamond of scale $\varkappa$, we have the same boundary conditions for c up to a global scaling by $\varkappa$.

Functions s, t and c are periodic on the universal cover of $\mathcal{A}$, and can be found as arguments of ratios of σ Weierstrass functions. The basic block of our harmonic extensions is a periodic step function defined on the infinite strip $\mathcal{S} = \mathbb{R} \times [0, \tau]$, which is the universal cover of the ring $\mathcal{A}$,

$$\frac{1}{\pi} \arg \left(\frac{\sigma(u-b)}{\sigma(u-a)} \right) \tag{4.3.12}$$

The plot of this function is as a step function with height 1 from a to b defined on the real axis,

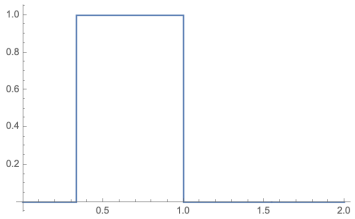

Figure 4.18: Example of plot of function S for $a = \frac{1}{3}$ and $b = 1$.

Although the symmetry of Aztec diamond allows as to write the harmonic extensions with several parameters,

$$s(u) = \frac{1}{\pi}\arg\frac{\sigma(u)\sigma(u-1/2)\sigma(u-(\tau-1/2))\sigma(u-(\tau-1/2+a))\sigma(u-(\tau+a))}{\sigma(u-1)\sigma(u+1/2)\sigma(u-(\tau-1/2-a))\sigma(u-(\tau-a))\sigma(u-\tau)}+ \\ +\frac{1}{\pi}\arg\frac{\sigma(u-(\tau+1-a))\sigma(u-(\tau+1))\sigma(u-(\tau+1/2-a))}{\sigma(u-(\tau+1/2+a))\sigma(u-(\tau+1+a))\sigma(u-(\tau+1/2))}. \quad (4.3.13)$$

The function $t(u)$ can be obtained by symmetry from $s(u)$ as $t(u) = s(u+1/2)$. These two functions are arguments of meromorphic functions as the product of σ function under the arg satisfy conditions of Theorem 4.3.1. For function c, however, the situation slightly different,

$$c(u) = \frac{1}{\pi}\arg\frac{\sigma(u+1/2)\sigma(u-1/2)}{\sigma(u-1)\sigma(u)}+\frac{\varkappa}{\pi}(\arg\frac{\sigma(u-(\tau-a))}{\sigma(u-(\tau-1/2-a))}+\arg\frac{\sigma(u-\tau)}{\sigma(u-(\tau-1/2))}+ \\ \arg\frac{\sigma(u-(\tau+a))}{\sigma(u-(\tau-1/2+a))}+\arg\frac{\sigma(u-(\tau+1-a))}{\sigma(u-(\tau+1/2-a))}+\arg\frac{\sigma(u-(\tau+1))}{\sigma(u-(\tau+1/2))}) \\ +\frac{1}{\pi}\arg\frac{\sigma(u-(\tau+1+a))}{\sigma(u-(\tau+1/2+a))}+K(a,b,\tau). \quad (4.3.14)$$

Here, the product of σ functions does not satisfy Theorem 4.3.1 like in the doubly-periodic Aztec diamond. Therefore, the resulting function changes after shift by a period, we subtract this change with the help of ζ-Weierstrass functions, this term is called $K(a,\varkappa,\tau)$. For example, for $\tau = \sqrt{-1}$, $K(a,\varkappa,\tau) = \frac{1}{2} + \frac{\eta_1}{\pi}(3\varkappa + \frac{1}{2})$.

Plot of the height function

In order to produce a parametric plot of the surface given by $\mathfrak{h}^\star$, we need to check that this surface is well-defined. In practice, it means that we need to look at intrinsic coordinate z, which is related with isothermal coordinate u by a rational transformation of degree 4(this is because, based on computer simulations, each frozen phase repeats 4 types going around the boundary).

At the critical points of $z(u)$, derivative z_u vanishes, therefore, the whole expression $s_z z_u + t_z z_u + c_u = 0$ vanish as well. Thus, we must have $c_u = 0$ at those points. Combining (4.3.13) with (4.2.14) we see that $z(u)$ is given by the expression in the argument of arg in $s(u)$,

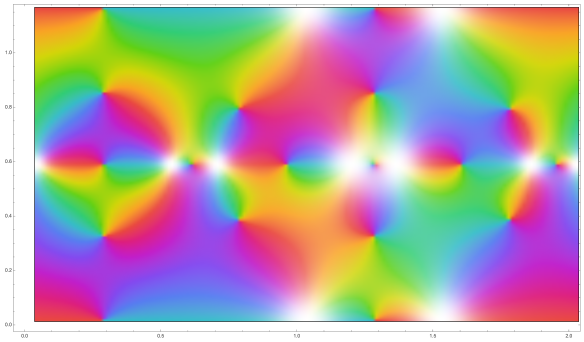

Figure 4.19: Plot of the derivative of $w(u)$ on the whole torus with two critical points inside the liquid region repeated 4 times

$$z(u) = \left(\frac{\sigma(u+\frac{1}{2})}{\sigma(u)}\right)\left(\frac{\sigma(u-(\tau-1+a))}{\sigma(u-a)}\right)\left(\frac{\sigma(u-(1-\frac{1}{2}))}{\sigma(u-(a+k))}\right)\left(\frac{\sigma(u-1)}{\sigma(u-(1+l))}\right)$$
$$\left(\frac{\sigma(u-(1+a))}{\sigma(u-1)}\right)\left(\frac{\sigma(u-(1+a+k))}{\sigma(u-(2-k))}\right). \quad (4.3.15)$$

.

Also, there is a similar expression for $w(u)$, which we omit. However, its plot shows that there is a unique critical point inside the liquid region in the fundamental domain.

On the figure 4.19 we see analytic properties of $w(u)$ on the whole torus. There are 8 zeros and 8 poles on the boundary of $\partial\mathcal{L}$, which are real zeros that we see directly from the expression. Moreover, there are 2 complex zeroes repeated 4 times in the interior of $\mathcal{L}$. They are linked by two involutions, the complex conjugation, and symmetry $w(u+1) = w(u^{-1})$.

This constraint determines the sets of parameters, which correspond to the actual limit shapes. We did not check it, and leave it for the future investigation.

The Tangent plane method for the constrained case

To obtain the constrained case, we need to modify only function c, more precisely add a multiple of $\mathrm{Im}(u)$(call this multiple r), which changes the value on the line $\mathrm{Im}u = 1$ keeping the value on the real axis unchanged. This modification makes $c(u)$ not exactly elliptic, however, for the sake of obtaining the arctic curves, it gives the right values. For intermediate values of r we obtain a deformed picture as on Figure 4.20.

We can also perform our computations for various sizes of the hole $\varkappa$.

Is it a circle?

Plots of the arctic curve for the doubly-periodic Aztec diamond and for the Aztec diamond with a hole share a feature that the outer connected component looks like a circle. Therefore, its worth investigating whether it is an actual circle, or not. To check it, we built the plot of function $x^2 + y^2$ on points of the curve (x, y). If the connected component was the circle given by $x^2 + y^2 = 2$, we would get a constant plot. However, it is not the case, and we obtain two slightly different non-constant plots, see the plot for the doubly-periodic Aztec diamond on Figure 4.23 and for Aztec diamond with a hole on Figure 4.24. These plots show that the outer connected components of the arctic curves are close to the circle up to approximately 99%, as the circle equation is satisfied up to a small error of order less than 1%, which is invisible for human vision.

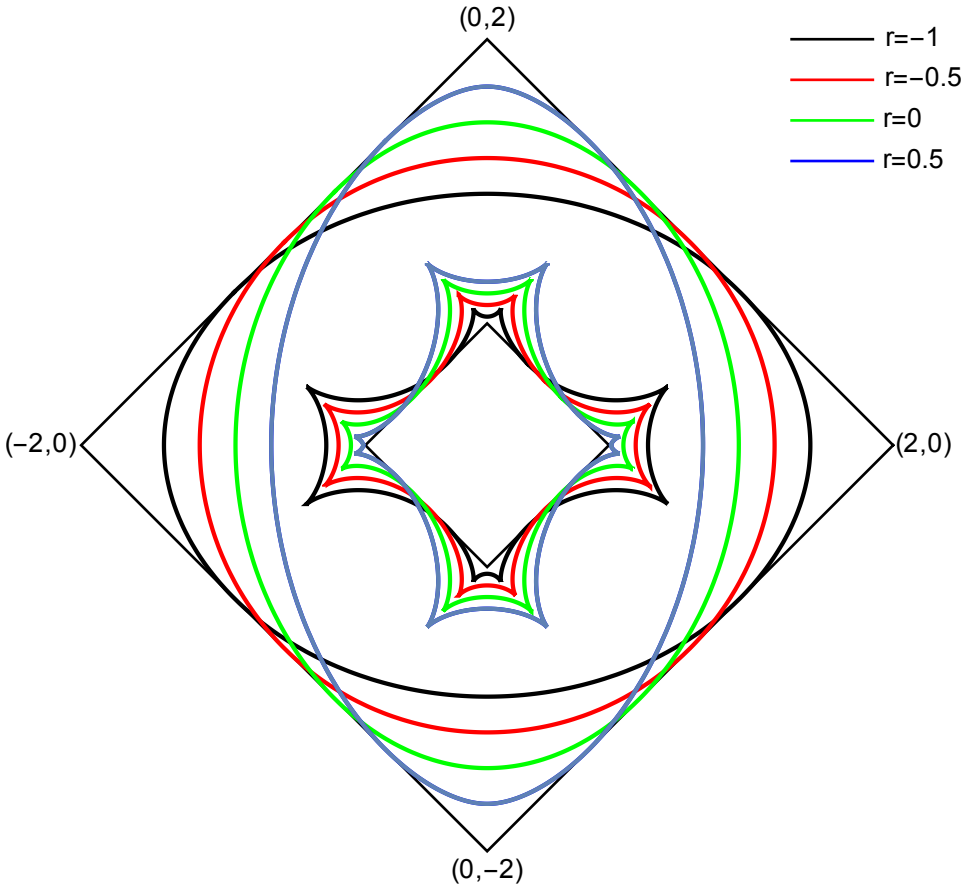

Figure 4.20: Limit shape for the Aztec diamond with a hole for different values of parameter r and $\varkappa = 0.3$.

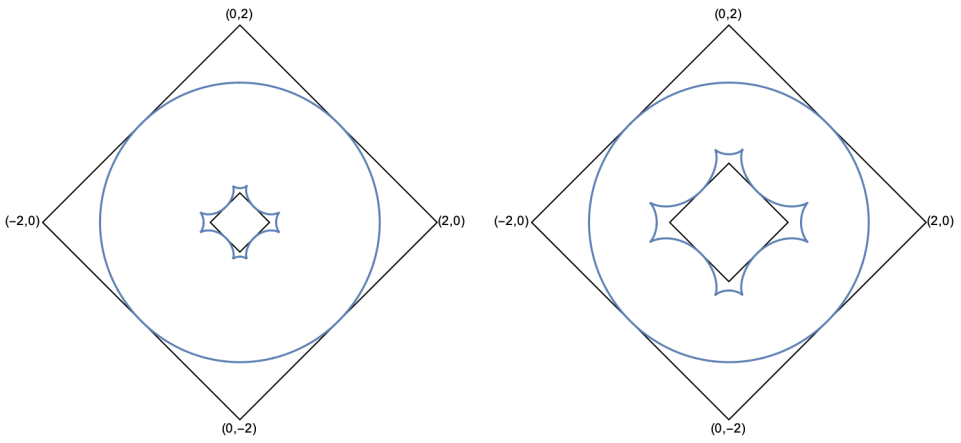

Figure 4.21: Plot of the frozen curve for unconstrained case with $\varkappa = 0.15$ on the left, and for $\varkappa = 0.6$ on the right.

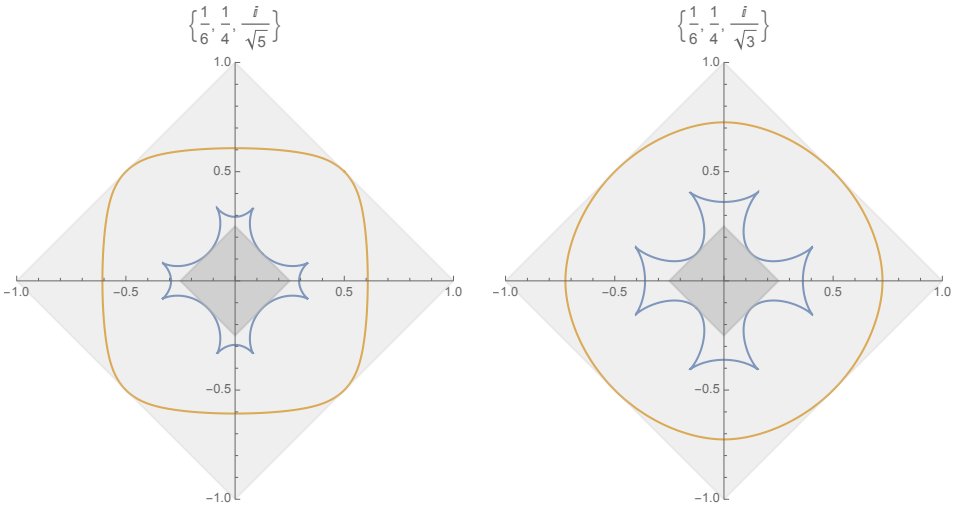

Figure 4.22: Plot of the frozen curve for unconstrained case with $\tau = \frac{\sqrt{-1}}{\sqrt{5}}$ on the left, and for $\tau = \frac{\sqrt{-1}}{\sqrt{3}}$ on the right.

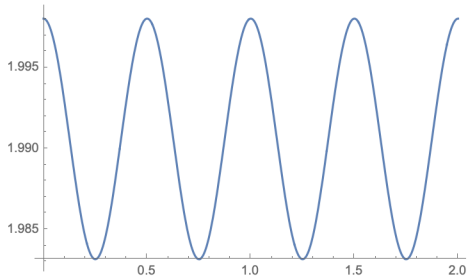

Figure 4.23: Plot of circle equation $x^2 + y^2$ on the external frozen boundary of doubly-periodic Aztec diamond.

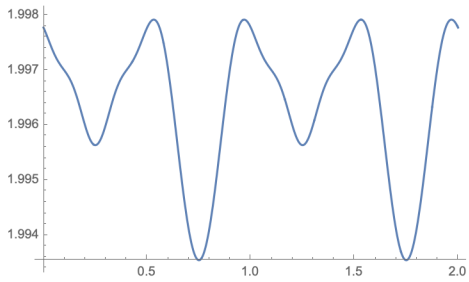

Figure 4.24: Plot of circle equation x^2+y^2 on the external frozen boundary of Aztec diamond with a hole.

Appendix to Chapter 4: Isothermal coordinates

Here we discuss Isothermal coordinates and the Beltrami equation on the Newton polygon $\mathcal{N}$ with a surface tension σ defined on it.

Since σ is convex, the Hessian of σ H_σ defines a non-degenerate metric g on $N \setminus \mathscr{G}$,

$$g = \sigma_{ss} ds^2 + 2\sigma_{st} ds dt + \sigma_{tt} dt^2. \tag{4.3.16}$$

Also note that since by Theorem 5.5 from [KOS06], $\det H_\sigma = \pi^2$.

In the isothermal coordinate $u := U(s,t) + iV(s,t)$ the metric g writes as

$$g = \rho(U,V)^2 (dU^2 + dV^2) \tag{4.3.17}$$

for a function $\rho(U,V)$. Isothermal coordinates exist on two-dimensional manifolds for metric with Hölder coefficients by result from [Kor14; Lic16]. For example, Theorem 18 i [Spi79] is the following,

Theorem 4.3.2. *Let Σ be a C^∞-smooth two-dimensional surface embedded into $\mathbb{R}^2$ with metric $g = \langle , \rangle$, and let $p \in \Sigma$ be a point, whose components with respect to the standard coordinate system are real analytic. Then, there exists a real analytic isothermal coordinate system in a neighborhood of p.*

Metric $g = \begin{pmatrix} a & b \\ b & c \end{pmatrix}$ defines scalar product $\langle \cdot, \cdot \rangle_g$ on vector fields on $\mathcal{N}$, and we can determine the isothermal coordinates after comparing $\langle \frac{\partial}{\partial U}, \frac{\partial}{\partial V} \rangle_g$ in coordinates s, t and U, V. In latter coordinates, it equals to zero by definition, while for coordinates s, t it becomes an equation. This condition together with $\langle \frac{\partial}{\partial V}, \frac{\partial}{\partial V} \rangle_g = \langle \frac{\partial}{\partial U}, \frac{\partial}{\partial U} \rangle_g$ results in the system of two real equations, which we call the Real Beltrami equations.

$$U_s = \rho(bV_s - aV_t), \tag{4.3.18}$$

$$U_t = -\rho(bV_t - cV_s). \tag{4.3.19}$$

This system naturally arises in the context of the dimer model as we are going to see in this Chapter. Further, it is equivalent to one complex equation for a complex coordinate u on $\mathcal{N}$, in terms of coordinates $u = U + iV, \bar{u} = U - iV$, the real Beltrami equations results in the usual Beltrami equation, used for example in [KP22]. In terms of u_s, u_t, it is the following equation,

$$\frac{\bar{\partial} u}{\partial u} = \frac{\frac{1}{2}(u_s + i u_t)}{\frac{1}{2}(u_s - i u_t)} = \frac{1}{\overline{\mu_\sigma}}. \tag{4.3.20}$$

where the Beltrami coefficient μ_σ is given by

$$\mu := \frac{\sigma_{ss} - \sigma_{tt} + 2i\sigma_{st}}{\sigma_{ss} + \sigma_{tt} - 2\sqrt{\sigma_{ss}\sigma_{tt} - \sigma_{st}^2}}. \tag{4.3.21}$$

Also, $\rho(U,V) = \sqrt{\sigma_{ss} + \sigma_{tt} - 2\sqrt{\sigma_{ss}\sigma_{tt}}}$.

Existence of a solution for this equation follows from the strict convexity of σ on $\mathring{\mathcal{N}}$, or in terms of Beltrami coefficient $|\mu_\sigma| < 1$. It is worth noting that the Beltrami equation for surface tension corresponding to the dimer model on hexagonal lattice is equivalent to the complex Burgers equation studied in [KO05].

Proof of Theorem 4.3.2. Let us first find Beltrami equation for real coordinates (U,V), let us start with $\langle \frac{\partial}{\partial U}, \frac{\partial}{\partial V} \rangle_g = 0$, which is just the definition of isothermal coordinates. In the (s,t) coordinates, it is non-trivial identity. First, the vector fields in (s,t) coordinates are

$$\begin{aligned} \frac{\partial}{\partial U} &= s_U \frac{\partial}{\partial s} + t_U \frac{\partial}{\partial t}, \\ \frac{\partial}{\partial V} &= \frac{\partial s}{\partial V}\frac{\partial}{\partial s} + \frac{\partial t}{\partial V}\frac{\partial}{\partial t}. \end{aligned} \tag{4.3.22}$$

Their scalar product is

$$\sigma_{ss} s_U s_V + \sigma_{st}(s_V t_U + s_U t_V) + \sigma_{tt} t_U t_V = 0. \tag{4.3.23}$$

Let us express 4.3.23 in terms of derivatives of U, V using the Jacobian matrix,

$$\mathcal{J} = \begin{pmatrix} \frac{\partial s}{\partial U} & \frac{\partial s}{\partial V} \\ \frac{\partial t}{\partial U} & \frac{\partial t}{\partial V}. \end{pmatrix} = \begin{pmatrix} \frac{\partial U}{\partial s} & \frac{\partial U}{\partial t} \\ \frac{\partial V}{\partial s} & \frac{\partial V}{\partial t} \end{pmatrix}^{-1} \tag{4.3.24}$$

Using $\mathcal{J}$, we express the desired derivatives as

$$s_u = V_t/\det\mathcal{J}, s_v = -U_t/\det\mathcal{J}, t_u = -V_s/\det\mathcal{J}, t_v = U_s/\det\mathcal{J}. \tag{4.3.25}$$

After substitution of derivatives to 4.3.23 and multiplying by $\det\mathcal{J}$ we obtain

$$U_t(V_s\sigma_{st} - V_t\sigma_{ss}) + U_s(V_t\sigma_{st} - V_s\sigma_{tt}) = 0. \tag{4.3.26}$$

From this equation, we see that U_s and U_t are proportional and thus there is such a ρ that

$$\begin{aligned} U_s &= \rho(V_s\sigma_{st} - V_t\sigma_{ss}), \\ U_t &= -\rho(V_t\sigma_{st} - V_s\sigma_{tt}). \end{aligned} \tag{4.3.27}$$

We also have the equation for the diagonal scalar products,

$$\langle \frac{\partial}{\partial U}, \frac{\partial}{\partial U} \rangle_g = \langle \frac{\partial}{\partial V}, \frac{\partial}{\partial V} \rangle_g. \tag{4.3.28}$$

Or more precisely,

$$\begin{aligned} \langle \frac{\partial}{\partial U}, \frac{\partial}{\partial U} \rangle_g = s_U^2\sigma_{ss} + t_U^2\sigma_{tt} + 2\sigma_{st}s_U t_U, \\ \langle \frac{\partial}{\partial V}, \frac{\partial}{\partial V} \rangle_g = s_V^2\sigma_{ss} + t_V^2\sigma_{tt} + 2\sigma_{st}(s_V t_V). \end{aligned} \tag{4.3.29}$$

Let us substitute (4.3.27) into (4.3.29) to find ρ. We need first to express the derivatives of s and t in terms of derivatives of U and V, and then use equations (4.3.27).

$$\rho = \langle \frac{\partial}{\partial U}, \frac{\partial}{\partial U} \rangle = \frac{1}{\det \mathcal{J}^2}(V_t^2 a + 2b(-V_s V_t) + cV_s^2),$$
$$\rho = \langle \frac{\partial}{\partial V}, \frac{\partial}{\partial V} \rangle = \frac{1}{\det \mathcal{J}^2}(aU_t^2 + cU_s^2 + 2b(-U_s U_t)) \quad (4.3.30)$$

$$V_t^2 a - 2bV_s V_t + cV_s^2,$$
$$a\rho^2(bV_t - cV_s)^2 + c\rho^2(bV_s - aV_t)^2 + 2b\rho^2(bV_s - aV_t)(bV_t - cV_s). \quad (4.3.31)$$

We see from comparison of coefficients in front of V_t^2 in both equations

$$a = \rho^2(ab^2 + ca^2 - 2bab)$$
$$1 = \rho^2(ca - b^2). \quad (4.3.32)$$

Similarly, for the coefficient in front of V_s^2,

$$c = \rho^2(ac^2 + cb^2 - 2bbc)$$
$$1 = \rho^2(ac - b^2). \quad (4.3.33)$$

Finally, the coefficient in front of $V_t \cdot V_s$,

$$-2b = -2a\rho^2 bc - 2c\rho^2 ba + 2b\rho^2(b^2 + ac)$$
$$1 = \rho^2 ca + \rho^2 pca - \rho^2(b^2 + ca)$$
$$1 = \rho^2(ca - b^2). \quad (4.3.34)$$

Thus, we deduce that $\rho = \sqrt{H_\sigma} := \sqrt{\sigma_{ss}\sigma_{tt} - \sigma_{st}^2}$.

In order to obtain the complex Beltrami equation, assume that we have a solution U, V of the real Beltrami equation (4.3.27). The let us look at their complex combination $u := U + iV$ ($\bar{u} := U - iV$), and the Wirtinger derivatives with respect to $u, \bar{u}$,

Using the Wirtinger derivatives, we have the following rules of computation of derivatives of a function w:

$$w_u = \frac{1}{2}(w_U - iw_V), \ w_{\bar{u}} = \frac{1}{2}(w_U + iw_V) \quad (4.3.35)$$

and

$$w_U = w_u + w_{\bar{u}}, \ w_V = \frac{w_{\bar{u}} - w_u}{i}. \quad (4.3.36)$$

Now, suppose U, V satisfy the Beltrami equations, then write

$$2w_{\bar{u}}\sqrt{ac - b^2} = (b - ia + i\sqrt{ac - b^2})V_x + (c - ib - \sqrt{ac - b^2})V_y \quad (4.3.37)$$

and

$$2w_z\sqrt{ac - b^2} = (b + ia + i\sqrt{ac - b^2})V_x + (c + ib + \sqrt{ac - b^2})V_y \quad (4.3.38)$$

Then, dividing the two equations and calculations, which we omit, we get an equivalent Beltrami equation in holomorphic coordinates,

$$\frac{w_{\bar{z}}}{w_z} = \frac{c - a - 2ib}{c + a + 2\sqrt{ac - b^2}}. \quad (4.3.39)$$

Or in other words,

$$w_{\bar{z}} = \mu w_z, \tag{4.3.40}$$

where $\mu = \frac{c-a-2ib}{c+a+2\sqrt{ac-b^2}}$ is the Beltrami coefficient.

Thus, we derived the Belrami equation for the conformal coordinates in two forms. Then, by the theory of elliptic PDE [AIM09], Beltrami equation admits a solution as long as $|\mu| < 1$, which is the condition of existence of isothermal coordinates. In the dimer model, it follows from strict convexity of σ[ADPZ20]. Therefore, inside the liquid region, where the gradient $\nabla\mathfrak{h}$ is in the interior of the Newton polygon, we have the existence of isothermal coordinates z.

□

Bibliography

[ADPZ20] K. Astala, E. Duse, I. Prause, and X. Zhong. "Dimer Models and Conformal Structures" (Apr. 2020).

[Agg19] A. Aggarwal. "Universality for Lozenge Tiling Local Statistics". *Annals, Pages 881-1012 from Volume 198 (2023), Issue 3* (July 2019).

[Agg20] . A. Aggarwal. "Arctic boundaries of the ice model on three-bundle domains". *Inventiones mathematicae* 220 (May 2020).

[AIM09] K. Astala, T. Iwaniec, and G. Martin. *Elliptic Partial Differential Equations and Quasiconformal Mappings in the Plane*. Jan. 2009.

[BCT23] C. Boutillier, D. Cimasoni, and B. de Tilière. "Elliptic dimer models on minimal graphs and genus 1 Harnack curves". *Communications in Mathematical Physics* 400.2 (Feb. 2023), pp. 1071–1136. arXiv: 2007.14699 [math.PR]. URL: https://doi.org/10.1007/s00220-022-04612-6.

[BF08] A. Borodin and P. L. Ferrari. "Large time asymptotics of growth models on space-like paths. I. PushASEP". *Electron. J. Probab.* 13 (2008), no. 50, 1380–1418. URL: https://doi.org/10.1214/EJP.v13-541.

[BG19] A. Bufetov and V. Gorin. "Fourier transform on high-dimensional unitary groups with applications to random tilings". *Duke Math. J.* 168.13 (2019), pp. 2559–2649. URL: https://doi.org/10.1215/00127094-2019-0023.

[BGG17] A. Borodin, V. Gorin, and A. Guionnet. "Gaussian asymptotics of discrete β-ensembles". *Publ. Math. Inst. Hautes Études Sci.* 125 (2017), pp. 1–78. URL: https://doi.org/10.1007/s10240-016-0085-5.

[BK16] A. Bufetov and A. Knizel. "Asymptotics of random domino tilings of rectangular Aztec diamonds". *Annales de l'institut Henri Poincare (B) Probability and Statistics* 54 (Apr. 2016).

[BLR19] N. Berestycki, B. Laslier, and G. Ray. *The dimer model on Riemann surfaces, I*. Aug. 2019.

[BT24] C. Boutillier and B. de Tilière. *Fock's dimer model on the Aztec diamond*. 2024. arXiv: 2405.20284.

[CEP96] H. Cohn, N. Elkies, and J. Propp. "Local statistics for random domino tilings of the Aztec diamond". *Duke Math. J.* 85.1 (1996), pp. 117–166. URL: https://doi.org/10.1215/S0012-7094-96-08506-3.

[CJ14] S. Chhita and K. Johansson. "Domino statistics of the two-periodic Aztec diamond". *Advances in Mathematics* 294 (Oct. 2014).

[CK01] R. Cerf and R. Kenyon. "The Low-Temperature Expansion of the Wulff Crystal in the 3D Ising Model". *Comm. Math. Phys.* 222 (Jan. 2001), pp. 147–179.

[CKP00] H. Cohn, R. Kenyon, and J. Propp. "A variational principle for domino tilings". *Journal of the American Mathematical Society* 14 (Aug. 2000).

[CL19] M. Ciucu and T. Lai. "Lozenge tilings of doubly-intruded hexagons". *J. Combin. Theory Ser. A* 167 (2019), pp. 294–339. URL: https://doi.org/10.1016/j.jcta.2019.05.004.

[Cos84] . A. Costa. "Examples of a Complete Minimal Immersion in $\mathbb{R}^3$ of Genus One and Three Embedded Ends." *Bil. Soc. Bras. Mat. 15, 47-54* (1984).

[CR08] D. Cimasoni and N. Reshetikhin. "Dimers on Surface Graphs and Spin Structures. II". *Communications in Mathematical Physics* 281 (July 2008), pp. 445–468.

[CS16] F. Colomo and A. Sportiello. "Arctic Curves of the Six-Vertex Model on Generic Domains: The Tangent Method". *Journal of Statistical Physics* 164 (Sept. 2016).

[CSW23] N. Chandgotia, S. Sheffield, and C. Wolfram. "Large deviations for the 3D dimer model". *arXiv preprint arXiv:2304.08468* (2023).

[DC04] S. V. Duzhin and B. D. Chebotarevsky. *Transformation groups for beginners*. Vol. 25. Student Mathematical Library. Translated and revised from the 1988 Russian original by Duzhin. American Mathematical Society, Providence, RI, 2004, pp. x+246. URL: https://doi.org/10.1090/stml/025.

[DDG20] B. Debin, P. Di Francesco, and E. Guitter. "Arctic curves of the twenty-vertex model with domain wall boundaries". *J. Stat. Phys.* 179.1 (2020), pp. 33–89. URL: https://doi.org/10.1007/s10955-020-02518-y.

[DS08] D. De Silva and O. Savin. "Minimizers of Convex Functionals Arising in Random Surfaces". *Duke Math. J.* 151 (Oct. 2008).

[DVZ00] A. Dembo, A. Vershik, and O. Zeitouni. "Large deviations for integer partitions". *Markov Process. Related Fields* 6.2 (2000), pp. 147–179.

[Eva10] L. C. Evans. *Partial differential equations*. American Mathematical Society, 2010.

[FGM95] H. Ferguson, A. Gray, and S. Markvorsen. "Costa's minimal surface via mathematica". *Volume 168 of Preprint, Differentialgeometrie und Quantenphysik SFB 288 Issue 168 of SFB 288 preprint, Sonderforschungsbereich Differentialgeometrie und Quantenphysik* (1995).

[Fou96] J. C. Fournier. "Pavage des figures planes sans trous par des dominos: fondement graphique de l'algorithme de Thurston, parallélisation, unicité et décomposition". In: vol. 159. 1. Selected papers from the "GASCOM '94" (Talence, 1994) and the "Polyominoes and Tilings" (Toulouse, 1994) Workshops. 1996, pp. 105–128. URL: https://doi.org/10.1016/0304-3975(95)00204-9.

[FRT54] J. S. Frame, G. d. B. Robinson, and R. M. Thrall. "The Hook Graphs of the Symmetric Group". *Canadian Journal of Mathematics* 6 (1954), pp. 316–324.

[GK11] A. Goncharov and R. Kenyon. "Dimers and cluster integrable systems". *Annales Scientifiques de l'Ecole Normale Superieure* 46 (July 2011).

[GNW79] C. Greene, A. Nijenhuis, and H. S. Wilf. "A probabilistic proof of a formula for the number of Young tableaux of a given shape". *Advances in Mathematics* 31.1 (1979), pp. 104–109. URL: https://www.sciencedirect.com/science/article/pii/0001870879900239.

[Gor21] V. Gorin. *Lectures on random lozenge tilings*. Vol. 193. Cambridge Studies in Advanced Mathematics. Cambridge University Press, Cambridge, 2021, pp. viii+250. URL: https://doi.org/10.1017/9781108921183.

[Hat02] A. Hatcher. *Algebraic topology*. Cambridge University Press, Cambridge, 2002, pp. xii+544.

[Joh05] K. Johansson. "The arctic circle boundary and the Airy process". *Ann. Probab.* 33.1 (2005), pp. 1–30. URL: https://doi.org/10.1214/009117904000000937.

[JPS98] W. Jockusch, J. Propp, and P. Shor. "Random Domino Tilings and the Arctic Circle Theorem" (Feb. 1998).

[Kas61] P. Kasteleyn. "The Statistics of Dimers on a Lattice". *Physica, 27, 1209-1225.* (1961).

[Ken09] R. Kenyon. "Lectures on dimers". In: *Statistical mechanics*. Vol. 16. IAS/Park City Math. Ser. Amer. Math. Soc., Providence, RI, 2009, pp. 191–230. URL: https://doi.org/10.1090/pcms/016/04.

[Ker03] S. Kerov. *Asymptotic Representation Theory of the Symmetric Group and its Applications in Analysis*. Translations of Mathematical Monographs Volume: 219; 2003; 201 pp, 2003.

[KO05] R. Kenyon and A. Okounkov. "Limit shapes and the complex Burgers equation". *Acta Math.* 199 (Aug. 2005).

[Kor14] Korn A. "Zwei Anwendungen der Methode der sukzessiven Anndherungen". *Schwarz Festschrift,pp.215-229* (1914).

[KOS06] R. Kenyon, A. Okounkov, and S. Sheffield. "Dimers and amoebae". *Ann. of Math. (2)* 163.3 (2006), pp. 1019–1056. URL: https://doi.org/10.4007/annals.2006.163.1019.

[KP22] R. Kenyon and I. Prause. "Gradient variational problems in $\mathbb{R}^2$". *Duke Mathematical Journal* 16 (Oct. 2022), pp. 3003–3022.

[KP24] R. Kenyon and I. Prause. “Limit shapes from harmonicity: dominos and the five vertex model”. *Journal of Physics A: Mathematical and Theoretical* 57 (Jan. 2024).

[Kuc17] N. Kuchumov. “Limit shapes for the dimer model” (Dec. 2017), p. 31.

[Kuc21] N. Kuchumov. “A variational principle for domino tilings of multiply-connected domains”. *preprint arXiv:2110.06896* (Oct. 2021), p. 32.

[Lan99] S. Lang. *Complex analysis*. Fourth. Vol. 103. Graduate Texts in Mathematics. Springer-Verlag, New York, 1999, pp. xiv+485. URL: https://doi.org/10.1007/978-1-4757-3083-8.

[Lic16] Lichtenstein L. “Zur Theorie der konformen Abbildung. Konforme Abbildung nichtana- lytischer, singularitdtenfreier Fldchenstficke auf ebene Gebiete”. *Bull. Int. del’Acad. Sci. Cracovie, ser. A pp. 192-217* (1916).

[LL58] L. Landau and E. Lifshitz. *Statistical Physics, Third Edition, Part 1: Volume 5 (Course of Theoretical Physics, Volume 5)*. Pergamon Press Ltd, 1958.

[LS77] B. F. Logan and L. A. Shepp. “A variational problem for random Young tableaux”. *Advances in Math.* 26.2 (1977), pp. 206–222. URL: https://doi.org/10.1016/0001-8708(77)90030-5.

[Mei08] J. Meier. *Groups, graphs and trees. An introduction to the geometry of infinite groups*. English. Vol. 73. Lond. Math. Soc. Stud. Texts. Cambridge: Cambridge University Press, 2008.

[MW73] B. M. McCoy and T. T. Wu. *The two-dimensional Ising model*. English. Cambridge, MA: Havard University Press, 1973.

[NIA90] N.I.Akhiezer. *Elements of the theory of elliptic functions, Chapter 3, Paragraph 14*. AMS vol 79, 1990.

[Oko15] A. Okounkov. “Limit shapes, real and imaginary”. *Bull. Amer. Math. Soc. (N.S.)53(2016), no.2, 187–216.* (2015).

[OR01] A. Okounkov and N. Reshetikhin. “Correlation function of Schur process with application to local geometry of a random 3-dimensional Young diagram”. *J. Amer. Math. Soc.* 16 (Aug. 2001).

[Pet12] L. Petrov. “Asymptotics of Random Lozenge Tilings via Gelfand-Tsetlin Schemes”. *Probability Theory and Related Fields* 160 (Feb. 2012).

[PST16] I. Pak, A. Sheffer, and M. Tassy. “Fast Domino Tileability”. *Discrete and Computational Geometry* 56 (Sept. 2016).

[PW96] J. G. Propp and D. B. Wilson. “Exact sampling with coupled Markov chains and applications to statistical mechanics”. In: *Proceedings of the Seventh International Conference on Random Structures and Algorithms (Atlanta, GA, 1995)*. Vol. 9. 1-2. 1996, pp. 223–252. URL: https://doi.org/10.1002/(SICI)1098-2418(199608/09)9:1/2%3C223::AID-RSA14%3E3.3.CO;2-R.

[RLa92] S. R.Lay. *Convex sets and their applications*. Krieger publishing company, Malabar, Florida, 1992.

[Ros23] S. Rostam. “Limit shape for regularisation of large partitions under the Plancherel measure” (Feb. 2023).

[RRS92] R. Dobrushin, R. Kotecký, and S. Shlosman. “*Wulff construction, volume 104 of* Translations of Mathematical Monographs”. *American Mathematical Society, Providence, RI* (1992).

[RS17] N. Reshetikhin and A. Sridhar. “Integrability of Limit Shapes of the Six Vertex Model”. *Communications in Mathematical Physics* 356 (Dec. 2017).

[Shl07] S. Shlosman. “The Wulff construction in statistical mechanics and combinatorics”. *Russian Mathematical Surveys* 56 (Oct. 2007), p. 709.

[Spi79] M. Spivak. *Comprehensive introduction to differential geometry. Vol.4, Chapter 9 addendum 1, Vol. 5 Chapter 19, Section 5*. Harvard University Press, 1979.

[STCR95] N. C. Saldanha, C. Tomei, M. A. Casarin Jr., and D. Romualdo. “Spaces of domino tilings”. *Discrete Comput. Geom.* 14.2 (1995), pp. 207–233. URL: https://doi.org/10.1007/BF02570703.

[Thu90] W. Thurston. “Conway’s Tiling Groups”. *American Mathematical Monthly* 97 (Oct. 1990).

[Val45] F. A. Valentine. “A Lipschitz condition preserving extension for a vector function”. *Amer. J. Math.* 67 (1945), pp. 83–93. URL: https://doi.org/10.2307/2371917.

[Ver96] A. M. Vershik. “Statistical Mechanics of Combinatorial Partitions, and Their Limit Shapes”. *Funktsional. Anal. i Prilozhen., 1996, Volume 30, Issue 2, 19–39* (1996).

[VK77] A. M. Vershik and S. V. Kerov. “Asymptotics of the Plancherel measure of the symmetric group and the limiting form of Young tableaux”. English. *Sov. Math., Dokl.* 18 (1977), pp. 527–531.

[Wul01] G. Wulff. “Xxv. zur frage der geschwindigkeit des wachsthums und der auflösung der krystallflächen”. *Zeitschrift für Kristallographie-Crystalline Materials* 34.1-6 (1901), pp. 449–530.